Fitted numerical methods to solve differential models describing unsteady magneto-hydrodynamic flow

George Buzuzi

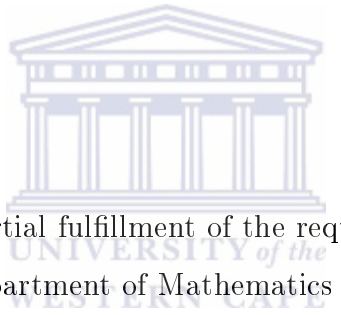

A Thesis submitted in partial fulfillment of the requirements for the degree of Doctor of Philosophy in the Department of Mathematics and Applied Mathematics at the Faculty of Natural Sciences, University of the Western Cape

Supervisor: Prof. Kailash C. Patidar

Co-supervisor: Dr. Justin B. Munyakazi

November 2013

KEYWORDS

Magneto-Hydrodynamic flows

Porus media

Differential equation models

Thermal radiation

Diffusion

Singular perturbation methods

Finite difference methods

Convergence and Stability analysis.

ABSTRACT

Fitted numerical methods to solve differential models describing unsteady magneto-hydrodynamic flow

by

George Buzuzi

PhD thesis, Department of Mathematics and Applied Mathematics, Faculty of Natural Sciences, University of the Western Cape

In this thesis, we consider some nonlinear differential models that govern unsteady magneto-hydrodynamic convective flow and mass transfer of viscous, incompressible, electrically conducting fluid past a porous plate with/without heat sources. The study focusses on the effect of a combination of a number of physical parameters (e.g., chemical reaction, suction, radiation, soret effect, thermophoresis and radiation absorption) which play vital role in these models. Non-dimensionalization of these models gives us sets of differential equations. Reliable solutions of such differential equations cannot be obtained by standard numerical techniques. We therefore resorted to the use of the singular perturbation approaches. To proceed, each of these model problems is discretized in time by using a suitable time-stepping method and then by using a fitted operator finite difference method in spatial direction. The combined methods are then analyzed for stability and convergence. Aiming to study the robustness of the proposed numerical schemes with respect to change in the values of the key parameters, we present extensive numerical simulations for each of these models. Finally, we confirm theoretical results through a set of specific numerical experiments.

November 2013.

DECLARATION

I declare that *Fitted numerical methods to solve differential models describing unsteady magneto-hydrodynamic flow* is my own work, that it has not been submitted before for any degree or examination at any other university, and that all sources I have used or quoted have been indicated and acknowledged by complete references.

George Buzuzi November 2013

Signed .....

ACKNOWLEDGEMENT

The preparation of this thesis would not have been possible without the support, encouragement and effort of various people.

I am deeply indebted to my supervisor, Prof. Kailash C. Patidar and my co-supervisor Dr. Justin B. Munyakazi for their commitment, encouragement, and persistent guidance throughout my PhD studies.

I wish to express my gratitude to the Department of Mathematics and Applied Mathematics of the University of the Western Cape for providing a conducive environment to carry out my studies. I also extend my thanks to the Department of Mathematics and Physics of Cape Peninsula University of Technology for supporting me in many ways to make my dreams come true.

I am grateful to Dr. Gift Muchatibaya, Gilbert Makanda, Martin Kudhina for their encouragement and support during my studies.

I finally wish to express my love to my family, friends and brethren of F.I.F.M.I. Cape Town. I am very grateful for my wife Perpetuah and my children, Addlight, Melody, Ashley and Andile for being there for me all the time.

DEDICATION

Dedicated to my mother Annie Grace Buzuzi.

Contents

List of Tables

List of Figures

List of Publications

Part of this thesis has been submitted in the form of the following research papers submitted to international journals for publications.

1. George Buzuzi, Justin B. Munyakazi and Kailash C. Patidar, Fitted numerical method to study the effects of chemical reaction and thermal radiation on unsteady mixed MHD convective flow and mass transfer of a fluid past an accelerated infinite porous plate in a porous medium, submitted for publication.

2. George Buzuzi, Justin B. Munyakazi and Kailash C. Patidar, A fitted numerical method to simulate a transient MHD free convective flow past an infinite vertical porous plate, submitted for publication.

3. George Buzuzi, Justin B. Munyakazi and Kailash C. Patidar, A novel finite difference method for an unsteady MHD free convection flow past a vertical plate with heat sources in the presence of a chemical reaction and suction, submitted for publication.

4. George Buzuzi, Justin B. Munyakazi and Kailash C. Patidar, The fitted method on the double-diffusive MHD flow over a moving vertical plate with heat generation and soret effects, submitted for publication.

5. George Buzuzi, Justin B. Munyakazi and Kailash C. Patidar, On the Fitted numerical method to investigate the effect of thermophoresis, viscosity, chemical reaction and radiation on an MHD flow over an inclined plate, submitted for publication.

6. George Buzuzi, Justin B. Munyakazi and Kailash C. Patidar, Fitted numerical analysis of radiation absorption and chemical effects on unsteady MHD free convection past a vertical permeable plate with heat source and suction or injection, submitted for publication.

Chapter 1

General introduction

In recent years, magnetohydrodynamic (MHD) problems have become increasingly important in industrial application. Metallurgical processes such as tinning of copper wires and drawing involve cooling of continuous strips by drawing them through a quiescent fluid [84]. Drawing such strips/filaments in an electrically conducting fluid subjected to a magnetic field affect the rate of cooling which of course controls the quality of the final product. In addition, hydromagnetics assists in the purification of molten metals from non-metallic inclusions by introducing a magnetic field [134].

1.1 Motivation for this research

The study of the rotation of electrically conducting fluids is important in several astrophysical and geophysical situations such as in the study the dynamics of rotating stars [15, 125]. Also the study of mixed convective MHD flow with mass transfer has been given much attention because of its application to nuclear research and the study of planets [125]. Permeability of the surface over which fluid flows has applications in biology and engineering such as transpiration cooling [117], urinary circulatory system and separation of Uranium-235 from Uranium-238 by gaseous exchange [125, 117]. Chemical reaction in a flow which affects concentration levels is useful in chemical processing industries such as fibre drawing, crystal pulling from melt and polymer pro-

duction. The problem of mixed convective MHD with mass transfer has been of much importance because of its application to nuclear research and the study of planets. In view of these, importance of studies of flow past a vertical wall has increased.

Mass transfer is encountered in chemical industry as well as in biological sciences [115]. Although many authors have studied mass transfer with or without radiation effects on the flow past oscillating vertical plate in the presence of magnetic field and free convection heat and variable mass diffusion, the case of a porous plate has not been considered so far. Moreover the use of perturbation techniques to solve such a problem has not been utilized to date.

The effect of chemical reaction on unsteady MHD flow past a moving semi-infinite vertical porous plate can also be investigated further. Chemical reactions can be considered either heterogenous or homogenous processes depending on whether the reaction occurs at an interface or as a single phase reaction. Many transport processes exist in nature and in industrial applications in which the simultaneous heat and mass transfer results from effects of both buoyancy and thermal diffusion and diffusion of chemical species [123, 124, 135, 155]. Free convection currents are caused by temperature differences. In addition, flow is affected by differences in concentration. Such study on concentration is useful in chemical processing industries such as crystal pulling and polymer production [84].

Magneto-convection is important in industrial applications including magnetic control of molten iron flow in the steel industry and liquid metal cooling in nuclear reactors [29, 124]. To the best of our knowledge, the singular perturbation techniques, are not fully explored to solve such problems to date.

In view of the above, one can see how complex the associated differential equation models can be. As is seen in the literature, they can not be solved analytically and hence we intend to design some efficient numerical methods to solve them.

Differential models describing the magnetohydrodynamic flows have been solved earlier using different methods such as the standard finite difference methods and finite element methods. In the models under study the coefficient of the first derivative

in the energy equation may be very large for certain combination of the given parameters rendering the equation singularly pertubed. In such instances, the standard methods fails to provide fairly accurate approximations of the true solution and to resolve the issue we design the robust, computationally more efficient fitted operator finite difference method (FOFDM). These FOFDMs were developed recently to solve singular perturbation problems (SPPs) (see e.g., Bashier and Patidar [14], Lubuma and Patidar [86], Munyakazi and Patidar [102, 103] and Patidar [121]). Singular perturbation problems are known to have solutions with large gradients when the coefficient of the highest derivative is very small. Boundary/interior layers develop which affect the convergence of the solution obtained using the usual standard numerical approach. The typical ranges of Prandtl numbers encountered in the current study include those for gases (0.7-1.0), water (1.7-13.7), light organic fluids (5-50) and oils (above 50).

1.2 Literature review

An early study on MHD problems was presented by Carrier and Greenspan [23]. Subsequently more works including [52, 61, 114] presented various aspects of such problems, for effect of mass transfer, wall temperature and magnetic field. Sakiadis [134] was the first to analyze the boundary layer on continuous surface of MHD problems.

Crane [40] presented a similarity solution for steady two dimensional boundary layer flow over a surface which is stretched in its own plane with a velocity varying linearly with the distance from a fixed point. Banks [13] considered a surface stretched with a velocity proportional to x^m, where x is the distance from a fixed point and m is a constant.

Magyari and Keller [88, 89] and Magyari *et al.* [90] considered the case when the mass transfer(suction/injection) is proportional to a power of the distance x. Carragher and Crane [22] considered the case where the temperature difference between the stretched surface and the ambient fluid is proportional to x^n, n being a constant. Kuiken [82] analyzed the boundary layer flow due to a moving sheet which obeys a

more general stretching law. Kuiken [82] showed that if the Reynolds number is large, a backward boundary layer exists along the moving sheet. Ishak *et al.* [74] reported the case of an electrically charged fluid experiencing transverse magnetic field. Ishak also discussed heat transfer assuming that the surface is maintained at a variable wall temperature $T_w(x)$ which is proportional to $(x_0/|x|)^m$ where m is a positive constant. Elshabeshy and Bazid [53] analyzed the stretching problem including a uniform porous medium. More recently, they analyzed the unsteady stretching problem. They analyzed both the steady and unsteady stretching surface with internal heat generation. They considered influence of variable viscosity of MHD flow and heat transfer over a porous stretching surface with internal heat generation. Ishak *et al.* [73] analyzed heat transfer over an unsteady stretching permeable surface with prescribed temperature. Subsequently, Hayat *et al.* [66] studied MHD flow and heat transfer over permeable stretching sheet with slip condition.

Alam and Sattar [9] investigated MHD heat and mass tranfer flow in a rotating system in presence of thermal diffusion. Brinkman [20] found the estimated viscous force imparted by a flowing fluid in a dense swarm of particles. Chandran *et al.* [33] studied the unsteady hydrodynamic free convection flow with heat flux and accelerated boundary motion. Choudhhury and Das [34] investigated the magnetohydrodynamic boundary layer flow of a non-Newtonian fluid past a flat plate.

Hasimoto [64] analyzed the boundary layer growth on a flat plate with suction and injection. Das *et al.* [48] numerically solved the mass transfer effects on unsteady flow past an accelerated vertical porous plate with suction. Mansutti *et al.* [93] studied the steady flows on non-newtonian fluids past a porous plate with suction and injection. In [120], Pathal *et al.* discussed the unsteady mass, momentum and heat transfer in MHD free convection flow past a vertical plate suddenly set in motion.

Raptis *et al.* [128] studied unsteady free convective flow through a porous medium adjacent to a semi-infinite vertical plate using finite difference scheme. Sharma and Pareek [141] have discussed the steady free convection MHD flow past a vertical porous moving surface. Das and Mitra [46] studied the unsteady mixed convective mass trans-

fer flow of viscous incompressible electrically conducting fluid past an accelerated infinite vertical porous plate with suction in the presence of transverse magnetic field. They solved this problem analytically and numerically using error function and the finite difference scheme, respectively. In the current study we applied both the analytical and perturbation technique.

The effect of chemical reaction on unsteady MHD flows past a moving semi-infinite plate has received considerable attention. Chambre and Young [25] analyzed a first order chemical reaction in the neighborhood of a horizontal plate. Das et al. [43] studied the effect of first order chemical reaction on the flow past an impulsively started infinite vertical plate with uniform heat flux and mass transfer. In addition, Das et al. [43] studied mass transfer effects on moving isothermal vertical plate in the presence of chemical reaction. Chandrakala [32] investigated the MHD flow past an impulsively started semi-infinite vertical plate with homogenous first order chemical reaction by implicit finite difference scheme of Crank-Nicolson type.

According to Deka and Neog [49], radiation in free convection has been studied by many authors because of its direct application in engineering and industry such as in nuclear power plants, space science and fossil fuel consumption. The industrial and engineering importance of radiation such as in liquid metal cooling, nuclear reactors, magnetic control of molten iron flow in steel industry are noted. Hydrodynamic flow is encountered in applications such as heat exchangers, nuclear engineering and MHD accelerators.

Exact solutions of free convection flow past a vertical oscillating plate in free convective flow was studied by Soundalgekar and Akolkar [153]. Before that, Soundalgekar [151] pioneered the study of flow past a vertical oscillating plate in free convective flow. The same problem with mass transfer effects was analyzed by soundalgekar and Alkolkar [153]. Das *et al.* [42] studied the effects of mass transfer on free convection flow past an impulsively started infinite vertical plate with constant heat flux and chemical reaction. Soundalgekar *et al.* [157] studied the effects of mass transfer on the flow past an infinite vertical oscillating plate with constant heat flux.

England and Emery [56] studied the thermal radiation effects on the laminar free and forced convection boundary layer of an absorbing gas bounded by a vertical stationary plate. Gupta and Gupta [62] studied the effects of radiation and combined free and forced convection of an electrically conducting fluid in the presence of transverse magnetic field. Das *et al.* [43] considered the case of radiation effects on flow past an impulsively started vertical plate. Mazumdar and Deka [94] studied the MHD flow past an impulsively started infinite vertical plate in the presence of thermal radiation.

Literature on the numerical techniques used for many of the models indicated above can also be found in some standard texts on Computational Fluid Dynamics.

Before we proceed further, we would like to mention here that the literature on individual problems treated subsequently in different chapters is provided in respective chapters.

1.3 Outline of the thesis

This thesis is concerned with the design, analysis and implimentation of a class of fitted operator finite difference methods to solve differential models describing unsteady magneto-hydrodynamic flow.

In Chapter 2, we study unsteady mixed MHD convective flow and mass transfer in a flow past an accelerated infinite porous plate with thermal radiation, chemical reaction and suction.

Chapter 3 is devoted to the analysis of the solution of a transient MHD flow of viscous incompressible electrically conducting fluid past a vertical infinite porous plate in the presence of a transverse magnetic field.

We investigate the effects of a chemical reaction on unsteady two-dimensional MHD free convection flow of viscous incompressible electrically conducting fluid past a vertical infinite porous plate with heat sources in the presence of a transverse magnetic field, chemical reaction and suction or injection in Chapter 4.

The solution of a double-diffusive convection-radiation interaction on a two dimen-

sional unsteady MHD laminar flow of viscous, incompressible, electrically conducting fluid past a semi-infinite vertical moving porous plate embedded in a porous, heat generation/absorption and thermal diffusion is dealt with in Chapter 5.

Chapter 6 tackles unsteady transient MHD free convective and mass transfer flow with thermophoresis past an inclined permeable plate in the presence of chemical reaction, thermal radiation and temperature dependent viscosity. medium subjected to a transverse magnetic field in the presence of a chemical reaction.

In Chapter 7, we study a two-dimensional unsteady MHD free convection flow of a viscous, incompressible, electrically conducting, heat generation/absorbing fluid past a vertical infinite porous flat plate in the presence of a transverse magnetic field, radiation absorption, chemical reaction and suction or injection.

Finally, in Chapter 8 concluding remarks and plans for further research are given.

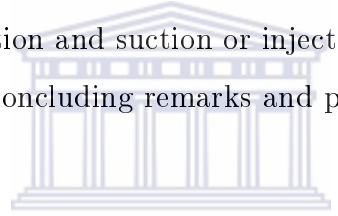

Chapter 2

A fitted numerical method to study the effects of chemical reaction and thermal radiation on unsteady mixed MHD convective flow and mass transfer of a fluid past an infinite porous plate in a porous medium

In this chapter, we study unsteady mixed MHD convective flow and mass transfer in a flow past an accelerated infinite porous plate with thermal radiation, chemical reaction and suction using a fitted operator finite difference method. We extend the work of Das and Mitra [46] by introducing the effects of radiation, chemical reaction and the presence of a porous media. Most of the works on this type of problems have considered standard numerical methods which are inappropriate as we have investigated with several cases. In this work, the governing partial differential equations describing the problem stated above are transformed by a suitable similarity transformation resulting

into a system of ordinary differential equations which are then solved using a fitted numerical method. We observe that for small values of the coefficient of the first derivative in the energy equation (2.2.3) the standard numerical method may still work but for relatively large values of these coefficients this approach fails to provide reasonably accurate numerical solution.

2.1 Introduction

Porous media arise in numerous geophysical and metallurgical flows. Chamka [28] analyzed the transient-free convection MHD boundary layer flow in a fluid-saturated porous medium channel. Later Chamka [29] extended this study to consider the influence of temperature-dependent properties on the hydrodynamic flow in a porous channel and inertial effects on the convection regime in the presence of heat source. Beg *et al.* [17] considered perturbation analysis of unsteady oscillatory magneto-convection in porous media with heat source effects. Later, Beg *et al.* [18] considered the transient radiation convection MHD flow past a vertical plate adjacent to a porous regime.

The fluid flow in the porous media may have chemical species diffusing into it which affects the mass transfer in the flow and therefore the study of chemical reaction cannot be ignored. Chemical reactions are classified as either homogenous or heterogenous depending on whether it is a single phase volume reaction or the reaction occur at an interface. Simultaneous heat and mass transfer in nature and in an industrial setting are triggered by the combined buoyancy effects of thermal diffusion and diffusion of chemical species. Free convection currents may be caused by temperature difference, concentration difference or both. Free convection flows due to difference in concentration is important in chemical processing industry in cases like fibre pulling, crystal pulling from the melt and in the production of polymers. Das *et al.* [47] analyzed the mass transfer effects on flow past an impulsively started infinite isothermal vertical plate with uniform mass flux. Later Das *et al.* [41] gave an analytical solution to the flow of a viscous incompressible fluid past an impulsively started vertical isothermal

plate in the presence of mass diffusion and first order chemical reaction. In both cases they solved the problems using the Laplace transform technique. Muthucumaraswamy and Ganesan [109] studied the effects of the first order homogenous chemical reaction on the flow characteristics of an unsteady flow past an impulsively started semi-infinite vertical plate with uniform mass flux. The governing equations were solved using implicit-finite difference scheme of the Crank Nicolson type. Chandrakala [31] used implicit finite-difference scheme to derive a solution to the transient natural convection flow of an incompressible viscous fluid past an impulsively started semi infinite isothermal vertical plate with uniform mass flux in the presence of a magnetic field and homogenous chemical reaction of the first order.

In recent years, the effect of heat transfer by radiation and free or mixed convection has become increasingly important industrially. Many processes in industry take place at high temperatures and the knowledge of radiation heat transfer enables the design of the relevant high temperature equipment such as nuclear power plants, solar fans, photo chemical reactors, missiles, satellites, glass production devices, furnace design equipments and propulsion devises for aircraft.

Takhar *et al.* [70, 159] analyzed the effect of radiation on mixed convection along a vertical plate with uniform surface temperature. Bakier and Gorla [12] studied the effect of radiation on mixed convection flow over horizontal surfaces embedded in a porous medium. Kim and Fedorov [80] analyzed the transient mixed radiative convective flow of a micro polar fluid past a moving semi-infinite vertical porous plate. Cookey *et al.* [75] investigated two dimensional flow with time dependent suction. Prasad *et al.* [124] analyzed a laminar mixed convective boundary layer flow of a radiating fluid along a semi-infinite vertical permeable moving plate with heat and mass transfer. Recently, Shateyi *et al.* [142] studied the effect of thermal radiation, Hall currents, Soret and Dufour on MHD flow by mixed convection over a vertical surface in porous media.

Many researchers have studied free or forced convective flows over a vertical plate due to their varied application in fields such as geophysics and astrophysics. Pathal *et al.* [120] discussed the unsteady mass, momentum and heat transfer in MHD free

convection flow past a vertical plate suddenly set in motion. Soundalgekar [152] analyzed the free convection effects on steady MHD flow past a vertical porous plate. Raptis *et al.* [128] have studied the unsteady free convective flow through a porous medium adjacent to semi infinite vertical plate using finite difference scheme. Satter [135] reported the free convection and mass transfer flow through a porous medium past an infinite vertical porous plate with time dependent temperature and concentration. Singh and Soundalgekar [149] investigated the transient free convection effect in cold water past an infinite vertical porous plate. Mansutti *et al.* [93] have analyzed the steady flows of non-Newtonian fluids past a porous plate with suction or injection. Sharma and Pareek [141] have discussed the steady free convection MHD flow past a vertical porous moving surface. Das *et al.* [48] solved numerically the equations that describe the mass transfer effects on unsteady flow past an accelerated vertical porous plate with suction. Das and Mitra [46] analyzed the unsteady mixed convective MHD flow and mass transfer past an accelerated infinite vertical porous plate with suction.

In this chapter, we study unsteady mixed MHD convective flow and mass transfer in a flow past an accelerated infinite porous plate with thermal radiation, chemical reaction and suction using a fitted operator finite difference method (FOFDM). We extend the work of Das and Mitra [46] by taking into account the effects of radiation, chemical reaction and the presence of a porous media. In the model under study the coefficient of the first derivative in the energy equation may become very large for certain combination of values of the Prandtl number, suction and radiation parameters. This renders the equation singularly perturbed. A vast amount of literature exists on singularly perturbed partial differential equations (see, [96, 131] and references therein). Cess [24] studied the interaction of radiation with laminar free convection heat transfer from a vertical plate using singular perturbation technique. Before we proceed further we would like to mention that such models have been simulated numerically as indicated in the literature above but to the best of our knowledge no work has been done to numerically study unsteady MHD flows using FOFDMs.

The rest of the chapter is organized as follows. In Section 2.2, the description of

the model problem under study is presented. Governing equations are developed and transformed into similarity form together with their boundary conditions. Section 2.3 deals with the construction of numerical method and its analysis. Section 2.4 contains the numerical results. Finally some concluding remarks are given in Section 2.5.

2.2 Description of the model

We consider the unsteady mixed convective mass transfer flow of a viscous incompressible electrically conducting fluid past an accelerating vertical infinite porous flat plate adjacent to a porous medium in the presence of a transverse magnetic field B_o and a chemical reaction with significant radiation effect. Let the $x-$axis be directed upward along the plate and the $y-$axis be normal to the plate. Let u and v be the velocity components along $x-$ and $y-$ axes, respectively. We assume that the plate is accelerating with a velocity $u = Ut$ in its own plane at time $t \geq 0$. Then the magnetohydrodynamic unsteady mixed convective boundary layer equations under usual Boussinesq's approximation (a modification of the model in [46]) read

$$\frac{\partial v}{\partial y} = 0, \tag{2.2.1}$$

$$\frac{\partial u}{\partial t} + v\frac{\partial u}{\partial y} = \nu\frac{\partial^2 u}{\partial y^2} + g\beta(T - T_\infty) + g\beta^*(\widetilde{C} - \widetilde{C}_\infty) - \frac{\sigma {B_0}^2}{\rho}u - \frac{\nu}{K^*}u, \tag{2.2.2}$$

$$\frac{\partial T}{\partial t} + v\frac{\partial T}{\partial y} = \alpha\frac{\partial^2 T}{\partial y^2} - \frac{1}{\rho c_p}\frac{\partial q_r}{\partial y}, \tag{2.2.3}$$

$$\frac{\partial \widetilde{C}}{\partial t} + v\frac{\partial \widetilde{C}}{\partial y} = D\frac{\partial^2 \widetilde{C}}{\partial y^2} - K_l(\widetilde{C} - \widetilde{C}_\infty), \tag{2.2.4}$$

where ν is the kinematic viscosity, β is the volumetric coefficient of thermal expansion, β^* is the volumetric coefficient of expansion with concentration, ρ is the density of the fluid, σ is the electrical conductivity of the fluid, g is the acceleration due to gravity, T is the temperature of the fluid in the boundary layer, T_∞ is the temperature of the fluid far away from the plate, $\widetilde{C}$ is the concentration of fluid in the boundary layer, $\widetilde{C}_\infty$ is the concentration of the fluid far away from the plate and D is the molecular diffusivity,

K^* is the permeability of the porous regime, K_l is the rate of chemical reaction, c_p is the specific heat capacity, α is the thermal diffusivity, q_r is the radiation heat flux and B_0 is the magnetic induction. The associated boundary conditions [46] are

$$\begin{aligned} &u = Ut,\ T = T_w,\ \widetilde{C} = \widetilde{C}_w \text{ at } y = 0, \\ &u \to 0,\ T \to T_\infty,\ \widetilde{C} \to \widetilde{C}_\infty \text{ as y} \to \infty \text{ for t} \to \infty. \end{aligned} \tag{2.2.5}$$

where U ia a scale of the free stream velocity. The radiative heat flux q_r is described by the Rosseland approximation (Prasad *et al.* [123]):

$$q_r = (4\sigma^*/3K_1)\partial T^4/\partial y, \tag{2.2.6}$$

where σ^* and K_1 are the Stefan-Boltzman constant and the mean absorption coefficient, respectively. Following Soundalgekar [149] and Das [46] we nondimensionalize (2.2.2)-(2.2.4) by introducing the following similarity variables

$$\begin{aligned} &\eta = y/(2\sqrt{\nu t}),\ \theta = (T - T_\infty)/(T_w - T_\infty),\ C = (\widetilde{C} - \widetilde{C}_\infty)/(\widetilde{C}_w - \widetilde{C}_\infty), \\ &M = (v\sigma B_o^2/\rho)/\nu^2,\ P_r = \nu/\kappa,\ S_c = \nu/D,\ G_r = 4g\beta(T_w - T_\infty)/U, \\ &G_c = 4g\beta^*(\widetilde{C}_w - \widetilde{C}_\infty)/U,\ \alpha = \kappa/\rho c_p,\ R = 4\sigma T_\infty^3/K_1\kappa, \\ &d = K_l\nu/v^2, \end{aligned} \tag{2.2.7}$$

where P_r is the Prandtl number, d is the chemical reaction parameter,G_r is the Grashof number of heat transfer, G_c is the Grashof number for mass transfer, R is the thermal radiation parameter, M is the magnetic parameter, κ is the thermal conductivity, K_l is the rate of chemical reaction and S_c is the Schmidt number.

In line with Hasimoto [64], Singh and Soundalgekar [149] and Das *et al.* [46], we consider

$$v = -a\,(\nu/t)^{1/2}, \tag{2.2.8}$$

where $a > 0$ is the suction parameter. Using (2.2.7) and (2.2.8), equations (2.2.2)-(2.2.4) reduce to

$$f'' + 2(\eta + a)f' - 4(1 + a^2(1/K^* + M))f = -G_r\theta - G_cC, \quad (2.2.9)$$

$$\theta'' + \frac{6(\eta + a)}{3 + 4R}P_r\theta' = 0, \quad (2.2.10)$$

$$C'' + 2(\eta + a)S_cC' - 4da^2S_cC = 0, \quad (2.2.11)$$

where $'$ denotes the differentiation with respect to η. The corresponding boundary conditions take the form

$$f(\eta) = 1,\ C(\eta) = 1,\ \theta(\eta) = 1 \text{ at } \eta = 0, \quad (2.2.12)$$

$$f(\eta) = 0,\ \theta(\eta) = 0,\ C(\eta) = 0 \text{ as } \eta \to \infty.$$

The non-dimensional local heat flux (in terms of Nusselt number, N_u) at the plate is given by

$$N_u = 2q_w\sqrt{\nu t}/(\kappa(T_w - T_\infty)) = -\theta'(0), \quad (2.2.13)$$

where q_w is the heat flux per unit area. We solve the above problem (2.2.9) - (2.2.12) using a fitted operator finite difference method described in next section.

2.3 Construction and analysis of the numerical method

In this section, we introduce a FOFDM to solve the energy equation (2.2.10). To begin with, let n be a positive integer. Consider the following partition of the interval [0,2]: $\eta_0 = 0,\ \eta_j = \eta_0 + jh,\ j = 1(1)n,\ h = \eta_j - \eta_{j-1},\ \eta_n = 2$. We take $\eta_n = 2$ since it lies well outside the boundary layer. Note that $j = 1(1)n$ means $j = 1, 2, 3, ...n$. On this partition, the standard finite difference method (SFDM) used to discretely approximate (2.2.10) reads

$$\frac{\widetilde{\nu}_{j+1} - 2\widetilde{\nu}_j + \widetilde{\nu}_{j-i}}{h^2} + A_j\frac{\widetilde{\nu}_{j+1} - \widetilde{\nu}_{j-1}}{2h} = 0, \quad (2.3.1)$$

where $\widetilde{\nu}$ is an approximation for θ and $A_j = 6(\eta_j + a)P_r/(3 + 4R)$. The choice for the central difference approximation for θ' using SFDM was arrived at after applying the double mesh principle which showed that the central difference approximation produced the least maximum absolute error. The central difference approximation was also used in the momentum and concentration equations (2.2.9) and (2.2.11), for the same reason. However, for relatively large values of $A_j\,'s$, the standard finite difference method (SFDM) fails to provide fairly accurate approximation of the true solution. To resolve this issue we design a fitted numerical technique whereby the denominator of the approximation to the second derivative h^2 is replaced by a function ψ_j^2, which is a function of h. The proposed FOFDM reads

$$L^h u_j \equiv \frac{u_{j+1} - 2u_j + u_{j-1}}{\psi_j^2} + A_j \frac{u_{j+1} - u_j}{h} = 0, \tag{2.3.2}$$

where u is an approximation for θ obtained by using this FOFDM and

$$\psi_j^2 = h\left(e^{A_j h} - 1\right)/A_j. \tag{2.3.3}$$

The function ψ_j^2 can be obtained by using the theory of finite differences as indicated in [86]. It captures significant behavior of the solution, particularly when the solution in the layer region has steep gradient. The layer region is located in the neighborhood of the vertical plate near the left end of the interval. Before we proceed with the numerical simulations, first we analyse the FOFDM (2.3.2) for stability and convergence.

Lemma 2.3.1. (Discrete minimum principle) *Assume that the mesh function ϕ_i satisfies $\phi_0 \geq 0$ and $\phi_n \geq 0$. Then, $L^h\phi_i \leq 0$ for $i = 1(1)n-1$ implies that $\phi_i \geq 0$ for all $i = 0(1)n$.*

Proof. The proof follows the same lines as the proof of the discrete minimum principle in [77] as shown below. Choose k such that $\phi_k = \min_i \phi_i$ and assume that $\phi_k \leq 0$. It

follows that $k \notin \{0, n\}$, $\phi_{k+1} - \phi_k \geq 0$ and $\phi_k - \phi_{k-1} \leq 0$. Then

$$\begin{aligned} L^h\phi_k &= \frac{1}{\psi_k^2}\left[\phi_{k+1} - 2\phi_k + \phi_{k-1}\right] + \frac{A_j}{h}\left[\phi_{k+1} - \phi_k\right], && (2.3.4)\\ &= \frac{1}{\psi_k^2}\left[\phi_{k+1} - \phi_k + \phi_{k-1} - \phi_k\right] + \frac{A_j}{h}\left[\phi_{k+1} - \phi_k\right] && (2.3.5)\\ &\geq 0, \end{aligned}$$

which is a contradiction. It follows that $\phi_k \geq 0$. Therefore, $\phi_i \geq 0$ for all $i,\ i(1)n$.

In what follows, $\widetilde{M}$ and $\mathcal{M}$ denote positive constants independent of h and ε.

Lemma 2.3.2. *Let θ be the solution of (2.2.10) with $\theta(0) = 1$ and $\theta(2) = 0$. Then for $0 \leq k \leq 3$,*

$$|\theta^{(k)}(\eta)| \leq \widetilde{M}\left(1 + B^k e^{-\lambda\eta}\right)$$

for all $\eta \in \overline{\Omega}$ where $B = \max_{\overline{\Omega}} A$, where $A \equiv A(\eta) = 6(\eta + a)P_r/(3 + 4R) > \lambda > 0$ and $\overline{\Omega} = [0, 2]$.

Proof. The proof follows the same lines as the proof of the bounds on the solution θ and its derivatives in [96]. Rewrite equation (2.2.10) in the form

$$L\phi \equiv \phi'' + A(\eta)\phi'. \tag{2.3.6}$$

We use the minimum principle to obtain a bound on the solution $\theta(\eta)$ of (2.2.10) as follows. We consider

$$\phi^{\pm}(\eta) = \widetilde{M}(2 - \eta) \pm \theta(\eta).$$

It is clear that

$$\phi^{\pm}(0) \geq 0,\ \phi^{\pm}(2) \geq 0,$$

and

$$L\phi^{\pm}(\eta) = \pm\theta''(\eta) + A(\eta)(\pm\theta)'(\eta) - A(\eta)\widetilde{M}, \tag{2.3.7}$$

$$= \pm L\theta(\eta) - A(\eta)\widetilde{M} \leq 0. \tag{2.3.8}$$

Then by the minimum principle $\phi^{\pm}(\eta) \geq 0$, and therefore

$$|\theta(\eta)| \leq \widetilde{M}(2-\eta) \leq 2\widetilde{M} \text{ for all } \eta \in \overline{\Omega}.$$

To obtain bounds on the derivatives of θ we differentiate k times the equation $L\theta = 0$ and obtain $L\theta^{(k)} = f_k$ where $1 \leq k \leq 3$,

$$f_k = -\Sigma_{r=0}^{k-1} \binom{n}{r} A^{(k-r)}\theta^{(r+1)}$$

and $f_0 = 0$. The quantity f_k depends on the derivatives of θ and the coefficient A. We therefore proceed with a proof by induction. We assume that the following estimates hold for all $0 \leq i \leq k$, for all $\eta \in \overline{\Omega}$, and $L\theta^{(k)} = f_k$:

$$|\theta^{(k)}(\eta)| \leq \widetilde{M}\left(1 + B^k e^{-\lambda\eta}\right), \tag{2.3.9}$$

and

$$|f_k(\eta)| \leq \widetilde{M}\left(1 + B^k e^{-\lambda\eta}\right). \tag{2.3.10}$$

At the boundary points

$$|\theta^{(k)}(0)| \leq \widetilde{M}\left(1 + B^k\right) \leq \widetilde{M}B^k, \tag{2.3.11}$$

and

$$|\theta^{(k)}(2)| \leq \widetilde{M}\left(1 + B^k e^{-2\lambda}\right) \leq \widetilde{M}B^k. \tag{2.3.12}$$

Let

$$w_k(\eta) = B\int_0^{\eta} f_k(t)e^{-B(H(\eta)-H(t))}dt, \tag{2.3.13}$$

where

$$H(\eta) = \int_0^{\eta} A(s)ds.$$

The particular solution of the equation $L\theta^{(k)} = f_k$ is given by

$$\theta_p^{(k)}(\eta) = -\int_0^{\eta} w_k(t)dt. \tag{2.3.14}$$

The general solution $\theta(k)$ is written in the form $\theta^{(k)} = \theta_p^{(k)} + \theta_h^{(k)}$ where $\theta_p^{(k)}$ is the particular solution and $\theta_h^{(k)}$ is the homogenous solution. $\theta^{(k)}$ satisfies

$$L\theta_h^{(k)} = 0,\ \theta_h^{(k)}(0) = \theta^{(k)}(0),\ \theta_h^{(k)}(2) = \theta^{(k)}(2) - \theta_p^{(k)}(2). \tag{2.3.15}$$

Let the function

$$\varphi(\eta) = \frac{\int_0^{\eta} e^{-H(t)}dt}{\int_0^{2} e^{-H(t)}dt},$$

then

$$L\varphi = 0, \quad \varphi(0) = 1, \quad \varphi(2) = 0, \quad 0 \le \varphi(\eta) \le 1.$$

Now $\theta_h^{(k)}$ is given by a linear combination of $\theta_h^{(k)}(0)$ and $\theta_h^{(k)}(2)$, that is

$$\theta_h^{(k)}(\eta) = \left(\theta^{(k)}(0)\right)\varphi(\eta) + \left(\theta^{(k)}(2) - \theta_p^{(k)}(2)\right)(1 - \varphi(\eta)). \tag{2.3.16}$$

Differentiating (2.3.16) with respect to η gives

$$\theta^{(k+1)}(\eta) = \left(\theta^{(k)}(0)\right)\varphi' - \left(\theta^{(k)}(2) - \theta_p^{(k)}(2)\right)\varphi'. \tag{2.3.17}$$

From (2.3.14) $\theta_p^{(k+1)}(\eta) = w_k$. It follows that

$$\begin{aligned}\theta^{(k+1)}(\eta) &= \theta_p^{k+1}(\eta) + \theta_h^{(k+1)}(\eta),\\ &= w_k + \theta_k(0)\varphi' - \left(\theta^{(k)}(2) - \theta_p^{(k)}(2)\right)\varphi',\\ &= w_k + \left(\theta^{(k)}(0) - \theta^{(k)}(2) + \theta_p^{(k)}(2)\right)\varphi'. \end{aligned}\tag{2.3.18}$$

Now

$$\varphi' = \frac{e^{-H(\eta)}}{\int_0^2 e^{-H(t)}dt}.$$

Therefore,

$$|\varphi'(\eta)| \leq |Ae^{-\lambda\eta}| \leq Be^{-\lambda\eta}. \tag{2.3.19}$$

Since $A \leq B$, we have

$$|w_k(\eta)| \leq B\widetilde{M}\int_0^\eta \left(1 + B^k e^{-\lambda t}\right) e^{-B(\lambda\eta - \lambda t)}dt. \tag{2.3.20}$$

Further simplification leads to

$$|w_k(\eta)| \leq \widetilde{M}Be^{-B\lambda\eta}\left(\frac{e^{B\lambda\eta}}{B} + B^k e^{(B\lambda-\lambda)\eta}\right). \tag{2.3.21}$$

Finally, we get

$$|w_k(\eta)| \leq \widetilde{M}\left(1 + B^{k+1}e^{-\lambda\eta}\right). \tag{2.3.22}$$

Since

$$\theta_k^{(k)}(2) = -\int_0^2 w_k(t)dt, \tag{2.3.23}$$

we get

$$|\theta_p^{(k)}(2)| \leq \widetilde{M}B^k. \tag{2.3.24}$$

We know that

$$|\theta^{(k+1)}| \leq \left(|w_k| + |\theta^{(k)}(0)| + |\theta^{(k)}(2)| + |\theta_p^{(k)}(2)|\right)\varphi', \tag{2.3.25}$$

so

$$|\theta^{(k+1)}| \leq \widetilde{M}\left(1 + B^{k+1}e^{-\lambda\eta}\right) + \left(\widetilde{M}B^k + \widetilde{M}B^k + \widetilde{M}B^k\right)Be^{-\lambda\eta}. \tag{2.3.26}$$

This reduces to

$$|\theta^{(k+1)}| \leq \widetilde{M}\left(1 + B^{k+1}e^{-\lambda\eta}\right), \tag{2.3.27}$$

which completes the proof.

The following lemma is a consequence of the discrete minimum principle (Lemma 2.3.1).

Lemma 2.3.3. (Uniform stability estimate) *If ξ_j is any mesh function such that $\xi_0 = \xi_n = 0$ then the operator L^h in (2.3.4) is uniformly stable if*

$$|\xi_j| \leq 2\mathcal{M}\max_{1\leq i\leq n-1}|L\xi_i| \quad for \quad 0 \leq j \leq n,$$

where $\mathcal{M}$ is a constant independent of the step size.

Proof. The proof follows the same lines as the proof of the uniform stability estimate

in [96]. Let

$$\widetilde{M} = \mathcal{M} \max_{1\le i\le n-1} |L\xi_i| .$$

and introduce the mesh functions $\vartheta_j^+, \vartheta_j^-$ defined by $\vartheta_j^\pm = \widetilde{M}(2-\eta_j)\pm\xi_j$. From equation (2.3.2)

$$\begin{aligned}
L^h\vartheta_j^\pm &= \frac{\left(\vartheta_{j+1}^\pm - 2\vartheta_j^\pm + \vartheta_{j-1}^\pm\right)}{\psi_j^2} + A_j\frac{\left(\vartheta_{j+1}^\pm - \vartheta_j^\pm\right)}{h}, \\
&= \frac{\left(\widetilde{M}(2-\eta_{j+1}) \pm \xi_{j+1} - 2\widetilde{M}(2-\eta_j) \pm \xi_j + \widetilde{M}(2-\eta_{j-1}) \pm \xi_{j-1}\right)}{\psi_j^2} \\
&\quad + A_j\frac{\left(\widetilde{M}(2-\eta_{j+1}) \pm \xi_{j+1} - \widetilde{M}(2-\eta_j) \pm \xi_j\right)}{h}, \\
&= \frac{(\pm\xi_{j+1} \pm 2\xi_{j+1} \pm \xi_{j-1})}{\psi_j^2} + A_j\frac{(\pm\xi_{j+1} \pm \xi_j)}{h} - A_j\widetilde{M}, \\
&= \pm L^h\xi_j - A_j\mathcal{M}\max|L^h\xi_i| \le 0, \quad 0 \le i \le n. \qquad (2.3.28)
\end{aligned}$$

From the discrete minimum principle, we have $\vartheta_j^\pm \ge 0$, for $0 \le j \le n$.
It follows $\widetilde{M}(2-\eta_j) \pm \xi_j \ge 0$ for $0 \le j \le n$, implies $|\xi_j| \le (2-\eta_j)\widetilde{M}$
$= (2-\eta_j)\mathcal{M}\max|L^h\vartheta_j^\pm| \le 2\mathcal{M}\max|L^h\vartheta_j^\pm|$, which completes the proof. Now the local truncation error of the FOFDM (2.3.2) is given by

$$\begin{aligned}
\left[L^h(\theta-u)_j\right] &= \left(\theta_j'' + A_j\theta_j'\right) - \left(\frac{\theta_{j+1} - 2\theta_j + \theta_{j-1}}{\psi_j^2} + A_j\frac{\theta_{j+1} - \theta_j}{h}\right), \qquad (2.3.29) \\
&= \theta_j'' + A_j\theta_j' - \frac{1}{\psi_j^2}\left[h^2\theta_j'' + h^4\theta^{(iv)}(\zeta_1)\right] \\
&\quad - \frac{A_j}{h}\left(h\theta_j' + \frac{h^2}{2}\theta_j'' + \frac{h^3}{6}\theta'''(\zeta_2)\right),
\end{aligned}$$

where $\zeta_1 \in (\eta_{j-1}, \eta_{j+1})$ and $\zeta_2 \in (\eta_j, \eta_{j+1})$. Using the Taylor series expansion, we have

$$\frac{1}{\psi_j^2} = \frac{A_j}{h}\left(\frac{1}{A_jh} - \frac{1}{2} + \frac{1}{12}A_jh + O(h^2)\right). \qquad (2.3.30)$$

This implies that

$$\begin{aligned}\left[L^h(\theta-u)_j\right] &= \theta_j'' + A_j\theta_j' \\ &\quad - \left[\frac{A_j}{h}\left(\frac{1}{A_jh} - \frac{1}{2} + \frac{1}{12}A_jh + O(h^2)\right)\right]\left[h^2\theta_j'' + O(h^4)\right] \\ &\quad - \frac{A_j}{h}\left(h\theta_j' + \frac{h^2}{2}\theta_j'' + \frac{h^3}{6}\theta'''(\zeta_2)\right).\end{aligned} \tag{2.3.31}$$

Further simplifications lead to

$$\left[L^h(\theta-u)_j\right] = -\left(\frac{A_j^2}{12}\theta_j'' + \frac{A_j}{6}\theta_j'''\right)h^2 + O(h^3).$$

Using Lemma 2.3.2 we obtain

$$\left|L^h(\theta-u)_j\right| \leq \left|\frac{A_j^2}{12}\widetilde{M}\left(1+\frac{B^2}{e^{\alpha\eta}}\right)\right|h^2 + \left|\frac{A_j\widetilde{M}}{6}\left(1+\frac{B^3}{e^{\alpha\eta}}\right)\right|h^2. \tag{2.3.32}$$

Applying Lemma 7 in [103]

$$\begin{aligned}\left|L^h(\theta-u)_j\right| &\leq \left(\frac{A_j^2\widetilde{M}}{12} + \frac{A_j\widetilde{M}}{6}\right)h^2, \\ &\leq \left(\frac{\overline{A}_j^2\widetilde{M}}{12} + \frac{\overline{A}_j\widetilde{M}}{6}\right)h^2, \\ &\leq \mathcal{M}h^2,\end{aligned} \tag{2.3.33}$$

where $\overline{A} = \max_j A_j$. The solutions to equations (2.2.9) and (2.2.11) are found simultaneously with equation (2.2.10). The system of equations are solved in such way that the improved solution of the energy equation obtained using the FOFDM is then used to obtain the solution of the velocity equation. This means that the final expression for the velocity equation gives a better solution compared to the case where the temperature values used are obtained using standard methods. Then by Lemma 2.3.3 and

(2.3.33), we have

$$\max_{0\le i\le n} |(\theta-u)_i| \;\le\; \max_{1\le i\le n-1} \left|L^h(\theta-u)_i\right| \le \mathcal{M}h^2.$$

2.4 Results and discussions

In this section, we present some numerical results followed by a thorough discussion of them.

The maximum absolute error at all mesh points are evaluated using the double mesh principle

$$E_n = \max_{0\le i\le n} |u_i^n - u_{2i}^{2n}|,$$

for different n and A_j where u_i is the numerical solution. Since A_j is directly proportional to P_r we calculate the maximum absolute error in the FOFDM solution by varying P_r and n while keeping other parameters constant. The numerical rates of convergence are computed using the formula ([51])

$$r_k := \log_2 \left(E_{n_k}/E_{2n_k}\right),\ k = 1, 2, \ldots.$$

The values for the maximum absolute errors and rates of convergence are depicted in Tables 2.4.1 and 2.4.2 respectively.

Table 2.4.1: Maximum absolute errors using FOFDM.

P_r	n= 10	n=20	n=40	n= 80
5	2.76E-3	6.83E-4	1.70E-4	4.27E-5
10	5.26E-3	1.40E-3	3.49E-4	8.71E-5
20	1.19E-2	2.89E-3	7.17E-4	1.79E-4
40	1.86E-2	5.92E-3	1.45E-3	3.71E-4

We compare the performance of the FOFDM with the SFDM. In Table 2.4.3, the results obtained by these two methods are compared for $a = 0.1, P_r = 7$, and $R = 1$. Similarly in Table 2.4.4, the two methods are compared for $a = 1, P_r = 10$, and $R = 2$. In these tables, SFDM-I and SFDM-II stands for standard finite difference

Table 2.4.2: Rates of convergence of FOFDM, $n_k = 10, 20, 40, 80$.

P_r	r_1	r_2	r_3
5	2.01	2.01	1.99
10	1.91	2.00	2.00
20	2.04	2.01	2.00
40	1.65	2.03	1.97

methods where forward difference approximation and central difference approximation are respectively used to approximate θ'.

Table 2.4.3: Maximum absolute errors for $a = 0.1$, $K = 1$, $M = 1$, $P_r = 7$, $S_c = 1$, $d = 1$, $R = 1$.

Method	$n = 10$	$n = 20$	$n = 40$	$n = 80$
SFDM-I	3.13E-2	1.86E-2	1.02E-2	5.33E-3
SFDM-II	1.33E-2	3.22E-3	8.00E-4	2.00E-4
FOFDM	3.87E-3	9.56E-4	2.42E-4	6.04E-5

Table 2.4.4: Maximum absolute errors for $a = 1$, $K = 1$, $M = 3$, $P_r = 10$, $S_c = 3$, $d = 2$, $R = 2$.

Method	$n = 10$	$n = 20$	$n = 40$	$n = 80$
SFDM-I	6.28E-2	3.99E-2	2.29E-2	1.26E-2
SFDM-II	5.27E-2	1.09E-2	2.64E-3	6.56E-4
FOFDM	4.25E-3	1.08E-3	2.83E-4	1.08E-5

We observe that if the coefficient of θ' is small (i.e. $P_r < 10$) both methods are reliable. However, if the coefficient of θ' is relatively large (i.e. $P_r > 20$) then the FOFDM is distinctly the better method as evidenced by the relatively small maximum absolute error. We observe that the larger the Prandtl number the smaller the maximum absolute error. The existence of an analytical solution in the energy equation allows us to compare the SFDM and the FOFDM as we observe the closeness of each of the solution to the exact solution. Figure 2.4.1 further confirm that the FOFDM is the better method for relatively large values of the coefficient of θ'.

Figure 2.4.1(a) shows that for $P_r = 0.71, a = 1$ and $R = 0.01$ both methods are reliable as both solutions coincides with the exact solution. However, Figure 2.4.1(b) shows that when using the SFDM with the parameters, $P_r = 50, a = 1$ and $R = 0.01$,

the solution oscillates and is therefore unreliable whereas the FOFDM gives accurate solution.

From the results obtained from the tables and graphs we conclude that the FOFDM is very reliable method for solving the energy equation. The momentum and concentration equations are therefore solved simultaneously as a combined system.

Using the FOFDM on the temperature equation, we study the effects of the flow parameters such as radiation parameter (R), permeability parameter (K), suction parameter (a), magnetic parameter (M), chemical reaction parameter (d) and Prandtl number (P_r), on velocity, temperature and concentration profiles. The effects of these parameters on the flow field are shown graphically for velocity profiles in Figure 2.4.2, temperature profile in Figure 2.4.3 and concentration profiles in Figure 2.4.4.

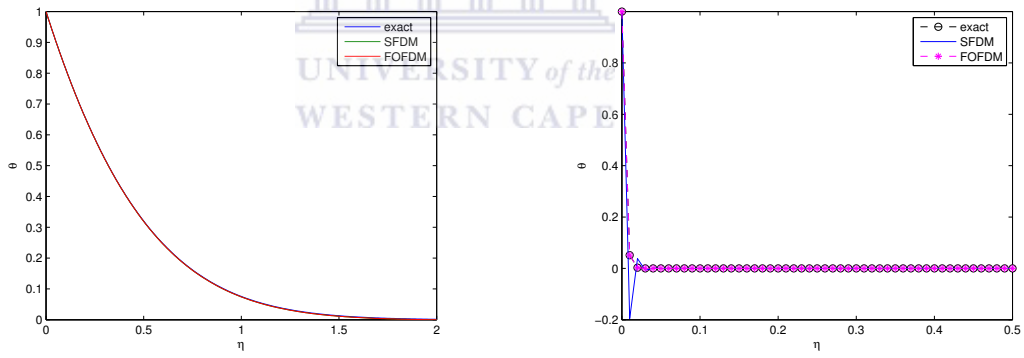

(a) Comparison of temperature values for $P_r = 0.71$, $a = 1$, $R = 0.01$, $n = 80$ which give small values for the coefficient of θ'.

(b) Comparison of temperature values for $P_r = 50$, $a = 3$, $R = 0.01$, $n = 80$ which give moderate values of the coefficient of θ'.

Figure 2.4.1: Comparison of temperature profiles for different combinations of parameters.

The effects of suction on velocity, temperature and concentration are depicted in Fig 2.4.2(a), Fig 2.4.3(a) and Fig 2.4.4(a), respectively. We note from these figures that the velocity, temperature, and concentration decrease with the increase of suction parameter confirming the fact that suction stabilizes the velocity, thermal and concentration layer growth.

The effect of the variation of chemical reaction parameter on velocity is shown in Fig 2.4.2(b). We observe that the velocity increases with decreasing chemical reaction

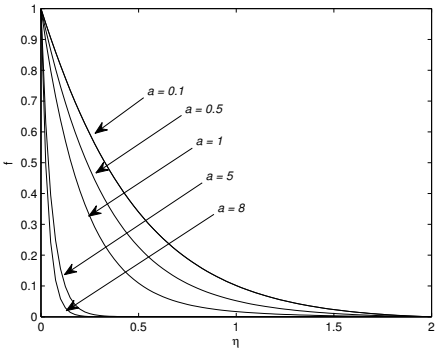

(a) Effect of suction on velocity with P_r = 50, $M = 1$, $K = 1$, $S_c = 0.22$, $G_r = 1$, G_c = 1,R =0.01, $d = 1$, $n = 80$.

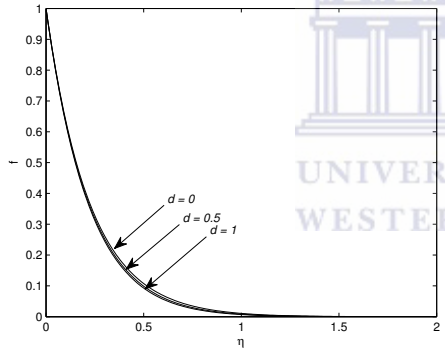

(b) Effect of chemical reaction parameter on velocity with $P_r = 50$, $M = 2$, $K = 1$, S_c = 0.22, $a = 2$, $n = 80$.

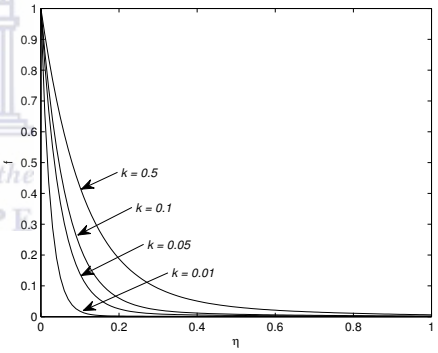

(c) Effect of permeability on velocity with P_r = 50, $M = 1$, $a = 2$, $S_c = 0.22$, $G_r = 2$, G_c = 5, R =0.01, $d = 1$, $n = 80$

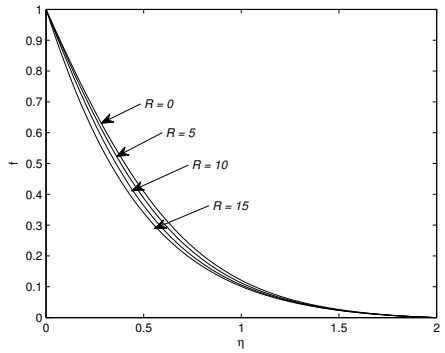

(d) Effect of thermal radiation parameter on Velocity with $P_r = 50$, $M = 2$, $K = 1$, a = 0.1, $S_c = 0.22$, $G_r = 3$, $G_c = 5$,$d = 1$, n = 80

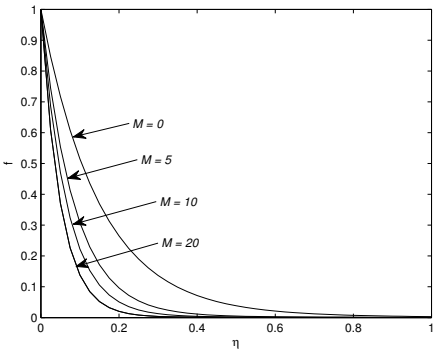

(e) Effect of magnetic parameter on velocity with P_r =50, $K = 1$, $a = 2$, $S_c = 0.22$, R =0.01, $d = 1$, $n = 80$.

Figure 2.4.2: Effects of different parameters on velocity.

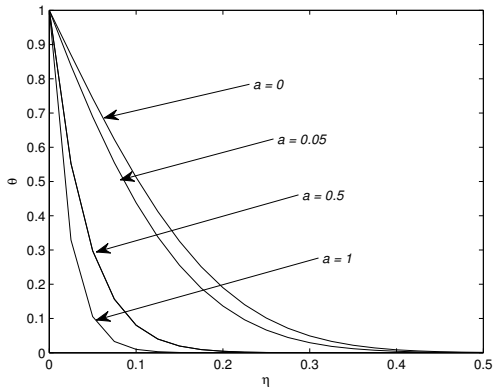

(a) Effect of suction on temperature with P_r = 50, R = 1, n = 80.

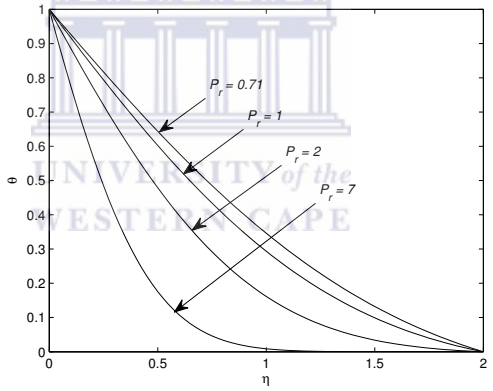

(b) Effect of P_r on temperature with a = 0.1, R = 1, n = 80.

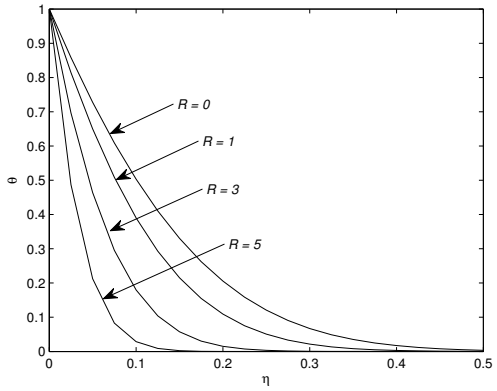

(c) Effect of thermal radiation parameter on temperature with P_r = 50, a = 2, n = 80.

Figure 2.4.3: Effects of different parameters on temperature.

parameter. The effect of the chemical reaction on concentration is depicted in Fig 2.4.4(b). We observe that the effect of chemical reaction on concentration is similar to its effect on velocity. However the effect of chemical reaction on concentration is more pronounced than its effect on velocity.

The effects of the permeability parameter (K) on velocity are displayed in Fig 2.4.2(c). From this figure we observe that velocity increases with increasing permeability.

From Fig 2.4.2(d) and Fig 2.4.3(c) we note that both velocity and temperature decrease with increase of thermal radiation parameter (R). Thus the thickness of the velocity and temperature boundary layer decrease with increasing radiation parameter (R).

Fig 2.4.2(e) shows the effect of magnetic parameter M on velocity. The presence of transverse magnetic field retards the velocity of flow field. The greater the magnetic field parameter the greater the reduction in the velocity of the flow field.

Fig 2.4.3(b) shows the effect of P_r on temperature. We observe that the temperature of the flow field decreases with increasing P_r. The greater the value of P_r the faster is the reduction of the plate temperature.

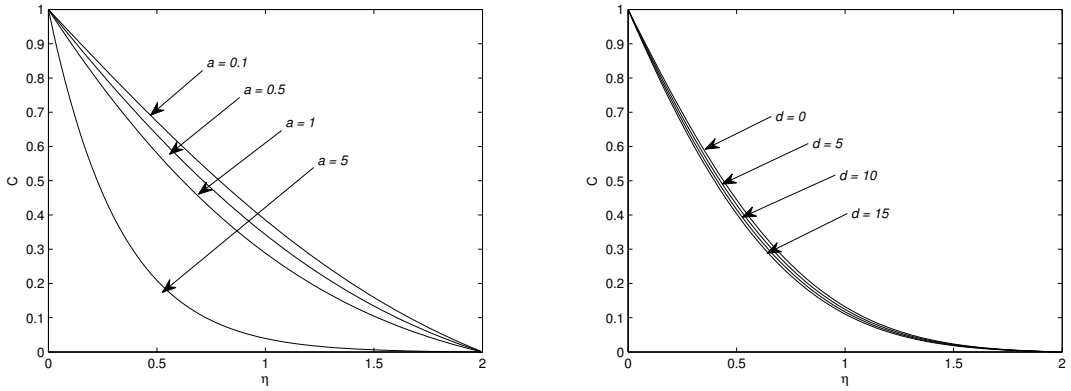

(a) Effect of suction on concentration $S_c = 0.22$, $M = 2$, $d = 0.1$, $n = 80$.

(b) Effect of chemical reaction parameter d on concentration with a= 0.1, $M = 2$, $P_r = 50$, R =0.01, $n = 80$.

Figure 2.4.4: Effects of different parameters on concentration.

In order to further assess the accuracy of this method we have compared our results, for the Nusselt number (N_u), with those of Das *et al.* [46] as shown in Table 2.4.5.

Table 2.4.5: Variation of heat flux (N_u) with suction for $P_r = 0.71$, $R = 0$.

	Das [46]	Our method
a	N_u=$\theta'(0)$	N_u=$\theta'(0)$
0.1	1.04299514	1.04299515
0.2	1.13865913	1.13865914
1	2.00275564	2.00275566
2	3.23732738	3.23732739

By letting $R = 0$, $K = 0$, $d = 0$, our problem reduces to that of Das *et al* [46]. Our result are in very good agreement with theirs. In addition, the velocity, temperature, and concentration profiles are also in agreement with those of Das [46]. In particular, our method and that of Das [46] are compared by considering the temperature profile depicted in Figure 2.4.5. The first few output values of the temperature for both methods are displayed in Table 2.4.6.

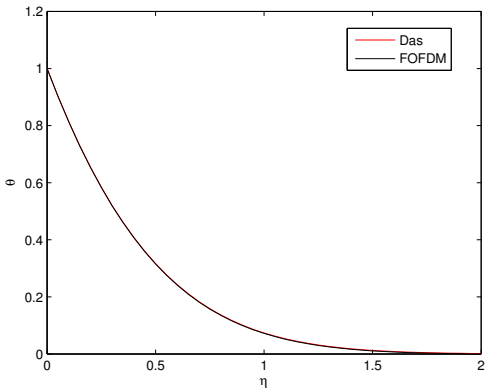

Figure 2.4.5: The temperature profile for $a = 1$, $M = 1$, $P_r = 0.71$, $R = 0$, $n = 40$ using our FOFDM and the method of Das [46].

Table 2.4.6: Temperature values for $a = 1$, $P_r = 0.71$, $R = 0$, $n = 40$

Das[46]	Our method
1.000	1.000
9.0339E-1	9.0322E-1
8.1372E-1	8.1340E-1
7.3078E-1	7.3032E-1
6.5435E-1	6.5376E-1

2.5 Summary

In this chapter we considered a mathematical model for unsteady MHD mixed convective mass transfer flow of a viscous incompressible electrically conducting fluid past an accelerated vertical infinite porous flat plate adjacent to a porous medium in the presence of a magnetic field and a chemical reaction with significant radiation effect with suction. The governing equations were transformed into a similarity form. The self-similar equations were solved numerically using a fitted operator finite difference method. We also noticed that the standard finite difference method fails to give reliable results for certain combinations of the key parameters.

Effects of the different parameters on velocity, temperature and concentration profiles are studied and the following conclusions are drawn

- Presence of radiation effects caused reduction in the velocity and temperature of the fluid.
- We noted that the increase in thermal radiation results in the reduction of the fluid velocity and fluid temperature.
- The presence of fluid wall suction led to the reduction in the velocity, temperature and concentration of the flow fluid. Suction thus stabilizes the velocity, temperature and concentration layer growth.
- Increase in permeability results in increased velocity of the fluid flow.
- Both fluid velocity and fluid concentration increases with decreasing chemical

reaction parameter.

- The presence of the magnetic field retards the velocity of the flow field.
- The greater the Prandtl number the faster the cooling of the plate.

Currently, we are extending our study to design FOFDM to simulate transient MHD flows as well as flows with soret effects and heat generation.

The next chapter treats a transient MHD free convective flow past an infinite vertical porous plate.

Chapter 3

A fitted numerical method to simulate a transient MHD free convective flow past an infinite vertical porous plate

In this chapter we analyze the solution of a transient MHD flow of viscous incompressible electrically conducting fluid past a vertical infinite porous plate in the presence of a transverse magnetic field using a fitted method. The governing partial differential equations that describe the problem stated above are transformed by a suitable similarity transformation resulting in a system of ordinary differential equations which are then solved using a fitted operator finite difference method (FOFDM) and results are compared with those obtained by using classical approaches. Using tools for numerical singular perturbation analysis, the method is analyzed for stability and convergence. We observe that for small values of the Prandtl number both the standard finite difference method (SFDM) and the FOFDM provide similar results but for relatively large values of the Prandtl number the SFDM fails to provide reliable numerical results. To confirm the theoretical estimates, we determine the velocity and temperature profiles via the proposed FOFDM. We noted that the transient temperature and transient velocity increases with time. The steady state temperature is reached faster with the

FOFDM than with the SFDM.

3.1 Introduction

Illingworth [72] was the first person to study the transient free convection flow of a viscous incompressible fluid past an infinite vertical plate. A few years later many papers were published on transient flow past an infinite plate (see Soundalgekar [158] and reference therein). Later Siegel [144] studied the transient free convection flow past a semi-infinite vertical plate using the momentum integral method. Thereafter Das [44]-[45] and Soundalgekar [152]-[158] studied the transient flow past an infinite plate whereas Hellums and Churchill [67] studied the same topic for flow past a semi-infinite plate.

Chamkha [28] analyzed the transient-free convection MHD boundary layer flow in a fluid-saturated porous medium channel. Beg *et al.* [18] considered the transient radiation-convection MHD flow past a vertical plate adjacent to a porous regime.

Singh [148] studied the effect of suction on the transient free convection flow past a vertical porous plate. Singh and Soundalgekar [149] investigated the transient free convection effect in cold water past an infinite vertical porous plate.

Chandrakala [31] used implicit finite-difference scheme to derive a solution to the transient natural convection flow of an incompressible viscous fluid past an impulsively started semi-infinite isothermal vertical plate with uniform mass flux in the presence of a magnetic field and homogenous chemical reaction of the first order.

We modify the work of Soundalgeker *et al.* [158] by introducing a transverse magnetic field and ignoring the effect of dissipative heat on the flow. For large values of the Prandtl number the energy equation reduces to a singular perturbation problem. The solution of singular perturbation problems is known to have large gradients when the coefficient of the highest derivative is very small. Boundary/interior layers develop which affect the convergence of the solution obtained using the usual standard numerical approach. It will be shown theoretically and numerically that the standard

finite difference method (SFDM) produces poor approximations when the perturbation parameter, ϵ becomes very small. For this reason we adopt the fitted operator finite difference method (FOFDM) which captures/mimics the behavior of the solution within the layer region. A vast amount of literature exists on singularly perturbed partial differential equations (see Beckett and Mackenzie [16], Kumar *et al.* [85], Patidar [121], Roos *et al.* [131], Miller *et al.* [96] and references therein.) To the best of our knowledge no work has been done to study transient free MHD viscous incompressible flows using the fitted operator finite difference method. Hence our current study is motivated.

The rest of the chapter is organized as follows. In Section 3.2 we describe the model of the problem. Section 3.3 focusses on numerical method and its analysis. Section 3.4 on the other hand deals with the presentation and discussion of the numerical results. Finally Section 3.5 gives concluding remarks.

3.2 Description of the model

We consider the unsteady free convective mass transfer flow of a viscous incompressible electrically conducting fluid past a vertical infinite porous flat plate in the presence of a transverse magnetic field. Let the x^*-axis be directed upward along the plate and the y^*-axis normal to the plate. Let u^* and v^* be the velocity components along x^* and y^* axes respectively. Then the magnetohydrodynamic unsteady free convective boundary layer equations under usual Boussinesq's approximation [158] read

$$\frac{\partial v^*}{\partial y^*} = 0, \tag{3.2.1}$$

$$\frac{\partial u^*}{\partial t^*} + v^*\frac{\partial u^*}{\partial y^*} = \nu\frac{\partial^2 u^*}{\partial y^{*2}} + g\beta(T^* - T^*_\infty) - \frac{\sigma {B_O}^2}{\rho}u^*, \tag{3.2.2}$$

$$\rho c_p\left[\frac{\partial T^*}{\partial t^*} + v^*\frac{\partial T^*}{\partial y^*}\right] = \kappa\frac{\partial^2 T^*}{\partial y^{*2}}, \tag{3.2.3}$$

where, ν is the kinematic viscosity, β is the volumetric coefficient of thermal expansion, ρ is the density, σ is the electrical conductivity of the fluid, g is the acceleration due to gravity, T^* is the temperature, T^*_∞ is the temperature of the fluid far away from the plate, c_p is the specific heat capacity, B_0 is the magnetic induction. From the continuity equation we deduce that the suction velocity $v(y) = -V_o$. The negative constant indicates that the suction is directed towards the plate. The necessary boundary conditions [158] are

$$\begin{aligned} t^* \leq 0,\ u^* = 0,\ T^* = T^*_\infty,\ \text{for all } y^*, \\ u^* = 0,\ T^* = T^*_w,\ \text{at } y^* = 0, \\ u^* = 0,\ T^* = T^*_\infty,\ \text{as } y^* \to \infty. \end{aligned} \tag{3.2.4}$$

We nondimensionalize (3.2.2) to (3.2.3) by introducing the following similarity variables

$$\begin{aligned} &u = u^*/u_0,\ \theta = (T^* - T^*_\infty)/(T^*_w - T^*_\infty),\ t = t^*/t_0, \\ &M = \sigma_0 B_o^2\ t_0/\rho,\ P_r = \mu c_p/k, \\ &\Delta T = T^*_w - T^*_\infty,\ V_o = v^*/u_o, \end{aligned} \tag{3.2.5}$$

with $u_0 = [\nu g\beta\Delta T]^{1/3}$, $L = [g\beta\Delta T/\nu^2]^{-1/3}$, $t_0 = [g\beta\Delta T]^{-2/3}/\nu^{-1/3}$, where M is the magnetic parameter, κ is the thermal conductivity, u_0 is the reference velocity, L is the reference length, t_0 is the reference time, V_o is the suction parameter. Using (3.2.4) and (3.2.5), equations (3.2.2)-(3.2.3) reduce to

$$\frac{\partial u}{\partial t} - V_o\frac{\partial u}{\partial y} = \frac{\partial^2 u}{\partial y^2} - Mu + \theta, \tag{3.2.6}$$

$$\frac{\partial \theta}{\partial t} - V_o\frac{\partial \theta}{\partial y} - \frac{1}{P_r}\frac{\partial^2 \theta}{\partial y^2} = 0. \tag{3.2.7}$$

The corresponding initial and boundary conditions [158] are

$$\begin{aligned} t \leq 0,\ u = 0,\ \theta = 0,\ \text{for all } y, \\ u = 0,\ \theta = 1,\ \text{at } y = 0, \\ u = 0,\ \theta = 0,\ \text{as } y \to \infty. \end{aligned} \tag{3.2.8}$$

3.3 Construction and analysis of the numerical method

We introduce the FOFDM to solve the energy equation (3.2.7). The FOFDM is compared with the standard finite difference method(SFDM). The energy equation is stated in the form

$$L\theta := \frac{\partial \theta}{\partial t} - V_o \frac{\partial \theta}{\partial y} - \frac{1}{P_r}\frac{\partial^2 \theta}{\partial y^2} = 0. \tag{3.3.1}$$

We will approximate the solution of the energy equation on a uniform mesh which we describe below.

Let N be a positive integer. Consider the following partition of the interval [0,4]:

$$y_0 = 0,\ y_i = y_0 + ih,\ i = 1(1)N,\ h = y_i - y_{i-1},\ y_N = 4.$$

Let τ be the uniform step size on

$$\Omega^{\tau,m} = \left\{ (y, t_j) : y \in \Omega, t_j = j\tau = \frac{j}{m},\ \forall\ 0 < j \leq m \right\}. \tag{3.3.2}$$

Denote the approximation of θ by the unknown ϖ. Performing the time semi-discretization by Euler method at time level n gives

$$\frac{\varpi^n - \varpi^{n-1}}{\tau} - V_o \varpi_y^n - \epsilon \varpi_{yy}^n = 0, \tag{3.3.3}$$

subject to

$$\varpi^n(0) = 1,\ 0 < n < m, \tag{3.3.4}$$

$$\varpi^n(4) = 0,\ 0 \leq n < m, \tag{3.3.5}$$

where $\epsilon = 1/P_r$. We rewrite (3.3) as

$$-\epsilon\varpi^n_{yy} - V_o\varpi^n_y + \frac{1}{\tau}\varpi^n = \frac{1}{\tau}\varpi^{n-1}. \tag{3.3.6}$$

For the sake of simplicity we omit the time level label "n" in (3.3.6). We are therefore concerned with the problem of finding $\varpi(y)$ such that

$$-\epsilon\varpi''(y) - V_o\varpi' - \frac{1}{\tau}\varpi(y) = \frac{1}{\tau}\varpi^*, \tag{3.3.7}$$

subject to

$$\varpi(0) = 1,\ \varpi(4) = 0, \tag{3.3.8}$$

where ϖ^* is the value of ϖ at the previous time level $n-1$.

The following lemma provides bounds on the solution of the problem (3.3.7)-(3.3.8).

Lemma 3.3.1. *Let ϖ be the solution of (3.3.7)- (3.3.8). Then for $0 \leq k \leq 4$,*

$$|\varpi^{(k)}(y)| \leq \widetilde{C}\left(1 + \epsilon^{-k}e^{-\lambda y/\epsilon}\right)$$

for all $y \in \overline{\Omega} = [0,4]$, where $0 < \epsilon \leq 1$, $\widetilde{C}$ is independent of ϵ, and $0 < \lambda < V_o$.

Proof. The inductive proof follows the idea of Miller *et al.* [96]. By using the maximum principle we are able to determine a bound on the solution $\varpi(y)$ of (3.3.7).

With reference to equation (3.3.7) we use the maximum principle to show that the solution $\varpi(y)$ of (3.3.7) is bounded. In a more general form we define the differential

operator L in (3.3.7) for all $\phi \in C^4\overline{\Omega}$ by

$$L\phi(y) = -\epsilon\phi''(y) - a(y)\phi(y) + b(y)\phi(y) = f(y) \tag{3.3.9}$$

Our particular case has $a = V_o$, $b = 1/\tau$ and $f = 1/\tau\phi^*$ where ϕ^* is the privious time level value of ϕ. Now we consider the function

$$\phi^{\pm}(y) = \widetilde{C}(4 - y) \pm \varpi(y).$$

It follows that

$$\phi^{\pm}(0) \geq 0,\ \phi^{\pm}(4) \geq 0,$$

and

$$\begin{aligned} L\phi^{\pm}(y) &= \pm\epsilon\varpi''(y) - a(y)(\pm\varpi)'(y) + (y)\varpi(y) + a(y)\widetilde{C}, & (3.3.10)\\ &= \pm L\varpi(y) + a(y)\widetilde{C} \geq 0. & (3.3.11) \end{aligned}$$

Then by the maximum principle

$$|\varpi(y)| \leq \widetilde{C}(4 - y) \leq 4\widetilde{C} \text{ for all } y \in \overline{\Omega}.$$

To obtain the estimate of the derivative of ϖ we differentiate k times the equation $L\varpi = f$ and obtain $L\varpi^{(k)} = f_k$ where $1 \leq k \leq 4$, where

$$f_k = f^{(k)} - \Sigma_{r=0}^{k-1} \binom{n}{r} a^{(k-r)}\varpi^{(r+1)}$$

and $f_0 = f$. It is clear that f_k depends on the derivatives of ϖ and the coefficient a. We assume that the following estimates hold

$$|\varpi^{(i)}(y)| \leq \widetilde{C}\left(1 + \epsilon^{-i}e^{-\lambda y/\epsilon}\right), \tag{3.3.12}$$

$\forall\ 0 \leq i \leq k$, $\forall\ y \in \overline{\Omega}$, and $L\varpi^{(k)} = f_k$ where

$$|\varpi^{(k)}(y)| \leq \widetilde{C}\left(1 + \epsilon^{-k}e^{-\lambda y/\epsilon}\right), \tag{3.3.13}$$

and

$$|f_k(y)| \leq \widetilde{C}\left(1 + \epsilon^{-k}e^{-\lambda y/\epsilon}\right). \tag{3.3.14}$$

At the end points

$$|\varpi^{(k)}(0)| \leq \widetilde{C}\left(1 + \epsilon^{-k}\right) \leq \widetilde{C}\epsilon^{-(k-1)}, \tag{3.3.15}$$

and

$$|\varpi^{k}(4)| \leq \widetilde{C}\left(1 + \epsilon^{-k}e^{-4\lambda/\epsilon}\right) \leq \widetilde{C}\epsilon^{-k}. \tag{3.3.16}$$

Let

$$\varsigma_k(y) = \epsilon^{-1}\int_0^y f_k(t)e^{-(H(y)-H(t))/\epsilon}dt, \tag{3.3.17}$$

where

$$H(y) = \int_0^y a(s)ds.$$

The particular solution of the equation $L\varpi^{(k)} = f_k$ is given by

$$\varpi_p^{(k)}(y) = -\int_0^y \varsigma_k(t)dt. \tag{3.3.18}$$

The general solution , $\varpi^{(k)}$ is written in the form $\varpi^{(k)} = \varpi_p^{(k)} + \varpi_h^{(k)}$ where $\varpi_h^{(k)}$ is the homogenous solution. The derivative $\varpi^{(k)}$ satisfies

$$L\varpi_h^{(k)} = 0,\ \varpi_h^{(k)}(0) = \varpi^{(k)}(0),\ \varpi_h^{(k)}(4) = \varpi^{(k)}(4) - \varpi_p^{(k)}(4). \tag{3.3.19}$$

Let the function

$$\psi(y) = \frac{\int_0^y e^{-H(t)/\epsilon}dt}{\int_0^4 e^{-H(t)/\epsilon}dt},$$

then

$$L^{h,\tau}\psi = 0, \quad \psi(0) = 1, \quad \psi(4) = 0, \quad 0 \leq \psi(y) \leq 1.$$

Now $\varpi_h^{(k)}$ is given by

$$\varpi_h^{(k)}(y) = \left(\varpi^{(k)}(0)\right)\psi(y) + \left(\varpi^{(k)}(4) - \varpi_p^{(k)}(4)\right)(1 - \psi(y)). \tag{3.3.20}$$

Differentiating (3.3.20) with respect to y gives

$$\varpi^{(k+1)}(y) = \left(\varpi^{(k)}(0)\right)\psi' - \left(\varpi^{(k)}(4) - \varpi_p^{(k)}(4)\right)\psi'. \tag{3.3.21}$$

From (3.3.18) $\varpi_p^{(k+1)}(y) = \varsigma_k$. It follows that

$$\begin{aligned} \varpi^{(k+1)}(y) &= \varpi_p^{(k+1)}(y) + \varpi_h^{(k+1)}(y), \\ &= \varsigma_k + \varpi_k(0)\psi' - \left(\varpi^{(k)}(4) - \varpi_p^{(k)}(4)\right)\psi', \\ &= \varsigma_k + \left(\varpi^{(k)}(0) - \varpi^{(k)}(4) + \varpi_p^{(k)}(4)\right)\psi'. \end{aligned} \tag{3.3.22}$$

Now

$$\psi' = \frac{-e^{H(y)/\epsilon}}{\int_0^4 e^{-H(t)/\epsilon}dt}.$$

Therefore, we get

$$|\psi'(y)| \leq |ae^{-\lambda y}| \leq \epsilon^{-1}\widetilde{C}e^{-\lambda y/\epsilon}. \tag{3.3.23}$$

Since $\lambda \leq a$, we have

$$\begin{aligned} |\varsigma_k(y)| &\leq \epsilon^{-1}\widetilde{C}\int_0^y \left(1 + \epsilon^{-k}e^{-\lambda t/\epsilon}\right)e^{-\lambda(y-t)/\epsilon}dt, \\ &\leq \widetilde{C}\left(1 + \epsilon^{-(k+1)}e^{-\lambda y/\epsilon}\right). \end{aligned} \tag{3.3.24}$$

Since

$$\varpi_k^{(k)}(4) = -\int_0^4 \varsigma_k(t)dt, \tag{3.3.25}$$

$$\begin{aligned} |\varpi_p^{(k)}(4)| &\leq \widetilde{C}\left(1+\epsilon^{-(k+1)}\right), \\ &\leq \widetilde{C}\left(1+\epsilon^{-k}\right), \\ &\leq \widetilde{C}\epsilon^{-k}. \end{aligned} \tag{3.3.26}$$

We know that

$$|\varpi^{(k+1)}| \leq \left(|\varsigma_k| + |\varpi^{(k)}(0)| + |\varpi^{(k)}(4)| + |\varpi_p^{(k)}(4)|\right)\psi', \tag{3.3.27}$$

therefore,

$$|\varpi^{(k+1)}| \leq \widetilde{C}\left(1+\epsilon^{-(k+1)}e^{-\lambda y/\epsilon}\right) + \left(\widetilde{C}\epsilon^{-(k-1)} + \widetilde{C}\epsilon^{-k} + \widetilde{C}\epsilon^{-k}\right)\epsilon^{-1}e^{-\lambda y/\epsilon}. \tag{3.3.28}$$

This reduces to

$$|\varpi^{(k+1)}| \leq \widetilde{C}\left(1+\epsilon^{-(k+1)}e^{-\lambda y/\epsilon}\right), \tag{3.3.29}$$

which completes the proof.

Next we discretize (3.3.7) in space using the standard finite difference method:

$$\mathcal{L}^{h,\tau}\widetilde{\nu}_j \equiv -\epsilon\frac{\widetilde{\nu}_{j+1} - 2\widetilde{\nu}_j + \widetilde{\nu}_{j-1}}{h^2} - V_o\frac{\widetilde{\nu}_{j+1} - \widetilde{\nu}_j}{h} + \frac{1}{\tau}\widetilde{\nu}_j = \frac{1}{\tau}\widetilde{\nu}_j^*, \tag{3.3.30}$$

where $\widetilde{\nu}$ is the approximation of ϖ and $\widetilde{\nu}^*$ is the previous time level value of $\widetilde{\nu}$. We will show later that for relatively small values of ϵ, the SFDM fails to provide fairly accurate approximation of the true solution by comparing the maximum absolute errors calculated. To obtain reliable results we discretize (3.3.7) as follows,

$$L^{h,\tau}u_j \equiv -\epsilon\frac{u_{j+1} - 2u_j + u_{j-1}}{\psi_j^2} - V_o\frac{u_{j+1} - u_j}{h} + \frac{1}{\tau}u_j = \frac{1}{\tau}u_j^*, \tag{3.3.31}$$

and

$$\psi_j^2 = \frac{\epsilon h\left(\exp\left(\frac{V_o h}{\epsilon}\right) - 1\right)}{V_o}, \tag{3.3.32}$$

where u is the numerical approximation of ϖ and u^* is value of ϖ at the previous time level.

The function ψ_j^2 captures the behavior of the solution in the boundary layer region. The layer region is located in the neighborhood of the vertical plate near the left end of the interval. Prior to the numerical simulation of the transient MHD free convective flow we analyse the FOFDM for stability and convergence.

Analysis of the numerical method

The local truncation error of the time semi-discritization by the forward implicit Euler scheme is denoted by $\tilde{e_n} = \theta(y, t_n) - \varpi(y)$, where $\varpi(y)$ is the solution of (3.3.7). The amount of error $\tilde{e_n}$ is the contribution of each time step to the global error of the time semi-discretizaton. The following lemmas depict the order of the local and global error related to the problem (3.3.7).

Lemma 3.3.2. (Local error estimate) *If* $|\varpi^{(k)}(y)| \leq \widetilde{C},\ y \in [0,4],\ 0 \leq k \leq 2$, *then the local error estimate is given by* $||\widetilde{e_n}|| \leq \widetilde{C}\tau^2$.

The following lemma relates to the global error, E_n.

Lemma 3.3.3. (Global error estimate) *The global error* $E_n = \Sigma_{n=0}^{m}\widetilde{e_n}$ *satisfies*

$$||E_n|| \leq \widetilde{C}\tau,\ \forall\ 1 \leq n \leq m.$$

Proof. Taking into account Lemma 3.3.2, we get the global error estimate at the

$(n+1)^{th}$ time step,

$$\begin{aligned} ||E_n||_\infty &\leq ||\Sigma_{i=1}^{n}\widetilde{e}_i|| \\ &\leq \widetilde{C}n\tau^2, \\ &\leq \widetilde{C}m\tau^2 \text{ (since } n \leq m), \\ &= \widetilde{C}\tau. \end{aligned} \tag{3.3.33}$$

since $m = 1/\tau$. Thus the global error of the time semi-discretization is of the first order, that is, $||\theta - \varpi|| \leq \widetilde{C}\tau$.

We discretize with respect to space and find the local truncation error $|(\varpi - u)|$ where ϖ is the exact solution with respect to space and u is the approximation of θ for the FOFDM. The following lemmas are pivotal in the analysis of the error of the solution obtained using the FOFDM.

From equation (3.3.31) the differential operator $L^{h,\tau}$ in (3.3.31) satisfies the following discrete maximum principle on Ω,

Lemma 3.3.4. (Discrete maximum principle) *Assume that the mesh function ϕ_i satisfies $\phi_0 \geq 0$ and $\phi_n \geq 0$. Then, $L\phi_i \geq$ for $i = 1(1)n-1$, which implies that $\phi_i \geq 0$ $\forall i$ $= 0(1)n$.*

Proof. The proof follows the same lines as the proof of the discrete maximum principle in [96] as shown below. Choose k such that $\phi_k = \min_i \phi_i$ and suppose that $\phi_k < 0$. Then $k \notin \{0, n\}$, $\phi_{k+1} - \phi_k \geq 0$ and $\phi_k - \phi_{k-1} \leq 0$. Thus

$$L^{h,\tau}\phi_k = -\frac{\epsilon}{\psi_k^2}\left[\phi_{k+1} - 2\phi_k + \phi_{k+1}\right] - \frac{V_o}{h}\left[\phi_{k+1} - \phi_k\right] + \frac{1}{\tau}\phi_k, \tag{3.3.34}$$

$$= -\frac{\epsilon}{\psi_k^2}\left[\phi_{k+1} - \phi_k + \phi_{k-1} - \phi_k\right] - \frac{V_o}{h}\left[\phi_{k+1} - \phi_k\right] + \frac{1}{\tau}\phi_k \tag{3.3.35}$$

$$< 0,$$

which is a contradiction. It follows that

$$\phi_k \geq 0 \text{ and so } \phi_i \geq 0 \ \forall i,\ i = 1(1)n.$$

The following Lemma is a consequence of the discrete maximum principle (Lemma 3.3.4).

Lemma 3.3.5. (Uniform stability estimate) *If ξ_i is any mesh function such that $\xi_0 = \xi_n = 0$ then $|\xi_i| \leq \frac{4}{\lambda} \max_{1\leq j\leq n-1} \left|L^{h,\tau}\xi_j\right|$ for $0 \leq i \leq n,\ 0 < \lambda \leq a_i$.*

Proof. Let

$$\widetilde{C} = \frac{1}{\lambda} \max_{1\leq j\leq n-1} \left|L^{h,\tau}\xi_j\right|,$$

and introduce the mesh functions $\vartheta_i^+, \vartheta_i^-$ such that $\vartheta_i^{\pm} = \widetilde{C}(4 - y_i) \pm \xi_i$.

From equation (3.3.31)

$$\begin{aligned} L^{h,\tau}\vartheta_i^{\pm} &= -\epsilon\frac{\vartheta_{i+1}^{\pm} - 2\vartheta_i^{\pm} + \vartheta_{i-1}^{\pm}}{\psi_i^2} - a_i\frac{\vartheta_{i+1}^{\pm} - \vartheta_i^{\pm}}{h} + b_i\vartheta_i^{\pm}, \\ &= -\epsilon\frac{\pm\xi_{i+1} \mp 2\xi_i \pm \xi_{i-1}}{\psi_i^2} - a_i\frac{(\pm\xi_{i+1} \mp \xi_i)}{h} + b_i(\pm\xi_i) + \widetilde{C}a_i, \\ &= \pm L^{h,\tau}\xi_i + \widetilde{C}a_i + b_i\widetilde{C}(4 - y_i), \\ &= \pm L^{h,\tau}\xi_i + \frac{a_i + b_i(4 - yi)}{\lambda} \max_{\Omega} \left|L^{h,\tau}\xi_i\right| \qquad (3.3.36) \\ &\geq 0, \end{aligned}$$

since $a_i/\lambda \geq 1$ and $y_i \leq 4$.

From the discrete maximum principle we have

$$\vartheta_i^{\pm} \geq 0 \text{ for } 0 \leq i \leq n,$$

and therefore

$$\vartheta_i^{\pm} = \widetilde{C}(4 - y_i) \pm \xi_i \geq 0 \text{ for } 0 \leq y_i \leq 4,$$

implies

$$|\xi_i| \leq \widetilde{C}(4 - y_i).$$

Since $4 - y_i \leq 4$,

$$|\xi_i| \leq \frac{4}{\lambda} \max_{1 \leq j \leq n-1} \left| L^{h,\tau} \xi_j \right|,$$

which completes the proof.

Next we establish the local truncation errors of the SFDM and the FOFDM. In the analysis of these errors, $\widetilde{M}$ and $\widetilde{B}$ denote positive constants, independent of h and ϵ which may assume different values in different inequalities and equations.

The local truncation error of the SFDM (3.3.30) is given by

$$\begin{aligned} \left| L^{h,\tau}(\theta - \widetilde{\nu})_j \right| &= \left| L^{h,\tau}(\theta - \varpi + \varpi - \widetilde{\nu})_j \right|, \\ &= \left| L^{h,\tau}(\theta - \varpi)_j \right| + \left| L^{h,\tau}(\varpi - \widetilde{\nu})_j \right|. \end{aligned} \tag{3.3.37}$$

From Lemma 3.3.3

$$\left| L^{h,\tau}(\theta - \widetilde{\nu})_j \right| = \widetilde{M}\tau. \tag{3.3.38}$$

Now the truncation error for the spatial descretization of the SFDM is given by

$$\begin{aligned} \left[L^{h,\tau}(\varpi - \widetilde{\nu})_j \right] &= -\epsilon \varpi_j'' - V_o \varpi_j' + \frac{1}{\tau}\varpi_j \\ &\quad - \left(-\epsilon \frac{\varpi_{j+1} - 2\varpi_j + \varpi_{j-1}}{h^2} - V_o \frac{\varpi_{j+1} - \varpi_j}{h} + \frac{1}{\tau}\varpi_j \right), \\ &= -\epsilon \varpi_j'' - V_o \varpi_j' + \frac{\epsilon}{h^2}\left[h^2 \varpi_j'' + \frac{h^4}{12}\varpi^{(iv)}(\zeta_1) \right] \\ &\quad + \frac{V_o h}{2}\left(\frac{\varpi_j''}{h} + \frac{h}{3}\varpi_j''' + \frac{h^2}{12}\varpi^{(iv)}(\zeta_2) \right), \\ &= \frac{V_o}{2}\varpi_j'' h + \left(\frac{\epsilon}{12}\varpi^{(iv)}(\zeta_1) + \frac{V_o}{6}\varpi''' \right) h^2 + O(h^5). \end{aligned} \tag{3.3.39}$$

where $\zeta_1 \in (y_{j-1}, y_{j+1})$ and $\zeta_2 \in (y_j, y_{j+1})$. Now

$$\begin{aligned} \left|L^{h,\tau}(\varpi - \widetilde{\nu})_j\right| &= \left|\frac{V_o}{2}\varpi_j'' h + \left(\frac{\epsilon}{12}\varpi^{(iv)}(\zeta_1) + \frac{V_o}{6}\varpi_j'''\right) h^2\right|, \\ &\leq \left|\frac{V_o}{2}\varpi_j''\right| h + \left|\left(\frac{\epsilon}{12}\varpi^{(iv)}(\zeta_1) + \frac{V_o}{6}\varpi'''\right)\right| h^2. \end{aligned}$$

Using Lemma 3.3.1 we obtain

$$\begin{aligned} \left|L^{h,\tau}(\varpi - \widetilde{\nu})_j\right| &\leq \frac{\widetilde{C}V_o}{2}\left(1 + \epsilon^{-2}e^{-\lambda y/\epsilon}\right) h + \frac{\widetilde{C}\epsilon}{12}\left(1 + \epsilon^{-4}e^{-\lambda y/\epsilon}\right) h^2 \\ &\quad + \frac{V_o\widetilde{C}}{6}\left(1 + \epsilon^{-3}e^{-\lambda y/\epsilon}\right) h^2. \end{aligned}$$

Using Lemma 7 in [103] yields

$$\begin{aligned} \left|L^{h,\tau}(\varpi - \widetilde{\nu})_j\right| &\leq \frac{\widetilde{C}V_o}{2} h + \left(\frac{\widetilde{C}}{12} + \frac{V_o\widetilde{C}}{6}\right) h^2, \\ &\leq \widetilde{M}h. \end{aligned}$$

Then by Lemma 3.3.1 and Lemma 3.3.5 we have

$$\begin{aligned} \max_{0\leq i\leq n} |(\varpi - \widetilde{\nu})_i| &\leq \max_{1\leq j\leq n-1} \left|L^{h,\tau}(\varpi - \widetilde{\nu})_j\right|, \\ &\leq \widetilde{M}h. \end{aligned} \tag{3.3.40}$$

From equations (3.3.38) and (3.3.40) the local truncation error of SFDM is given by

$$\begin{aligned} \left|L^{h,\tau}(\theta - \widetilde{\nu})_j\right| &= \left|L^{h,\tau}(\theta - \varpi + \varpi - \widetilde{\nu}_j\right|, \\ &\leq \left|L^{h,\tau}(\theta - \varpi)_j\right| + \left|L^{h,\tau}(\varpi - \widetilde{\nu})_j\right)|, \\ &\leq \widetilde{M}\left(\tau + h\right). \end{aligned} \tag{3.3.41}$$

Then using Lemma 3.3.5 to estimate the bounds on $|(\theta - \widetilde{\nu})|$, we get

$$\max_{0\leq i\leq n} |(\theta - \widetilde{\nu})_i| \leq \max_{1\leq j\leq n-1} \left|L^{h,\tau}(\theta - \widetilde{\nu})_j\right| \leq \widetilde{M}(\tau + h). \tag{3.3.42}$$

Similarly the local truncation error of the FOFDM (3.3.31) is given by

$$\left|L^{h,\tau}(\theta - u)_j\right| = \left|L^{h,\tau}(\theta - \varpi + \varpi - u)_j\right| = \left|L^{h,\tau}(\theta - \varpi)_j\right| + \left|L^{h,\tau}(\varpi - u)_j\right| . \tag{3.3.43}$$

From Lemma 3.3.3

$$\left|L^{h,\tau}(\theta - \varpi)_j\right| = \widetilde{B}\tau. \tag{3.3.44}$$

Now the truncation error for the spatial descretization is given by

$$\begin{aligned}
\left[L^{h,\tau}(\varpi - u)_j\right] &= -\epsilon\varpi_j'' - V_o\varpi_j' + \frac{1}{\tau}\varpi_j \\
&\quad - \left(-\epsilon\frac{\varpi_{j+1} - 2\varpi_j + \varpi_{j-1}}{\psi_j^2} - V_o\frac{\varpi_{j+1} - \varpi_j}{h} + \frac{1}{\tau}\varpi_j\right), \\
&= -\epsilon\varpi_j'' - V_o\varpi_j' + \frac{\epsilon}{\psi_j^2}\left[h^2\varpi_j'', + \frac{h^4}{12}\varpi^{(iv)}(\zeta_1)\right] \\
&\quad + \frac{V_o h}{2}\left(\frac{2\varpi_j'}{h} + \varpi_j'' + \frac{h}{3}\varpi_j''' + \frac{h^2}{12}\varpi^{(iv)}(\zeta_2)\right),
\end{aligned} \tag{3.3.45}$$

where $\zeta_1 \in (y_{j-1}, y_{j+1})$ and $\zeta_2 \in (y_j, y_{j+1})$. Using the Taylor series expansion, we have

$$\frac{\epsilon}{\psi_j^2} = \frac{\epsilon}{h^2} - \frac{V_o}{2h} + \ldots. \tag{3.3.46}$$

This implies that

$$\begin{aligned}
L^{h,\tau}(\varpi - u)_j &= -\epsilon\varpi_j'' \\
&\quad + \left[\frac{\epsilon}{h^2} - \frac{V_o}{2h} + \ldots\right]\left[h^2\varpi_j'' + \frac{\varpi^{(iv)}(\zeta_1)}{12}h^4\right] \\
&\quad + \frac{V_o}{2}\left(h\varpi_j'' + a\frac{h^2}{3}\varpi_j''' + \frac{\varpi^{(iv)}(\zeta_2)}{12}h^3\right).
\end{aligned} \tag{3.3.47}$$

Further simplifications lead to

$$L^{h,\tau}(\varpi-u)_j \;=\; \left(\frac{\epsilon\varpi^{(iv)}(\zeta_1)}{12}+\frac{V_o}{6}\varpi_j'''\right)h^2-\left(\frac{V_o\varpi^{(iv)}(\zeta_1)}{24}\right)h^3+O(h^5). \quad (3.3.48)$$

Using Lemma 3.3.1 we obtain

$$\left|L^{h,\tau}(\varpi-u)_j\right| \;\leq\; \left|\frac{\widetilde{C}\epsilon}{12}\left(1+\epsilon^{-4}e^{-\lambda y/\epsilon}\right)+\frac{\widetilde{C}V_o}{6}\left(1+\epsilon^{-3}e^{-\lambda y/\epsilon}\right)\right|h^2+O(h^5).$$

Now applying Lemma 7 in [103] yields

$$\begin{aligned}\left|L^{h,\tau}(\varpi-u)_j\right| &\leq \widetilde{C}\left(\frac{\epsilon h^2}{12}+\frac{V_o h^2}{6}\right)+O(h^5),\\ &\leq \widetilde{B}h^2,\end{aligned} \quad (3.3.49)$$

since $\epsilon h^2 < h^2$. Then by Lemma 3.3.1 and 3.3.5 we have

$$\begin{aligned}\max_{0\leq i\leq n}\left|(\varpi-u)_i\right|, &\leq \max_{1\leq j\leq n-1}\left|L^{h,\tau}(\varpi-u)_j\right|,\\ &\leq \widetilde{B}h^2.\end{aligned} \quad (3.3.50)$$

From equations (3.3.44) and (3.3.50) the local truncation error of FOFDM is given by

$$\begin{aligned}\left|L^{h,\tau}(\theta-u)_j\right| &= \left|L^{h,\tau}(\theta-\varpi+\varpi-u)_j\right|,\\ &\leq \left|L^{h,\tau}(\theta-\varpi)_j\right|+\left|L^{h,\tau}(\varpi-u_j)\right|,\\ &\leq \widetilde{B}\left(\tau+h^2\right).\end{aligned} \quad (3.3.51)$$

Then using Lemma 3.3.5 to estimate the bounds on $|(\theta-u)|$, we get

$$\max_{0\leq i\leq n}\left|(\theta-u)_i\right| \;\leq\; \max_{1\leq j\leq n-1}\left|L^{h,\tau}(\theta-u)_j\right|\leq\widetilde{B}\left(\tau+h^2\right).$$

We therefore establish that

$$\max_{0\leq i\leq n}|(\theta-u)_i|\leq \widetilde{B}\left(\tau+h^2\right). \tag{3.3.52}$$

3.4 Results and discussions

In this section we present and discuss numerical results. Since the exact solution is not available the pointwise errors are estimated using the double mesh principle, that is

$$e^{\Delta t,N}(y,t)=|u^N(y,t)-u^{2N}(y,t)|, \tag{3.4.1}$$

where N is the spatial discretization parameter and Δt is the time discretization parameter. The maximum absolute errors are given by

$$E^{N,\Delta t}=\max_N e^{\Delta t,N}(y,t), \tag{3.4.2}$$

and the rates of convergence are computed using the formula [85]

$$r_N=\frac{\log(E^{N,\Delta t}/E^{2N,\Delta t/4})}{\log 2}. \tag{3.4.3}$$

Equation (3.2.7) is solved using the SFDM and the FOFDM. It is observed that the maximum absolute errors of the fitted method is smaller than that of the standard method. This is depicted in Table 3.4.1. For a fixed value of ϵ the maximum absolute error decreases as the number of grid points, N increases. Results in Table 3.4.1 confirm our theoetical estimates stated in (3.3.42) and (3.3.52). From the results obtained from the tables it is evident that the maximum absolute errors and order of convergence of the fitted method are smaller and larger than that of the standard method. Since the value of P_r can assume large values in this paper we use the FOFDM to analyze the temperature and velocity profiles of the transient MHD free convective flow past an infinite vertical porous plate.

If the values of temperature and velocity at a time $t = t_n$ is known then the values of temperature and velocity at subsequent time levels is calculated as follows. We substitute $j = 1, 2, 3, 4, \ldots n-1$ in equation (3.3.31) which results in a tri-diagonal system of equations in unknown θ and is solved using the direct approach or the Thomas algorithm. Once θ is known at all values of y at the current time level ($t = t_n$), we then calculate the velocity, u from equation (3.2.6) using the same procedure as for temperature. The procedure is followed to obtain solution till desired time t.

The steady state value of time, t is the time such that values of temperature or velocity no longer changes. The limiting value of temperature or velocity is termed the steady state temperature or the steady state velocity respectively. The steady state temperatures for different values of the Prandtl number are shown in Figure 3.4.1(a). We observe that the time taken to reach the steady state temperature is less for FOFDM than for SFDM. We also notice from calculations and Figure 3.4.1(a) that the steady state temperatures obtained using FOFDM are less than for SFDM.

Figure 3.4.1(b) depicts the transient temperature variation with time. It also displays the effect of P_r on the transient temperature. We notice that if P_r and V_o are kept constant the transient temperature increases with time. We also show that if V_o and t are kept constant the transient temperature decreases with increasing P_r. From Figure 3.4.1(c) we observe that the transient temperature decreases with increasing value of the suction parameter V_o. Figure 3.4.2(a) depicts the effect of time, suction parameter and Prandtl number on transient velocity. We observe that the transient velocity increases with time. We also notice that transient velocity decreases with increasing value of either the Prandtl number or the suction parameter. Figure 3.4.2(b) on the other hand shows that the presence of a transverse magnetic field retards the velocity of the flow field.

3.5 Summary

We considered the unsteady free convective mass transfer flow of viscous incompressible electrically conducting fluid past a vertical infinite porous plate in the presence of a transverse

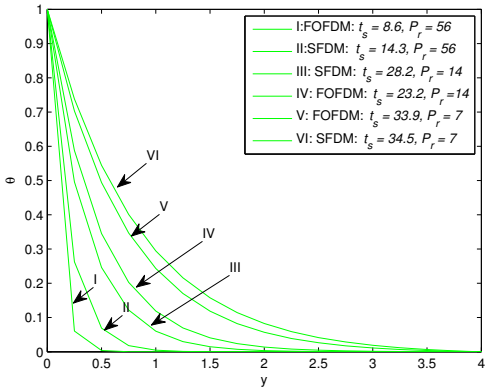

(a) Steady state temperatures for different values of the Prandtl numbers with $N = 16$.

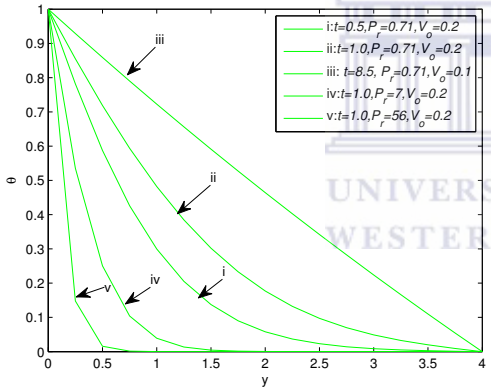

(b) The effect of P_r and t on the transient temperature profile with $N = 16$.

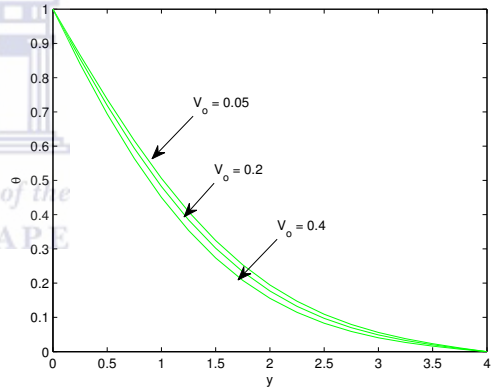

(c) The effect of V_o on the transient temperature profiles with $N = 16$.

Figure 3.4.1: Temperature profiles for $N = 16$.

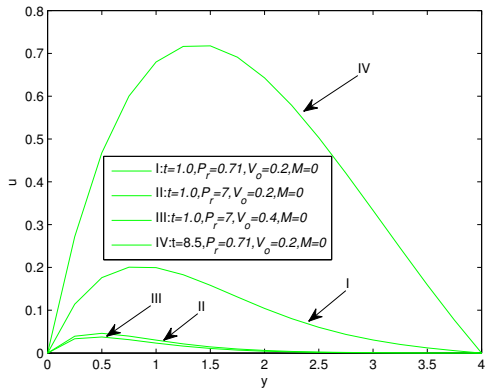

(a) The effect of P_r, V_o, and t on transient velocity with $N = 16$.

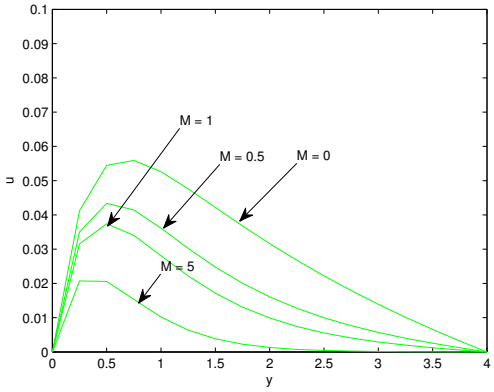

(b) The effect of M on transient velocity for $P_r = 25, V_o = 0.2$ and $N = 16$.

Figure 3.4.2: Velocity profiles for $N = 16$.

Table 3.4.1: Maximum absolute errors and orders of convergence associated with SFDM and FOFDM for $V_o = 0.2$ and $\tau = 0.1$.

P_r	N	10	20	40	80
	Δt	0.1	0.1/4	$0.1/4^2$	$0.1/4^3$
	SFDM	3.17E-2	3.13E-2	3.11E-2	3.10E-2
	r_N	0.02	0.01	0.01	
5	FOFDM	1.00E-2	2.70E-3	6.85E-4	1.71E-4
	r_N	1.88	1.98	2.00	
	SFDM	3.78E-2	3.71E-2	3.66E-2	3.64E-2
	r_N	0.03	0.02	0.01	
10	FOFDM	5.30E-3	3.30E-3	8.02E-4	2.07E-4
	r_N	0.68	2.04	1.95	
	SFDM	4.72E-2	4.14E-2	4.01E-2	3.97E-2
	r_N	0.19	0.05	0.01	
20	FOFDM	5.20E-3	4.10E-3	1.10E-3	2.85E-4
	r_N	0.34	1.90	1.95	
	SFDM	4.93E-2	5.49E-2	4.31E-2	4.18E-2
	r_N	-	0.35	0.04	
40	FOFDM	3.10E-3	2.00E-3	1.80E-3	4.43E-4
	r_N	0.63	0.20	2.02	

magnetic field. The governing equations were non-dimensionalized by introducing similarity variables and then solved numerically using the standard finite difference method and the fitted operator finite difference method. For small values of the Prandtl number both methods were applicable. However as the value of P_r became increasingly bigger the fitted operator method became clearly the better choice by taking into account the maximum absolute errors. We used the fitted operator finite difference to analyze the temperature and velocity profiles as parameters such as γ, P_r and M vary. The effect of the different parameters on the transient velocity and transient temperature are summarized as follows.

- The steady state temperature obtained using the fitted operator finite difference method is lower than that obtained when the standard finite difference method is used.
- The time taken for the temperature to reach steady state is less when the fitted operator finite difference method is used than when the standard finite difference method is used.
- The transient temperature and transient velocity increases with time.

- The transient temperature decreases with increasing value of the suction parameter.
- The transient temperature decreases with increasing value of the Prandtl number.
- The presence of the magnetic field retards the velocity of the flow field.

In the next chapter, we study unsteady MHD free convection flow past a vertical plate with heat sources in the presence of a chemical reaction and suction.

Chapter 4

A novel finite difference method for an unsteady MHD free convection flow past a vertical plate with heat sources in the presence of a chemical reaction and suction

This chapter investigates the effects of a chemical reaction on unsteady two-dimensional MHD free convection flow of viscous incompressible electrically conducting fluid past a vertical infinite porous plate with heat sources in the presence of a transverse magnetic field, chemical reaction and suction or injection. The governing equations of flow field in the current model are transformed by a suitable similarity transformation to a system of ordinary differential equations and simulated using a suitably designed fitted operator finite difference method (FOFDM). We show that the standard finite difference method (SFDM) and the FOFDM are first order and second order convergent respectively. The effect of Richardson extrapolation on the order of convergence is considered. We noted that this convergence acceleration technique improves the accuracy of the FOFDM although the order of convergence remains the same. We study the effects of various parameters on the velocity, temperature and concentration

profiles to confirm the theoretical estimates. We observe that the temperature flow field increases with an increase in the heat source parameter and decreases with an increase in the suction parameter.

4.1 Introduction

The study of heat and mass transfer problems with chemical reactions have received considerable amount of attention in recent years. It has practical applications in engineering and science. MHD flows find applications in planetary magneto-spheres, aeronautics, materiology, cosmic fluid dynamics, MHD generator, MHD accelerators and construction of centrifugal machines. Free convection currents is mostly caused by temperature difference though in some instances it may be caused by concentration differences where foreign gases are injected or where a substrate is coated with a material and thereby evaporated through the process of heating.

Singh [147] studied unsteady free convection flow of an incompressible micro-polar fluid past an infinite vertical plate with temperature gradient dependent heat source. Singh [146] also studied the effects of thermal diffusion on MHD free convection flow through a vertical channel. Acharya *et al.* [3] studied heat and mass transfer over an accelerated surface with heat source in the presence of suction and injection. Singh [145] investigated the effects of mass transfer on free convection in MHD flow of a viscous fluid. Cortell [39] considered flow and heat transfer of an electrically conducting fluid of second grade over a stretching sheet subject to suction and a transverse magnetic field. On the other hand Gebhart and Pera [58] did a study on combined heat and mass transfer flow and Helmy [68] examined an MHD unsteady free convection flow past a vertical porous plate. Kandasamy [79] analyzed heat and mass transfer along a wedge with heat source and convection in the presence of suction and injection.

The study of the development of two dimensional boundary layer with an applied magnetic field due to an impulsive motion was studied by Kumari and Nath [83]. Muthukumaraswamy and Ganesan [112] studied unsteady flow past an impulsively started vertical plate with heat and mass transfer and Kim [81] investigated the unsteady flow past an impulsively started vertical plate with heat and mass transfer. Raptis [126] examined the thermal radiation and

free convection flow through a porous medium bounded by a vertical infinite porous plate by using a regular perturbation method. Pantokratoras [118] considered a non-Darcian forced convection heat transfer over a flat plate in a porous medium with variable viscosity and variable Prandtl number. Sacheti [133] presented an analysis on exact solutions for unsteady magneto-hydrodynamics free convection flow with constant flux.

The study of the effects of chemical reaction and radiation absorption on transient hydromagnetic natural convection flow with wall transpiration and heat source was carried out by Ibrahim [71]. Devi [50] investigated the effects of a chemical reaction on the MHD flow in the presence of heat transfer. Mansour [92] examined the effects of chemical reaction on MHD natural convection flows saturated in porous media with suction and injection. Recently Shivaiah [143] studied the effects of chemical reaction on unsteady MHD free convection flow past a vertical porous plate in the presence of suction or injection using the finite element method.

Our current study entails the use of the fitted operator finite difference method (FOFDM) to examine the same model studied by Shivaiah [143]. We examine the singularly perturbed part of the governing equations of flow field using the FOFDM. The solution of the singular perturbation problems (SPPs) is known to have large gradients when the coefficient of the highest derivative is very small. We will show theoretically and numerically that the standard finite difference method (SFDM) produces very poor approximations in the layer region when ϵ become very small. This is why we adopt the FOFDM which is chosen so as to capture the behavior of the solution within the boundary layer developed. Sources of literature consulted on singularly perturbed partial differential equations include, Doolan *et al.* [51], Roos *et al.* [131], Miller *et al.* [96] and references therein. Beckett and Mackenzie [16] studied the convergence of finite difference approximations on equally distributed grids to a singularly perturbed boundary value problem using an upwind scheme.

Besides using a different approach to solve the the SPPs our problem differs from that of Beckett and Mackenzie [16] in that our flow is unsteady whereas Beckett and Mackenzie investigated steady flows. Research on singularly perturbed steady convection diffusion problems have been carried out using different methods as stated in Beckett and Mackenzie [16] but none of the methods used our proposed approach. In an attempt to achieve better accuracy with fewer mesh points we use Richardson extrapolation method. Munyakazi and

Patidar [102] investigated the performance of Richardson extrapolation when applied to some FOFDMs for some singular perturbation problems. They found out that the performance of Richardson extrapolation is dependent on the FOFDM scheme employed.

The rest of the chapter is organized as follows. In Section 4.2, the description of our model is presented. Section 4.3 deals with the construction of the numerical method, its analysis and the implementation of the Richardson extrapolation technique. Section 4.4 on the other hand is concerned with the numerical results which supports the theory as well as the study of the effects of the flow parameters using FOFDM. Finally Section 4.5 presents the concluding remarks of the chapter.

4.2 Description of the model

We consider the unsteady two-dimensional free convective mass transfer flow of a viscous incompressible electrically conducting fluid past a vertical infinite porous flat plate in the presence of a transverse magnetic field in the presence of suction or injection. Let the x^*-axis be directed upward along the plate and the y^*-axis normal to the plate. Let u^* and v^* be the velocity components along x^* and y^* axes respectively. At $t^* = 0$, the plate and fluid are at the same temperature T^*_∞ and same concentration C^*_∞. Then the magnetohydrodynamic unsteady free convective boundary layer equations under usual Boussinesq's approximation [143] read

$$\frac{\partial v^*}{\partial y^*} = 0, \tag{4.2.1}$$

$$\frac{\partial u^*}{\partial t^*} + v^*\frac{\partial u^*}{\partial y^*} = \nu\frac{\partial^2 u^*}{\partial y^{*2}} + g\beta(T^* - T^*_\infty) + g\beta^*(C^* - C^*_\infty) - (\frac{\sigma {B_O}^2}{\rho} + \frac{\nu}{\kappa_p})u^*, \tag{4.2.2}$$

$$\frac{\partial T^*}{\partial t^*} + v^*\frac{\partial T^*}{\partial y^*} = \alpha\frac{\partial^2 T^*}{\partial y^{*2}} + \frac{Q_0}{\rho c_p}(T^* - T^*_\infty), \tag{4.2.3}$$

$$\frac{\partial C^*}{\partial t^*} + v^*\frac{\partial C^*}{\partial y^*} = D\frac{\partial^2 C^*}{\partial y^* 2} - K^*_l(C^* - C^*_\infty), \tag{4.2.4}$$

where, ν is the kinematic viscosity, α is the thermal diffusivity, β is the volumetric coefficient of thermal expansion, β^* is the volumetric coefficient of expansion with concentration, ρ is the density, σ is the electrical conductivity of the fluid, g is the acceleration due to gravity, T^* is the temperature of fluid inside thermal boundary, T^*_∞ is the temperature of the fluid

in the free stream, C^* is the species concentration in the boundary layer, C^*_∞ is the species concentration in the free stream, c_p is the specific heat capacity, B_0 is the magnetic induction, Q_o is the heat generation constant, K^* is the permeability of the porous medium, D is the molecular diffusivity, K^*_l is the rate of chemical reaction. The boundary conditions [143] are

$$\begin{aligned} t^* \leq 0: \ & u^* = 0, \ v^* = 0, \ T^* = T^*_\infty, \ C = C^*_\infty \text{ for all } y^*, \\ t^* > 0: \ & u^* = 0, \ v^* = v(t), \ T^* = T^*_w, \ C^* = C_w \text{ at } y^* = 0, \\ & u^* = 0, \ T^* = T^*_\infty, \ C^* = C^* = C^*_\infty \text{ as } y^* \to \infty, \end{aligned} \tag{4.2.5}$$

where, $v(t)$ is the suction velocity at the plate. From the continuity equation we deduce that the suction velocity $v(t) = -V_o$. The negative constant indicates that the suction is directed towards the plate. We nondimensionalize (4.2.2) to (4.2.4) by introducing the following non-dimensional quantities

$$\begin{aligned} & u = u^*/\widetilde{V_0}, \ V_o = v^*/\widetilde{V_o}, \ y = \widetilde{V_o} y^*/V_o, \ \theta = (T^* - T^*_\infty)/(T^*_w - T^*_\infty), \ t = \widetilde{V_o}^2 t^*/V_o, \\ & \widetilde{\phi} = (C^* - C^*_\infty)/(C^*_w - C^*_\infty), \ M = \sigma B_o^2 \ V_o/\rho\widetilde{V_o}^2, \ P_r = V_o \rho C_p/k, \\ & K = k_p \widetilde{V_o}^2/V_o^2, \ G_r = g\beta V_o(T^*_w - T^*_\infty)/\widetilde{V_o}^3, \ G_m = g\beta^* V_o(C^*_w - C^*_\infty)/\widetilde{V_o}^3, \\ & Q = Q_o V_o/\rho C_p \widetilde{V_o}^2, \ K_l = K^*_l V_o^2/\widetilde{V_o}^2, \ S_c = V_o/D, \end{aligned} \tag{4.2.6}$$

where, M is the magnetic parameter, κ is the thermal conductivity, $\widetilde{V_0}$ is the reference velocity, K_l is the chemical reaction parameter, G_r is the Grashof number of heat transfer, G_m is the Grashof number of mass transfer, S_c is the Schmidt number, Q is the heat source parameter. Using (4.2.5) and (4.2.6), equations (4.2.2)-(4.2.4) reduces to

$$\frac{\partial u}{\partial t} - V_o \frac{\partial u}{\partial y} = \frac{\partial^2 u}{\partial y^2} + G_r\theta + G_m C - \left(M + \frac{1}{K}\right) u, \tag{4.2.7}$$

$$\frac{\partial \theta}{\partial t} - V_o \frac{\partial \theta}{\partial y} = \frac{1}{P_r}\frac{\partial^2 \theta}{\partial y^2} + Q\theta, \tag{4.2.8}$$

$$\frac{\partial C}{\partial t} - V_o \frac{\partial C}{\partial y} = \frac{1}{Sc}\frac{\partial^2 C}{\partial y^2} - K_l C. \tag{4.2.9}$$

The corresponding initial and boundary conditions are

$$\begin{aligned} t \leq 0: \ & u = 0, \ \theta = 0, \ C = 0 \text{ for all } y, \\ t \geq 0: \ & u = 0, \ \theta = 1, \ C = 1 \text{ at } y = 0, \\ & u \to 0, \ \theta \to 0, \ C \to 0, \text{ as } y \to \infty. \end{aligned} \tag{4.2.10}$$

The set of equations (4.2.7) to (4.2.9) together with the corresponding boundary conditions (4.2.10) are non-linear and coupled and so analytical solutions are difficult to find. The finite difference method is used to find an approximate solution to the problem. To solve the perturbed part of the differential model we employ the FOFDM which arises when P_r is relatively large.

4.3 Construction and analysis of the numerical method

We introduce the FOFDM to solve the energy equation. The FOFDM is compared with the standard finite difference method (SFDM). The energy equation (4.2.8) is stated in the form:

$$L\theta := \frac{\partial \theta}{\partial t} - V_o \frac{\partial \theta}{\partial y} - \frac{1}{P_r} \frac{\partial^2 \theta}{\partial y^2} - Q\theta = 0. \tag{4.3.1}$$

We denote by N a positive integer and approximate the solution to (4.3.1) on a uniform mesh and let the interval [0,4] be divided into N equal sub-intervals

$$y_0 = 0, \ y_i = y_0 + ih, \ i = 1(1)N, \ h = y_i - y_{i-1}, \ y_N = 4.$$

Let τ be the uniform step size on

$$\Omega^{\tau,m} = \left\{ (y, t_j) : y \in \Omega, t_j = j\tau = j\frac{1}{m}, \ \forall \ 0 < j \leq m \right\}. \tag{4.3.2}$$

Denote the approximation of θ by the unknown ϖ. By performing the time semi-discretization by Euler method at time level n gives

$$\frac{\varpi^n - \varpi^{n-1}}{\tau} - V_o \varpi_y^n - \epsilon \varpi_{yy}^n - Q\varpi^n = 0, \tag{4.3.3}$$

subject to

$$\varpi^n(0) = 1 \ 0 < n < m, \tag{4.3.4}$$
$$\varpi^n(4) = 0 \ 0 \leq n < m,$$

where $\epsilon = 1/P_r$. This implies

$$-\epsilon\varpi^n_{yy} - V_o\varpi^n_y + \left(\frac{1}{\tau} - Q\right)\varpi^n = \widetilde{f}, \tag{4.3.5}$$

subject to

$$\varpi^n(0) = 1, \ \varpi^n(4) = 0, \tag{4.3.6}$$

where $\widetilde{f} = (1/\tau)\widetilde{v}^{n-1}$.

For the sake of simplicity we rewrite equation (4.3.5) without the time level notation "n" in the following form

$$-\epsilon\varpi''(y) - \gamma\varpi' - \frac{1}{\tau}\varpi(y) = \frac{1}{\tau}\varpi^*, \tag{4.3.7}$$

subject to

$$\varpi(0) = 1, \ \varpi(4) = 0, \tag{4.3.8}$$

Note that ϖ^* is defined as the previous time level value of ϖ.

The following lemma provides bounds on the solution of the problem (4.3.7).

Lemma 4.3.1. *Let ϖ be the solution of (4.3.7). Then for $0 \leq k \leq 4$,*

$$|\varpi^{(k)}(y)| \leq \widetilde{C}\left(1 + \epsilon^{-k}e^{-\lambda y/\epsilon}\right)$$

for all $y \in \overline{\Omega} = [0, 4]$, where $0 < \epsilon \leq 1$, $\widetilde{C}$ is independent of ϵ, and $0 < \lambda < V_o$.

Proof. See [96].

Next we discretize (4.3.7) in space using the standard finite difference method and denote the approximation of ϖ by $\widetilde{\nu}$ to give

$$L^{h,\tau}\widetilde{\nu}_j \equiv -\epsilon\frac{\widetilde{\nu}_{j+1} - 2\widetilde{\nu}_j + \widetilde{\nu}_{j-1}}{h_j^2} - V_0\frac{\widetilde{\nu}_{j+1} - \widetilde{\nu}_j}{h} + \left(\frac{1}{\tau} - Q\right)\widetilde{\nu}_j = \widetilde{f}_j. \tag{4.3.9}$$

In this chapter SFDM stand for the standard finite difference method, FOFDM stand for fitted operator finite difference method. For very small values of ϵ, the SFDM gives inaccurate approximation of the true solution as the maximum absolute errors suggest. We design a fitted numerical technique so as to achieve reliable results by replacing the denominator of the approximation to the second derivative h^2 by a function ψ_j^2, which is a function of P_r, V_o and h. Let u be the approximation of ϖ for the FOFDM and the resulting FOFDM is given by

$$L^{h,\tau}u_j \equiv -\epsilon\frac{u_{j+1}-2u_j+u_{j-1}}{\psi_j^2} - V_0\frac{u_{j+1}-u_j}{h} + \left(\frac{1}{\tau}-Q\right)u_j = \widetilde{f}_j, \tag{4.3.10}$$

where,

$$\psi_j^2 = \frac{\epsilon h}{V_0}\left(\exp\left(\frac{V_0 h}{\epsilon}\right)-1\right). \tag{4.3.11}$$

The function ψ_j^2 mimics the behavior of the solution in the boundary layer region. The layer region is located in the neighborhood of the vertical plate near the left end of the interval. Before the numerical simulation of the MHD flow using the FOFDM we begin by analyzing the FOFDM for stability and convergence.

The local truncation error of the time semi-discritization by the forward implicit Euler scheme is denoted by $\widetilde{e_n} = \theta(y,t_n)-\varpi(y)$, where $\varpi(y)$ is the solution of (4.3.7). The amount of error $\widetilde{e_n}$ is the contribution of each time step to the global error of the time semi-discretizaton. The following lemmas depict the order of the local and global error related to the problem (4.3.7).

Lemma 4.3.2. (Local error estimate) *If* $|\varpi^{(k)}(y)| \leq \widetilde{C},\ y \in [0,4],\ 0 \leq k \leq 2$, *then the local error estimate is given by* $||\widetilde{e_n}|| \leq \widetilde{C}\tau^2$.

The following lemma relates to the global error, E_n.

Lemma 4.3.3. Global error estimate. *The global error* $E_n = \Sigma_{n=0}^{m}\widetilde{e_n}$ *satisfies*

$$||E_n|| \leq \widetilde{C}\tau,\ \forall\ 1 \leq n \leq m.$$

The global error of the time semi-discretization is of the first order, that is, $||\theta-\varpi|| \leq \widetilde{C}\tau$.

We discretize spatially to find the local truncation error $|(\varpi - u)|$ where ϖ is the exact solution with respect to space and u is the approximation of θ for the FOFDM. We are going to consider a few lemmas which are pivotal in the analysis of the error of the solution obtained using the fitted operator finite difference method.

We analyse (4.3.10) for stability and convergence. The differential operator $L^{h,\tau}$ in (4.3.10) satisfies the following discrete maximum principle on Ω,

Lemma 4.3.4. (Discrete maximum principle). *Assume that the mesh function $\varphi(y)$ satisfies $\phi(0) \geq 0$ and $\phi(4) \geq 0$. Then, $L^{h,\tau}\phi(y) \geq 0$ for all $y \in \Omega = (0,4)$ implies that $\phi(y) \geq 0$ for all $y \in \overline{\Omega}$.*

Proof. The proof follows the same lines as the proof of the discrete maximum principle in [96] as shown below. Choose k such that $\phi_k = \min_i \phi_i$ and suppose that $\phi_k \leq 0$. Then $k \notin \{0, n\}$, $\phi_{k+1} - \phi_k \geq 0$ and $\phi_k - \phi_{k-1} \leq 0$. Thus

$$\begin{aligned} L^{h,\tau}\phi_k &= -\frac{\epsilon}{\psi_k^2}(\phi_{k+1} - 2\phi_k + \phi_{k-1}) - \frac{V_o}{h}(\phi_{k+1} - \phi_k) + (\frac{1}{\tau} - Q)\phi_k, \qquad (4.3.12) \\ &= -\frac{\epsilon}{\psi_k^2}(\phi_{k+1} - \phi_k + \varphi_{k-1} - \phi_k) - \frac{V_o}{h}(\phi_{k+1} - \phi_k) + (\frac{1}{\tau} - Q)\phi_k \\ &\leq 0, \end{aligned}$$

which is a contradiction. It follows $\phi_k \geq 0$ and so $\phi_i \geq 0 \ \forall i,\ i = 1(1)n$, which completes the proof. The following lemma is a consequence of the discrete maximum principle in Lemma 4.3.4.

Lemma 4.3.5. (Uniform stability estimate) *If ξ_i is any mesh function such that $\xi_0 = \xi_n = 0$ then $|\xi_i| \leq \frac{4}{\lambda} \max_{1\leq j\leq n-1} \left|L^h \xi_j\right|$ for $0 \leq i \leq n$.*

Proof. We consider a general case of the form:

$$L^{h,\tau}\vartheta(y) = -\epsilon\vartheta''(y) - a(y)\vartheta(y) + b(y)\vartheta(y), \qquad (4.3.13)$$

where $a(y) > \lambda > 0$. Let

$$\widetilde{C} = \frac{1}{\lambda} \max_{1\leq j\leq n-1} |L^n \xi_j|,$$

and introduce the mesh functions $\vartheta_i^+, \vartheta_i^-$ where $\vartheta_i^\pm = \widetilde{C}(4-y_i) \pm \xi_i$. Then

$$\begin{aligned} L^{h,\tau}\vartheta_i^\pm &= -\epsilon\frac{\vartheta_{i+1}^\pm - 2\vartheta_i^\pm + \vartheta_{i-1}^\pm}{\psi_i^2} - a_i\frac{\vartheta_{i+1}^\pm - \vartheta_i^\pm}{h} + b_i\vartheta_i^\pm, \\ &= -\epsilon\frac{\pm\xi_{i+1} \mp 2\xi_i \pm \xi_{i-1}}{\psi_i^2} - a_i\frac{(\pm\xi_{i+1} \mp \xi_i)}{h} + b_i(\pm\xi_i) + \widetilde{C}a_i, \\ &= \pm L^{h,\tau}\xi_i + \widetilde{C}a_i + b_i\widetilde{C}(4-y_i), \\ &= \pm L^{h,\tau}\xi_i + \frac{a_i + b_i(4-yi)}{\lambda}\max_{\Omega}\left|L^{h,\tau}\xi_i\right| \qquad (4.3.14) \\ &\geq 0, \end{aligned}$$

since $a_i/\lambda \geq 1$. By the maximum principle it implies

$$\vartheta_i^\pm \geq 0 \text{ for } 0 \leq i \leq n,$$

and therefore

$$\vartheta_i^\pm = \widetilde{C}(4-y_i) \pm \xi_i \geq 0 \text{ for } 0 \leq y_i \leq 4.$$

This reduces to

$$|\xi_i| \leq \widetilde{C}(4-y_i),$$

since $4 - y_i \leq 4$ and so

$$|\xi_i| \leq \frac{4}{\lambda}|L^{h,\tau}\xi_i|, \qquad (4.3.15)$$

which completes the proof.

Now we attempt to establish the local truncation error of the FOFDM. In the analysis of these errors, $\widetilde{M}$ denote a positive constant, independent of h and ϵ and may assume different values in different inequalities and equations. The local truncation error of the FOFDM (4.3.10) is given by

$$\left|L^{h,\tau}(\theta-u)_j\right| = \left|L^{h,\tau}(\theta-\varpi+\varpi-u)_j\right| = \left|L^{h,\tau}(\theta-\varpi)_j\right| + \left|L^{h,\tau}(\varpi-u)_j\right|. \qquad (4.3.16)$$

From lemma 4.3.3

$$\left|L^{h,\tau}(\theta - u_j\right| = \widetilde{M}\tau. \tag{4.3.17}$$

Now the truncation error for the spatial descretization is given by

$$\begin{aligned} L^{h,\tau}(\varpi - u)_j &= -\epsilon\varpi_j'' - V_o\varpi_j' + \left(\frac{1}{\tau} - Q\right)\varpi_j - \left(-\epsilon\frac{\varpi_{j+1} - 2\varpi_j + \varpi_{j-1}}{\psi_j^2} - V_o\frac{\varpi_{j+1} - \varpi_j}{h}\right) \\ &\quad - \left(\frac{1}{\tau} - Q\right)\varpi_j, \\ &= -\epsilon\varpi_j'' + V_o\varpi_j' - \frac{\epsilon}{\psi_j^2}\left[h^2\varpi_j'' + \frac{\varpi^{(iv)}(\zeta_1)}{12}h^4\right] + \frac{V_o h}{2}\left(\varpi_j'' + \frac{h}{3}\varpi_j'''\right) \\ &\quad + \frac{h^2}{12}\varpi^{(iv)}(\zeta_2), \end{aligned} \tag{4.3.18}$$

where $\zeta_1 \in (y_{j-1}, y_{j+1})$ and $\zeta_2 \in (y_j, y_{j+1})$. Using the Taylor series expansion, we have

$$\frac{\epsilon}{\psi_j^2} = \frac{\epsilon}{h^2} - \frac{V_o}{2h} + \ldots.$$

This implies that

$$\begin{aligned} L^{h,\tau}(\varpi - u)_j &= -\epsilon\varpi_j'' \\ &\quad + \left[\frac{\epsilon}{h^2} - \frac{V_o}{2h} + \ldots\right]\left[h^2\varpi_j'' + \frac{\varpi^{(iv)}(\zeta_1)}{12}h^4\right] \\ &\quad + \frac{V_o}{2}\left(h\varpi_j'' + \frac{h^2}{3}\varpi_j''' + \frac{\varpi^{(iv)}(\zeta_2)}{12}h^3\right). \end{aligned}$$

Further simplifications lead to

$$L^{h,\tau}(\varpi - u)_j = \left(\frac{\epsilon\varpi^{(iv)}(\zeta_1)}{12} + \frac{V_o}{6}\varpi_j'''\right)h^2 - \left(\frac{V_o\varpi^{(iv)}(\zeta_1)}{24}\right)h^3 + O(h^5).$$

Using Lemma 4.3.1 to estimate the bounds on the derivatives, we obtain

$$\left|L^{h,\tau}(\varpi - u)_j\right| \leq \left|\frac{\widetilde{C}\epsilon}{12}\left(1 + \epsilon^{-4}e^{-\lambda y/\epsilon}\right) + \frac{\widetilde{C}V_o}{6}\left(1 + \epsilon^{-3}e^{-\lambda y/\epsilon}\right)\right|h^2 + O(h^5).$$

Now applying Lemma 7 in [103] yields

$$\begin{aligned} \left|L^{h,\tau}(\varpi-u)_j\right| &\leq \widetilde{C}\left(\frac{\epsilon h^2}{12}+\frac{V_o h^2}{6}\right)+O(h^5) \\ &\leq \widetilde{M}h^2, \end{aligned} \tag{4.3.19}$$

since $\epsilon h^2 < h^2$. Then by Lemma 4.3.5 and (4.3.19) we have

$$\begin{aligned} \max_{0\leq i\leq n}\left|(\varpi-u)_i\right|, &\leq \max_{1\leq j\leq n-1}\left|L^{h,\tau}(\varpi-u)_j\right|, \\ &\leq \widetilde{M}h^2. \end{aligned} \tag{4.3.20}$$

From equation (4.3.17) and (4.3.19) the local truncation error is given by

$$\begin{aligned} \left|L^{h,\tau}(\theta-u)_j\right| &= \left|L^{h,\tau}(\theta-\varpi+\varpi-u)_j\right|, \\ &\leq \left|L^{h,\tau}(\theta-\varpi)_j\right|+\left|L^{h,\tau}(\varpi-u)_j\right|, \\ &\leq \widetilde{M}\left(\tau+h^2\right). \end{aligned} \tag{4.3.21}$$

Richardson extrapolation

We implement the Richardson extrapolation, a convergence acceleration technique. The technique improves the accuracy of the numerical approximation. It involves two linear solutions on a nested mesh whose linear combination results in a third solution which produces better or improved approximations.

Let N be a positive integer. We implement the FOFDM over N mesh intervals

$$y_0=0,\ y_i=y_0+ih,\ i=1(1)N,\ h=y_i-y_{i-1},\ y_N=4.$$

The above mesh is denoted by π_N. We introduce another mesh π_{2N} by bisecting each mesh interval in π_N

$$\widetilde{y}_0=0,\ \widetilde{y}_i=\widetilde{y}_0+i\widetilde{h},\ i=1(1)2N,\ \widetilde{h}=\widetilde{y}_i-\widetilde{y}_{i-1}=\frac{h}{2},\ \widetilde{y}_N=4.$$

The two meshes, π_N and π_{2N} are used to derive the Richardson extrapolation formula.

Extrapolation formula

The FOFDM on the mesh π_N satisfies (4.3.19). Denoting by $\widetilde{w}$ the numerical solution computed on the mesh π_{2N},

$$\begin{aligned}\left[L^{\frac{h}{2},\tau}\left(\varpi-\widetilde{u}\right)_j\right] &= -\epsilon\varpi_j''-V_o\varpi_j'+\left(\frac{1}{\tau}-Q\right)\varpi_j \\ &\quad -\left[-\epsilon\frac{\varpi_{j+1}-2\varpi_j+\varpi_{j-1}}{\psi_j^2}-\frac{V_o}{h/2}\left(\varpi_{j+1}-\varpi_j\right)\right] \\ &\quad -\left(\frac{1}{\tau}-Q\right)\varpi_j, \\ &= -\epsilon\varpi_j''+\frac{\epsilon}{\psi_j^2}\left(\frac{h^2}{4}\varpi_j''+\frac{h^4}{192}\varpi_j^{(iv)}+O(h^6)\right)+\frac{hV_o}{4}\varpi_j'' \\ &\quad +\frac{h^2V_o}{24}\varpi_j'''+\frac{h^3V_o}{192}\varpi_j^{(iv)}+O(h^4). \end{aligned} \tag{4.3.22}$$

Using Taylor series expansion

$$\frac{\epsilon}{\psi_j^2} = \frac{2V_o}{h}\left[\frac{e^{\frac{-V_oh}{2\epsilon}}}{1-e^{\frac{V_oh}{2\epsilon}}}\right]=\left(\frac{4\epsilon}{h^2}-\frac{V_o}{h}+\ldots\right). \tag{4.3.23}$$

Therefore

$$\begin{aligned} L^{\frac{h}{2},\tau}\left(\varpi-\widetilde{u}\right)_j &= -\epsilon\varpi_j''+\left(\frac{4\epsilon}{h^2}-\frac{V_o}{h}+\ldots\right)\left(\frac{h^2}{4}\varpi_j''+\frac{h^4\varpi_j^{(iv)}}{192}\right) \\ &\quad + \frac{hV_o}{4}\varpi_j''+\frac{h^2V_o}{24}\varpi_j'''+\frac{h^3V_o}{192}\varpi_j^{(iv)}, \\ &= \left(\frac{\epsilon\varpi_j^{(iv)}}{48}+\frac{V_o\varpi_j'''}{24}\right)h^2+O(h^5). \end{aligned} \tag{4.3.24}$$

The FOFDM on the mesh π_N satisfies (4.3.19) and reads

$$\max_{0\le j\le n}\left|\left(\varpi-u\right)_j\right|\le\widetilde{M}h^2.$$

It follows that

$$\varpi(y_j)-u_j=\widetilde{M}h^2+R_N(y_j),\ 1\le j\le N-1,$$

and

$$\varpi(\tilde{y}_j) - \tilde{u}_j = \widetilde{M}\left(\frac{h}{2}\right)^2 + R_{2N}(y_j),\ 1 \leq j \leq 2N-1,$$

where both the remainders $R_N(y_j)$ and $R_{2N}(y_j)$ are $O(h^2)$.

Therefore,

$$\varpi(y_j) - u_j - 16(\varpi(y_j) - \tilde{u}_j) = R_N(y_j) - 16R_{2N}(y_j) = O(h^2), \forall y_j \in \pi_N, \tag{4.3.25}$$

and consequently

$$\varpi(y_j) - \frac{16\tilde{(u)} - u}{15} = O(h^2)\ \forall y_j \in \pi_N. \tag{4.3.26}$$

This suggests an extrapolation formula:

$$u_j^{extr} := \frac{16\widetilde{u} - u}{15},\ j = 1(1)N-1 \tag{4.3.27}$$

where u_j^{extr} is the solution of (4.3.10) obtained after extrapolation. The local truncation error after extrapolation is thus given by

$$\begin{aligned}\left|L^h(\varpi - u^{extr})_j\right| &= \frac{16}{15}\left[L^{\frac{h}{2},\tau}\left(\varpi - \widetilde{u}\right)_j\right] - \frac{1}{15}L^{h,\tau}(\varpi - u)_j \\ &= \left(\frac{\epsilon\varpi^{(iv)}}{60} + \frac{V_o\varpi'''}{30}\right)h^2 + O(h^5).\end{aligned} \tag{4.3.28}$$

Hence

$$\left|L^h(\varpi - u^{extr})_j\right| = \left|\frac{\epsilon\varpi^{(iv)}}{60} + \frac{V_o\varpi'''}{30}\right|h^2 + O(h^5),$$

Applying Lemma 4.3.1 and Lemma 7 in [103] yields

$$\begin{aligned}\left|L^h(\varpi - u^{extr})_j\right| &= \left|\frac{\epsilon\varpi^{(iv)}}{60} + \frac{V_o\varpi'''}{30}\right| h^2 + O(h^5),\\ &\leq \left(\frac{\epsilon\widetilde{C}}{60}\left(1+\epsilon^{-4}e^{-\lambda y/\epsilon}\right) + \frac{V_o\widetilde{C}}{30}\left(1+\epsilon^{-3}e^{-\lambda y/\epsilon}\right)\right)h^2,\\ &\leq \widetilde{C}\left(\frac{1+2V_o}{60}\right)h^2,\\ &\leq \widetilde{M}h^2.\end{aligned}$$

From equation (4.3.17) and (4.3.29) the local truncation error is given by

$$\begin{aligned}\left|L^{h,\tau}(\theta - u^{extr})_j\right| &= \left|L^{h,\tau}(\theta - \varpi + \varpi - u^{extr})_j\right|,\\ &\leq \left|L^{h,\tau}(\theta-\varpi)_j\right| | + \left|L^{h,\tau}(\varpi - u^{extr})_j\right|,\\ &\leq \widetilde{M}\left(\tau + h^2\right).\end{aligned} \tag{4.3.29}$$

4.4 Results and discussions

Since the exact solution is not available the maximum errors at all the mesh points are estimated using the double mesh principle as:

$$e^{\Delta t,N}(y,t) = |u^N(y,t) - u^{2N}(y,t)|, \quad \text{before extrapolation,} \tag{4.4.1}$$

and

$$e^{\Delta t,N,extr}(y,t) = |u^{N,extr}(y,t) - u^{2N,extr}(y,t)|, \text{ after extrapolation,} \tag{4.4.2}$$

where N is the spatial discretization parameter, Δt is the time discretization parameter, u^{2N} is the solution of (4.3.1) before extrapolation and $w^{2N,extr}$ is the solution after extrapolation. The maximum absolute errors are given by

$$E^{N,\Delta t} = \max_N e^{\Delta t,N}(y,t), \text{ before extrapolation,} \tag{4.4.3}$$

and

$$E^{N,\Delta t,extr} = \max_N e^{\Delta t,N,extr}(y,t), \text{ after extrapolation,} \tag{4.4.4}$$

and the rates of convergence are given by

$$r_N = \frac{\log(E^{N,\Delta t}/E^{2N,\Delta t/4})}{\log 2}, \text{ before extrapolation,} \tag{4.4.5}$$

and

$$r_N = \frac{\log(E^{N,\Delta t,extr}/E^{2N,\Delta t/4,extr})}{\log 2}, \text{ after extrapolation.} \tag{4.4.6}$$

Table 4.4.1: Maximum absolute errors and orders of convergence associated with SFDM and FOFDM for $V_o = 0.2$, $\tau = 0.1$ and $Q = 1.5$.

P_r	N	10	20	40	80
	Δt	0.1	0.1/4	$0.1/4^2$	$0.1/4^3$
5	SFDM	2.87E-2	1.50E-2	8.20E-3	4.40E-3
	r_N	0.94	0.87	0.90	
	FOFDM	1.96E-2	5.30E-3	1.30E-3	3.27E-4
	r_N	1.89	2.03	1.99	
10	SFDM	4.10E-2	2.51E-2	1.52E-2	8.50E-3
	r_N	0.71	0.60	0.84	
	FOFDM	1.56E-2	8.00E-3	2.10E-3	5.28E-4
	r_N	0.96	1.93	1.99	
20	SFDM	6.32E-2	4.10E-2	2.80E-2	1.64E-2
	r_N	0.62	0.55	0.77	
	FOFDM	4.30E-3	1.41E-2	3.50E-3	8.69E-4
	r_N	-	2.01	2.01	
40	SFDM	7.49E-2	6.65E-2	4.78E-2	3.05E-2
	r_N	0.17	0.48	0.65	
	FOFDM	3.30E-3	1.26E-2	5.30E-3	1.40E-3
	r_N	-	1.25	1.92	

Equation (4.3.1) was solved using the standard finite difference method and the fitted operator finite difference method. Since the exact solution is not available the double mesh principle is applied and we observe that the maximum absolute errors of the fitted method are less than that of the standard method. These are depicted in Tables 4.4.1. For a fixed

Table 4.4.2: Maximum absolute errors and orders of convergence associated with FOFDM **before** and **after** extrapolation.

P_r	N	10	20	40	80
	Δt	0.1	0.1/4	$0.1/4^2$	$0.1/4^3$
5	Before extrapolation	1.96E-2	5.30E-3	1.30E-3	3.27E-4
	r_N	1.89	2.03	1.99	
	After extrapolation	2.90E-3	6.95E-4	1.79E-4	4.48E-5
	r_N	2.06	1.96	2.00	
10	Before extrapolation	1.56E-2	8.00E-3	2.10E-3	5.28E-4
	r_N	0.96	1.93	1.99	
	After extrapolation	5.10E-3	1.30E-3	3.38E-4	8.45E-5
	r_N	1.97	1.94	2.00	
20	Before extrapolation	4.30E-3	1.41E-2	3.50E-3	8.69E-4
	r_N	-	2.01	2.01	
	After extrapolation	3.00E-3	2.50E-3	6.03E-4	1.50E-4
	r_N	0.26	2.04	2.00	
40	Before extrapolation	3.30E-3	1.26E-2	5.30E-3	1.40E-3
	r_N	-	1.25	1.92	
	After extrapolation	7.37E-4	3.60E-3	8.81E-4	2.48E-4
	r_N	-	2.03	1.83	

value of ϵ the maximum absolute error decreases as the number of grid points, N increases. In Table 4.4.1 the spatial descretization takes the values $N = 10,\ 20,\ 40,\ 80$ and the time descretization parameter take the values $\Delta t = 0.1\ , 0.1/4,\ 0.1/4^2,\ 0.1/4^3$. We have divided the step sizes into a different ratio so that we accommodate at the same time the first order convergence in time and the second order convergence in space. From the table of results the maximum absolute errors suggest the second order convergence in space. The result agrees with theoretical results which showed that the local truncation error is of order $O\left(\tau + h^2\right)$. From the tabulated results it is clear that the maximum absolute errors of the FOFDM are comparatively smaller than the usual standard methods. On the other hand the order of convergence of the FOFDM are slightly larger than the order of convergence of the SFDM.

In Table 4.4.2 the spatial descretization takes the values $N = 10,\ 20,\ 40,\ 80$ and the time descretization parameter take the values $\Delta t = 0.1\ , 0.1/4,\ 0.1/4^2,\ 0.1/4^3$. As displayed in Table 4.4.2 implementation of Richardson extrapolation results in the generation of smaller error values but does not improve the order of convergence. Since we regard large values of

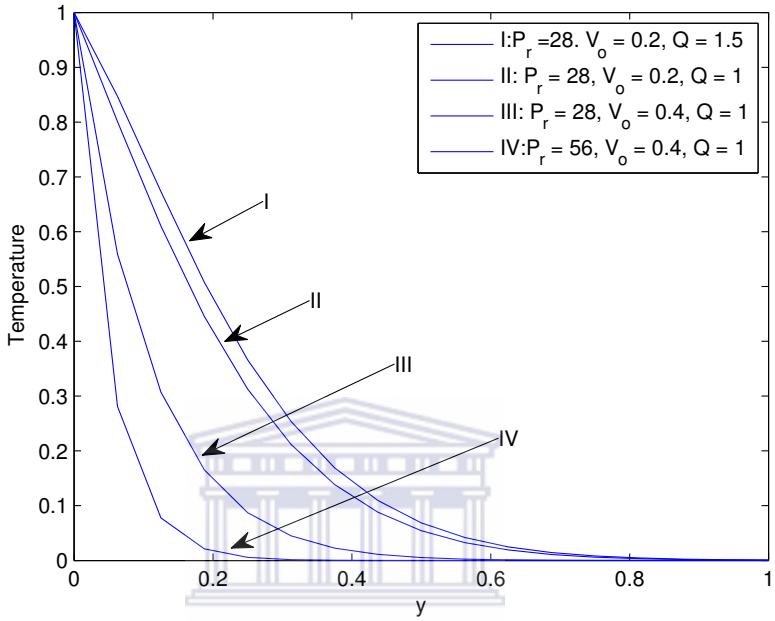

Figure 4.4.1: The effect of P_r, v_o and Q on the temperature profile for $N = 64$.

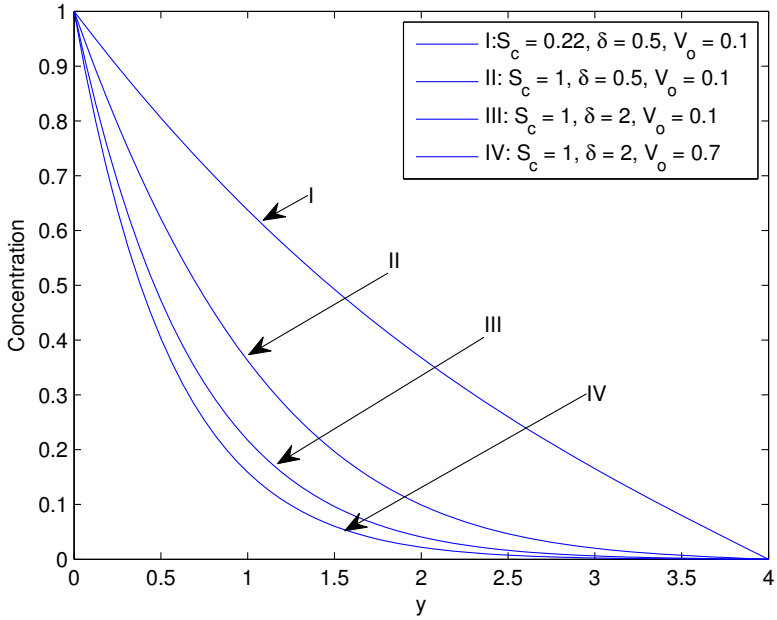

Figure 4.4.2: The effect of S_c, V_o and K_l on the concentration profile for $N = 64$.

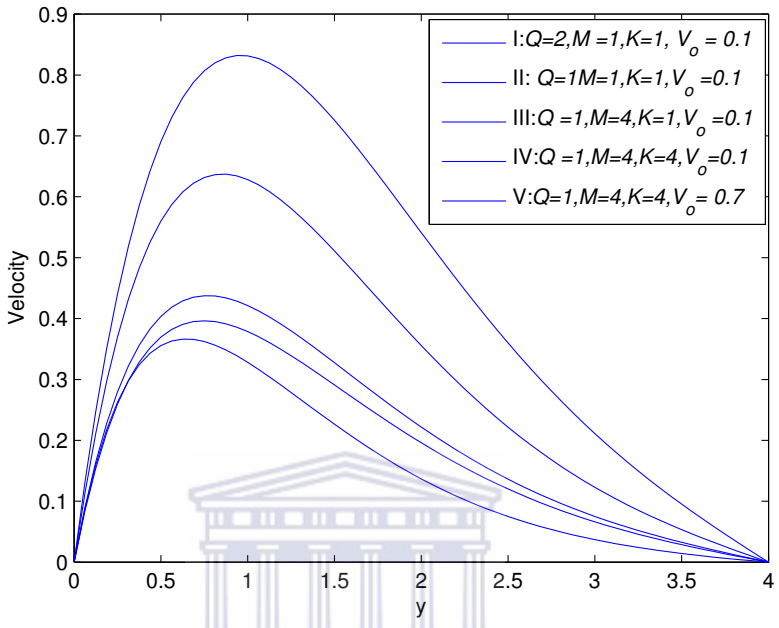

Figure 4.4.3: The effect of M, V_o, Q and K on the velocity profile for $N = 64$.

P_r in this paper we use the FOFDM to analyze the temperature, velocity and concentration profiles of the MHD free convective flow past an infinite vertical porous plate with heat sources in the presence of a chemical reaction and suction or injection. Figure 4.4.1 depicts the effects of the Prandtl number, suction parameter and heat source parameter on the temperature profile. We notice from Figure 4.4.1 that the temperature flow field increases as the heat source parameter Q increases. On the other hand the temperature flow field decreases with increasing Prandtl number P_r and suction parameter V_o. Figure 4.4.2 shows the effect of parameters such as the Schmidt number S_c, chemical reaction parameter K_l and suction parameter V_o on the concentration profile. We observe that the concentration distribution decreases with increasing Schmidt number, chemical reaction parameter and suction parameter. The effects of magnetic parameter M, suction parameter V_o, permeability parameter K and heat source parameter Q are depicted in Figure 4.4.3. As expected we observe that the magnetic parameter and suction parameter retards the velocity flow field. We also observe that the velocity flow field increases with increasing permeability parameter and increasing heat source parameter.

4.5 Summary

The study of unsteady free convective mass transfer flow of viscous incompressible electrically conducting fluid past a vertical infinite porous plate with heat sources in the presence of a chemical reaction, transverse magnetic field and suction/injection using the FOFDM was carried out. The governing equations are non-dimensionalized by introducing similarity variables and then solved numerically using the fitted operator finite difference method. The Richardson extrapolation technique is implemented and it is deduced that the extrapolation improves the accuracy of the results whereas the order of convergence is not improved. Since large values of P_r are assumed in this paper the fitted operator finite difference method is used to analyze the temperature, concentration and velocity profiles as parameters such as the suction parameter, Prandtl number, Schmidt number, magnetic parameter, permeability parameter, chemical reaction parameter and heat source parameter vary. The effect of the different parameters on the velocity, concentration and temperature profiles are summarized as follows.

- The temperature flow field increases with the increase in the heat source parameter whereas it decreases with the increase in Prandtl number and suction parameter.
- The concentration flow field decreases with the increase in the Schmidt number, chemical reaction parameter and suction.
- The velocity flow field decreases with increasing magnetic parameter and suction parameter whereas it increases with increasing permeability parameter and heat source parameter.

In Chapter 5 we investigate the double-diffusive MHD flow over a moving plate with heat generation and soret effects.

Chapter 5

A fitted method on the double-diffusive MHD flow over a moving vertical plate with heat generation and soret effects

In this chapter we investigate the solution of a double-diffusive convection-radiation interaction on a two dimensional unsteady MHD laminar flow of viscous, incompressible, electrically conducting fluid past a semi-infinite vertical moving porous plate embedded in a porous medium subjected to a transverse magnetic field in the presence of a chemical reaction, heat generation/absorption and thermal diffusion. The plate moves with constant velocity in the direction of fluid flow and the free stream velocity follows the exponentially increasing small perturbation law. The porous surface absorbs fluid with a suction velocity that is time-dependent. The Rosseland approximation is used to describe the radiative heat flux in the energy equation. In this work, the governing partial differential equations describing the problem are transformed by a similarity transformation resulting in a system of ordinary differential equations. The singularly perturbed part of the differential model is simulated using the fitted operator finite difference method (FOFDM) and results are compared with those obtained using classical approaches. We analyze the proposed approach for stability

and convergence. Numerical results are presented to confirm our theoretical findings. We observe that both temperature and concentration profiles increases with an increase in the value of the Soret number. We also note that the temperature increases with an increase in the heat generation parameter.

5.1 Introduction

Heat and mass transfer problems with chemical reaction have received much attention in recent years because of of their application in engineering and science. Muthucumaraswamy and Ganesan [109] studied the effect of the chemical reaction and injection on flow in unsteady vertical isothermal plate. Das *et al.* [42] analyzed the effect of the first order homogenous chemical reaction in unsteady flow past an infinite vertical plate with constant heat and mass transfer. Muthucumaraswamy and Ganesan [111] studied the effects of a chemical reaction in the unsteady flow past an impulsively started semi-infinite vertical plate subjected to uniform heat flux. Muthucumaraswamy and Ganesan [106] investigated the effects of suction on heat and mass transfer along a moving vertical surface in the presence of a chemical reaction. Raptis and Perdikis [127] studied the effects of a chemical reaction of an electrically conducting viscous fluid over a quadratic semi-infinite stretching sheet in the presence of a constant magnetic field. Ibrahim *et al.* [71] investigated the effects of the chemical reaction and radiation absorption on the unsteady MHD free convection flow past a semi-infinite porous moving plate with suction and heat source. Seddeck *et al.* [140] studied the effects of chemical reaction, radiation and variable viscosity on hydromagnetic mixed convection heat and mass transfer for Hiemenz flow through porous media.

The existence of various physical problems that undergo exothermic and endothermic chemical reaction have led to the study of heat generation effects in moving fluids. Hossain *et al.* [69] investigated the problem of a natural convection flow along a vertical wavy surface with uniform surface temperature in the presence of heat generation. Chamkha [30] studied unsteady convective heat and mass transfer past a semi-infinite porous moving plate with heat generation/absorption. Alam *et al.* [6] analyzed the problem of free convection heat and mass transfer flow past an inclined semi-infinite heated surface of an MHD flow in the presence of heat generation.

The study of radiation interaction with convection for heat and mass transfer in fluids is important in view of its significance in free convection problems involving absorbing-emitting fluids. El-Naby [55] investigated the effect of radiation on MHD unsteady free convection flow past a semi-infinite vertical porous plate using the implicit finite difference methods. The study of unsteady fluid flow past a non porous moving plate in the presence of free convection and radiation were done by Cogley *et al.* [36], Das *et al.* [43], Ganesan and Loganathan [57] and Mbeledogu *et al.* [95] only to mention a few.

Several studies have been carried out involving a porous medium. El-Hakiem [54] investigated the unsteady MHD oscillatory flow in free convection-radiation through a porous medium with a vertical infinite surface that absorbs the fluid with constant velocity. Cookey *et al.* [37] studied the effect of viscous dissipation and radiation on unsteady MHD free convection flow past an infinite heated vertical plate in a porous medium with time-dependent suction. Kim [81] analyzed the unsteady MHD convective heat transfer past a semi-infinite vertical porous moving plate with suction.

Mohamed [99] investigated the double-diffusive convection -radiation interaction on unsteady MHD flow over a vertical moving porous plate with heat generation and soret effects and solved the set of differential equations analytically using the harmonic and non-harmonic functions. Roja *et al.* [130] investigated a model similar to that of Mohamed [99] except that the MHD flow was of micropolar fluid. Our current study focusses on the differential model by Mohamed [99] and we assume that the perturbation parameter, the coefficient of the highest derivative ϵ in the heat equation may become small enough to render it singularly perturbed. The solution of the singular perturbation problems is known to have large gradients within the boundary layer which affect the convergence of the solution obtained using the usual standard numerical approach. It is shown theoretically and numerically that the SFDM produces poor approximations when ϵ is very small. Hence the reason why we adopt the fitted operator finite difference method (FOFDM) which captures the behavior of the solution within the layer region.

A vast amount of literature exists on singularly perturbed partial differential equations (see Beckett and Mackenzie [16], Gracia and Lisbona [60], Patidar [121], Roos *et al.* [131], Miller *et al.* [96], Doolan *et al.* [51] and references therein.)

To the best of our knowledge no work has been done to study double-diffusive convection-

radiation interaction on unsteady MHD flow over a vertical moving porous plate with heat generation and thermal diffusion using the fitted operator finite difference method.

The rest of the chapter is organized as follows. In Section 5.2 we describe the model of our problem. Section 5.3 focusses on the numerical method and its analysis. Section 5.4 on the other hand deals with the presentation and discussion of the numerical results. Finally Section 5.5 is devoted to the conclusion of the chapter.

5.2 Description of the model

We consider a two dimensional unsteady flow of a laminar, viscous, incompressible, electrically conducting and heat generating fluid past a moving vertical semi-infinite porous plate immersed in a uniform porous medium in the presence of a transverse magnetic field with double-diffusive free convection, thermal diffusion, chemical reaction, and thermal radiation effects. Let the x^*-axis be directed upward along the plate and the y^*-axis normal to the plate. Let u^* and v^* be the velocity components along x^* and y^* axes respectively. Then the magnetohydrodynamic unsteady free convective boundary layer equations based on the balances of mass, momentum, heat, and concentration species [99] read

$$\frac{\partial v^*}{\partial y^*} = 0, \tag{5.2.1}$$

$$\rho\left(\frac{\partial u^*}{\partial t^*} + v^*\frac{\partial u^*}{\partial y^*}\right) = -\frac{\partial p^*}{\partial x^*} + \mu\frac{\partial^2 u^*}{\partial y^{*2}} - \rho g - \frac{\mu}{K^*}u^* - \frac{\sigma {B_O}^2}{\rho}u^*, \tag{5.2.2}$$

$$\frac{\partial T^*}{\partial t^*} + v^*\frac{\partial T^*}{\partial y^*} = \frac{\kappa}{\rho c_p}\frac{\partial^2 T^*}{\partial y^{*2}} + \frac{Q_o}{\rho c_p}\left(T^* - T^*_\infty\right) - \frac{1}{\rho c_p}\frac{\partial q_r}{\partial y^*}, \tag{5.2.3}$$

$$\frac{\partial C^*}{\partial t^*} + v^*\frac{\partial C^*}{\partial y^*} = D\frac{\partial^2 C^*}{\partial y^{*2}} + D_T\frac{\partial^2 T^*}{\partial y^{*2}} - K^*_l\left(C^* - {C^*}_\infty\right), \tag{5.2.4}$$

where, ν is the kinematic viscosity, K^* is the permeability of the porous medium, D is the coefficient of chemical molecular diffusivity, D_T is the coefficient of thermal diffusivity, ρ is the density, σ is the electrical conductivity of the fluid, g is the acceleration due to gravity, T^* is the temperature, T^*_∞ is the temperature of the fluid far away from the plate, C^* is the dimensional concentration, q_r is the local radiative heat flux, K_l is the reaction rate constant, Q_o is the heat generation constant, c_p is the specific heat capacity, B_0 is the magnetic induction. The

necessary boundary conditions [99] are

$$\begin{aligned} u^* &= u_p^*,\ T^* = T_w^* + \iota\left(T_w^* - T_\infty^*\right)e^{N^*t^*},\ C^* = C_w^* + \iota\left(C_w^* - C_\infty^*\right)e^{N^*t^*} \text{ at } y = 0, \\ u^* &= U_p^* = U_o\left(1 + \iota e^{N^*t^*}\right),\ T^* \to T_\infty^*,\ C^* \to C_\infty^* \text{ as } y \to \infty, \end{aligned} \tag{5.2.5}$$

where, T_w^* and C_w^* are the wall dimensional temperature and concentration respectively, C_∞^* is the stream dimensional concentration, U_o and N^* are constants.

From the continuity equation it is deduced that the suction velocity is a function of time only and it is assumed to take the form

$$v^* = -V_o\left(1 + \iota A e^{N^*t^*}\right), \tag{5.2.6}$$

where, A is a real positive constant, ι and ιA are less than unity and the non zero positive constant, V_o is a scale of suction velocity. Far from the plate we get

$$\rho\frac{dU_\infty^*}{dt^*} = -\frac{\partial p^*}{\partial x^*} - \rho_\infty g - \frac{\mu}{K^*}U^*{}_\infty - \rho B_o^* U^*. \tag{5.2.7}$$

By eliminating $\partial p^*/\partial x^*$ between equation (5.2.3) and (5.2.7) and using the equation of state [65]

$$\rho_\infty - \rho = \rho\beta\left(T^* - T_\infty^*\right) + \rho\beta^*\left(C^* - C_\infty^*\right), \tag{5.2.8}$$

we obtain

$$\begin{aligned} \frac{\partial u^*}{\partial t^*} + v^*\frac{\partial u^*}{\partial y^*} &= \frac{dU_\infty^*}{dt^*} + \nu\frac{\partial^2 u^*}{\partial y^{*2}} + g\beta\left(T^* - T_\infty^*\right) + g\beta^*\left(C^* - C_\infty^*\right) \\ &+ \frac{\nu}{K^*}\left(U_\infty^* - u^*\right) + \frac{\sigma B_o^2}{\rho}\left(U_\infty^* - u^*\right), \end{aligned} \tag{5.2.9}$$

where, β is the volumetric coefficient of thermal expansion, β^* the volumetric coefficient of expansion with concentration, ρ_∞ the density of the fluid far away from the surface and ν is the coefficient of kinematic viscosity.

Assuming the Rosseland approximations the radiative heat flux term is given by

$$q_r = -(4\rho^*/3k_1^*)\partial T^{*4}/\partial y^*, \tag{5.2.10}$$

where, ρ^* and k_1^* are the Stefan-Boltzman constant and the mean absorption coefficient respectively. Assuming that the temperature difference within the flow are so small that T^{*4} may be expressed as a linear function of the temperature. By using Taylor series expansion and neglecting higher order terms we get

$$T^{*4} \equiv 4T^{*3}_{\infty}T^* - 3T^{*4}_{\infty}. \tag{5.2.11}$$

By using equations (5.2.10) and (5.2.11) the heat equation is reduced to

$$\frac{\partial T^*}{\partial t^*} + v^*\frac{\partial T^*}{\partial y^*} = \frac{\kappa}{\rho c_p}\frac{\partial^2 T^*}{\partial y^{*2}} + \frac{Q_o}{\rho c_p}(T^* - T^*_{\infty}) + \frac{16\sigma^* T^{*3}_{\infty}}{3\rho c_p k^*_1}\frac{\partial^2 T^*}{\partial y^{*2}}. \tag{5.2.12}$$

We non-dimensionalize (5.2.4), (5.2.9) and (5.2.12) by introducing the following similarity variables

$$\begin{aligned} &v^* = uV_o,\ u^* = uU_o,\ y^* = y\mu/V_o,\ U^* = U_\infty U_o,\ u_p^* = U_p U_o,\ t^* = t\nu/V_o^2,\ N^* = (V_o^2 N_1)/\mu, \\ &K^* = K\mu/V_o^2,\ T^* = T^*_\infty + \theta\left(T^*_w - T^*_\infty\right),\ C^* = C^*_\infty + C\left(C^*_w - C^*_\infty\right), \end{aligned} \tag{5.2.13}$$

and obtain the following dimensionless differential equations,

$$\frac{\partial u}{\partial t} - \left(1 + \iota A e^{N_1 t}\right)\frac{\partial u}{\partial y} = \frac{dU}{dt} + \frac{\partial^2 u}{\partial y^2} + Gr\theta + G_m C + W\left(U_\infty - u\right), \tag{5.2.14}$$

$$\frac{\partial \theta}{\partial t} - \left(1 + \iota A e^{N_1 t}\right)\frac{\partial \theta}{\partial y} = \frac{1}{P_r}\left(1 + \frac{4R}{3}\right)\frac{\partial^2 \theta}{\partial y^2} + Q\theta, \tag{5.2.15}$$

$$\frac{\partial C}{\partial t} - \left(1 + \iota A e^{N_1 t}\right)\frac{\partial C}{\partial y} = \frac{1}{S_c}\frac{\partial^2 C}{\partial y^2} + S_o\frac{\partial^2 \theta}{\partial y^2} - \delta C, \tag{5.2.16}$$

subject to the following boundary conditions

$$u = U_p,\ \theta = 1 + \iota e^{N_1 t},\ C = 1 + \iota e^{N_1 t} \text{ as } y = 0, \tag{5.2.17}$$

$$u = U_\infty \to 1 + \iota e^{N_1 t},\ \theta \to 0,\ C \to 0 \text{ as } y \to \infty, \tag{5.2.18}$$

where,

$G_r = \nu\beta g\,(T_w^* - T_\infty^*)/V_o^2 U_o$ is the thermal Grashof number, $G_m = \nu\beta^* g\,(C_w^* - C_\infty^*)/V_o^2 U_o$ is the solutal Grashof number, $M = \sigma B_o^2 \nu/\rho V_o^2$ is the magnetic field parameter, $P_r = \nu\rho c_p/\kappa$ is the Prandtl number, $R = 4\sigma T_\infty^*/\kappa\kappa_1^*$ is the thermal radiation parameter, $S_c = \nu/D$ is the Schmidt number, $Q = \nu Q_o/\rho V_o^2 c_p$ is the dimensionless heat generation coefficient, $S_o = D\,(T_w^* - T_\infty^*)/\nu\,(C_w^* - C_\infty^*)$ is the soret number, $\delta = K_l\nu/D$ is the chemical reaction parameter and $W = M + 1/K$.

5.3 Construction and analysis of the numerical method

In this section we construct the numerical method followed by its analysis. We introduce the FOFDM to solve the energy equation. The FOFDM is compared with the standard finite difference method (SFDM) and the analytical approximate solution. The energy equation (5.2.15) is stated in the form

$$L\theta := \frac{\partial\theta}{\partial t} - \left(1 + \iota A e^{N_1 t}\right)\frac{\partial\theta}{\partial y} - \frac{1}{P_r}\left(1 + \frac{4R}{3}\right)\frac{\partial^2\theta}{\partial y^2} - Q\theta = 0. \tag{5.3.1}$$

We will approximate the solution above on a uniform mesh which we describe below.

Let N be a positive integer. Consider the following partition of the interval [0,4]:

$y_0 = 0,\ y_i = y_0 + ih,\ i = 1(1)N,\ h = y_i - y_{i-1},\ y_N = 4.$

Let τ be the uniform step size on

$$\Omega^{\tau,m} = \left\{(y, t_j) : y \in \Omega, t_j = j\tau = \frac{j}{m},\ \forall\ 0 < j \leq m\right\}. \tag{5.3.2}$$

Denote the approximation of θ by the unknown ϖ. Performing the time semi-discretization by Euler method at time level n gives

$$\frac{\varpi^n - \varpi^{n-1}}{\tau} - \left(1 + \iota A e^{N_1 t}\right)\varpi_y^n - \frac{1}{P_r}\left(1 + \frac{4R}{3}\right)\varpi^n{}_{yy} - Q\varpi^n = 0, \tag{5.3.3}$$

subject to

$$\varpi^n(0) = 1 + \iota e^{N_1 t} \text{ for } 0 < n < m, \tag{5.3.4}$$

$$\varpi^n(4) = 0 \text{ for } 0 \leq n < m. \tag{5.3.5}$$

We rewrite (5.3.3) as

$$-\epsilon\, \varpi^n_{yy} - \left(1 + \iota A e^{N_1 t}\right) \varpi^n_y + \left(\frac{1}{\tau} - Q\right) \varpi^n = \frac{1}{\tau}\varpi^{n-1}. \tag{5.3.6}$$

subject to

$$\varpi^n(0) = \left(1 + \iota e^{N_1 t}\right) \text{and } \varpi^n(4) = 0, \tag{5.3.7}$$

where $\epsilon = (1/P_r)\,(1 + 4R/3)$. For the sake of simplicity we omit the time level label "n" in (5.3.6). We are therefore concerned with the problem of finding ϖ such that

$$-\epsilon\varpi''(y) - \left(1 + \iota e^{N_1 t}\right) \varpi' + \left(\frac{1}{\tau} - Q\right) \varpi(y) = \frac{1}{\tau}\varpi^*, \tag{5.3.8}$$

subject to

$$\varpi(0) = 1 + \iota e^{N_1 t} \text{ and } \varpi(4) = 0, \tag{5.3.9}$$

where ϖ^* is the value of ϖ at the previous time level $n - 1$.

The following lemma provides bounds on the solution of the problem (5.3.8)-(5.3.9).

Lemma 5.3.1. *Let ϖ be the solution of (5.3.8)-(5.3.9). Then for $0 \leq k \leq 4$,*

$$|\varpi^{(k)}(y)| \leq \widetilde{C}\left(1 + \epsilon^{-k} e^{-\lambda y/\epsilon}\right)$$

for all $y \in \overline{\Omega} = [0, 4]$, where $0 < \epsilon \leq 1$, $\widetilde{C}$ is independent of ϵ, and $0 < \lambda < \left(1 + \iota A e^{N_1 t}\right)$.

Proof. See [96].

Discretizing (5.3.8) in space using the standard finite difference method and denoting the approximation of ϖ by $\widetilde{\nu}$ to give

$$\mathcal{L}^{h,\tau}\nu_j \equiv -\epsilon\, \frac{\widetilde{\nu}_{j+1} - 2\widetilde{\nu}_j + \widetilde{\nu}_{j-1}}{h^2} - \left(1 + \iota A e^{N_1 t}\right) \frac{\widetilde{\nu}_{j+1} - \widetilde{\nu}_j}{h} + \left(\frac{1}{\tau} - Q\right) \widetilde{\nu}_j = \frac{1}{\tau}\widetilde{\nu^*}_j. \tag{5.3.10}$$

We will show later that for relatively small values of ϵ, the SFDM fails to provide fairly accurate approximation of the true solution by comparing the maximum absolute errors calculated. To obtain reliable results we discretize (5.3.8) as follows,

$$L^{h,\tau}u_j \equiv -\epsilon\,\frac{u_{j+1}-2u_j+u_{j-1}}{\psi_j^2}-\left(1+\iota Ae^{N_1 t}\right)\frac{u_{j+1}-u_j}{h}+\left(\frac{1}{\tau}-Q\right)u_j=\frac{1}{\tau}u_j^*. \tag{5.3.11}$$

and

$$\psi_j^2=\frac{\epsilon\left(1+\frac{4R}{3}\right)h}{\left(1+\iota Ae^{N_1 t}\right)}\left(\exp\left(\frac{\left(1+\iota Ae^{N_1 t}\right)h}{\epsilon\left(1+\frac{4R}{3}\right)}\right)-1\right). \tag{5.3.12}$$

The proposed scheme (5.3.11) and (5.3.12) is refered to as FOFDM. The function ψ_j^2 captures the behavior of the solution in the boundary layer region which is located in the near the left end of the interval.

Next we analyze the FOFDM. The local truncation error of the time semi-discritization by the forward implicit Euler scheme is denoted by $\widetilde{e_n}=\theta(y,t_n)-\varpi(y)$, where $\varpi(y)$ is the solution of (5.3.6). The amount of error $\widetilde{e_n}$ is the contribution of each time step to the global error of the time semi-discretizaton. The following lemmas depict the order of the local and global error related to the problem (5.3.6).

Lemma 5.3.2. (Local error estimate) *If* $|\varpi^{(k)}(y)|\leq\widetilde{C},\ y\in[0,4],\ 0\leq k\leq 2$, *then the local error estimate is given by* $||\widetilde{e_n}||\leq\widetilde{C}\tau^2$.

The following lemma relates to the global error, E_n.

Lemma 5.3.3. (Global error estimate) *The global error* $E_n=\Sigma_{n=0}^{m}\widetilde{e_n}$ *satisfies*

$$||E_n||\leq\widetilde{C}\tau,\ \forall\ 1\leq n\leq m.$$

We discretize in space and find the local truncation error $|(\varpi-u)|$ where ϖ is the exact solution with respect to space and u is the approximation of θ for the FOFDM. The following lemmas are pivotal in the analysis of the error of the solution obtained using the FOFDM. We will show later that for relatively small values of ϵ, the SFDM fails to provide fairly accurate approximation of the true solution by comparing the maximum absolute errors calculated. To obtain reliable results we discretize (5.3.8) as follows, We analyse the FOFDM (5.3.11)

for stability and convergence. The differential operator $L^{h,\tau}$ in (5.3.11) satisfies the following discrete maximum principle on Ω,

Lemma 5.3.4. (Discrete maximum principle) *Assume that the mesh function ϕ_i satisfies $\phi_0 \geq 0$ and $\phi_n \geq 0$. Then, $L^{h,\tau}\phi_i \geq 0$ for $i = 1(1)n-1$ which implies that $\phi_i \geq 0$ $\forall i$=0(1)n.*

Proof. The proof follows the same lines as the proof of the discrete maximum principle in [96] as shown below. Choose k such that $\phi_k = \min_i \phi_i$ and suppose that $\phi_i \leq 0$. Then $k \notin \{0, n\}$, $\phi_{k+1} - \phi_k \geq 0$ and $\phi_k - \phi_{k-1} \leq 0$. Thus

$$\begin{aligned} L^{h,\phi_k} &= -\epsilon \frac{\phi_{k+1} - 2\phi_k + \phi_{k-1}}{\psi_k^2} - a\frac{\phi_{k+1} - \phi_k}{h} + b\phi_k, \\ &= -\epsilon \frac{\phi_{k+1} - \phi_k + \phi_{k-1} - \phi_k}{\psi_k^2} - a\frac{\phi_{k+1} - \phi_k}{h} + b\phi_k \\ &< 0, \end{aligned}$$

a clear contradiction. Then

$$\phi_k \geq 0, \text{ which implies } \phi_i \geq 0, \ \forall i = 1(1)n, \text{ which completes the proof.}$$

The following lemma is a consequence of the discrete maximum principle.

Lemma 5.3.5. (Uniform stability estimate) *If ξ_i is any mesh function such that $\xi_0 = \xi_n = 0$ then*

$$|\xi_i| \leq \frac{4}{\lambda} \max_{1 \leq j \leq n-1} \left| L^h \xi_j \right| \text{ for } 0 \leq i \leq n.$$

Proof. Let

$$\widetilde{C} = \frac{1}{\lambda} \max_{1 \leq j \leq n-1} |L^n \xi_j|,$$

and introduce the mesh functions $\vartheta_i^+, \vartheta_i^-$ defined by $\vartheta_i^{\pm} = \widetilde{C}(4 - y_i) \pm \xi_i$. From (5.3.11), we

have

$$\begin{aligned} L^{h,\tau}\vartheta_i^{\pm} &= -\epsilon\frac{\vartheta_{i+1}^{\pm}-2\vartheta_i^{\pm}+\vartheta_{i-1}^{\pm}}{\psi_i^2}-a_i\frac{\vartheta_{i+1}^{\pm}-\vartheta_i^{\pm}}{h}+b_i\vartheta_i^{\pm}, \\ &= -\epsilon\frac{\pm\xi_{i+1}\mp 2\xi_i\pm\xi_{i-1}}{\psi_i^2}-a_i\frac{(\pm\xi_{i+1}\mp\xi_i)}{h}+b_i(\pm\xi_i)+\widetilde{C}a_i, \\ &= \pm L^{h,\tau}\xi_i+\widetilde{C}a_i+b_i\widetilde{C}(4-y_i), \\ &= \pm L^{h,\tau}\xi_i+\frac{a_i+b_i(4-yi)}{\lambda}\max_{\Omega}\left|L^{h,\tau}\xi_i\right| \\ &\geq 0, \end{aligned} \tag{5.3.13}$$

since $a_i/\lambda \geq 1$.

By the maximum principle, it implies that

$$\vartheta_i^{\pm} \geq 0 \text{ for } 0 \leq i \leq n,$$

and

$$\vartheta_i^{\pm} = \widetilde{C}(4-\ y_i) \pm \xi_i \geq 0 \text{ for } 0 \leq y_i \leq 4.$$

Since $4 - y_i \leq 4$,

$$|\xi_i| \leq \widetilde{C}(4-y_i) \leq 4\widetilde{C},$$

and therefore

$$|\xi_i| \leq \frac{4}{\lambda}\max_{1\leq j\leq n-1}\left|L^n\xi_j\right|,$$

which completes the proof.

Our next attempt is to establish the local truncation error of the SFDM and the FOFDM. In the analysis $\widetilde{M}$ and $\widetilde{S}$ denote positive constants independent of h and ϵ and may assume different values in different equations and inequalities.The local truncation error of the SFDM (5.3.10) is given by

$$\left|\mathcal{L}^{h,\tau}(\theta-\widetilde{u})_j\right| = \left|\mathcal{L}^{h,\tau}(\theta-\varpi+\varpi-\widetilde{u})_j\right| = \left|\mathcal{L}^{h,\tau}(\theta-\varpi)_j\right| + \left|\mathcal{L}^{h,\tau}(\varpi-\widetilde{u})_j\right|. \tag{5.3.14}$$

From lemma 5.3.3

$$\left|\mathcal{L}^{h,\tau}(\theta-\varpi)_j\right| = \widetilde{M}\tau. \tag{5.3.15}$$

The truncation error for the spatial descretization of the SFDM is given by

$$\begin{aligned}\left[\mathcal{L}^{h,\tau}(\varpi-\widetilde{u})_j\right] &= -\epsilon\ \varpi_j'' - B\varpi_j' + \left(\frac{1}{\tau}-Q\right)\varpi_j - \left(-\epsilon\ \frac{\varpi_{j+1}-2\varpi_j+\varpi_{j-1}}{h^2}\right)\\ &\quad +B\frac{\varpi_{j+1}-\varpi_j}{h} - (\frac{1}{\tau}-Q)\varpi_j,\\ &= -\epsilon\varpi_j'' + \frac{\epsilon}{h^2}\left[h^2\varpi_j'' + \frac{h^4}{12}\varpi^{(iv)}(\zeta_1)\right]\\ &\quad +\frac{Bh}{2}\left(\varpi_j'' + \frac{h}{3}\varpi_j''' + \frac{h^2}{12}\varpi^{(iv)}(\zeta_2)\right),\\ &= \frac{B}{2}\varpi_j''h + \left(\frac{\epsilon}{12}\varpi^{(iv)}(\zeta_1) + \frac{B}{6}\varpi_j'''\right)h^2 + \frac{B}{24}\varpi^{(iv)}(\zeta_2)h^3, \end{aligned}\tag{5.3.16}$$

where $B = \left(1+\iota Ae^{N_1 t}\right)$, $\zeta_1 \in (y_{j-1}, y_{j+1})$ and $\zeta_2 \in (y_j, y_{j+1})$. Now

$$\begin{aligned}\left|\mathcal{L}^{h,\tau}(\varpi-\widetilde{u})_j\right| &= \left|\frac{B}{2}\varpi_j''h + \left(\frac{\epsilon}{12}\varpi^{(iv)}(\zeta_1) + \frac{B}{6}\varpi_j'''\right)h^2 + \frac{B}{24}\varpi^{(iv)}(\zeta_2)h^3\right|,\\ &\leq \left|\frac{B}{2}\varpi_j''\right|h + \left|\left(\frac{\epsilon}{12}\varpi^{(iv)}(\zeta_1) + \frac{B}{6}\varpi_j'''\right)\right|h^2\\ &\quad +\left|\frac{B}{24}\varpi^{(iv)}(\zeta_2)\right|h^3. \end{aligned}\tag{5.3.17}$$

Using Lemma 5.3.1 we obtain

$$\begin{aligned}\left|L^{h,\tau}(\varpi-\widetilde{\nu})_j\right| &\leq \frac{\widetilde{C}B}{2}\left(1+\epsilon^{-2}e^{-\lambda y/\epsilon}\right)h + \frac{\widetilde{C}\epsilon}{12}\left(1+\epsilon^{-4}e^{-\lambda y/\epsilon}\right)h^2\\ &\quad +\frac{B\widetilde{C}}{6}\left(1+\epsilon^{-3}e^{-\lambda y/\epsilon}\right)h^2 + O(h^3).\end{aligned}$$

Using Lemma 7 in [103]

$$\begin{aligned}\left|L^{h,\tau}(\varpi-\widetilde{\nu})_j\right| &\leq \frac{\widetilde{C}B}{2}h + \left(\frac{\widetilde{C}}{12}+\frac{B\widetilde{C}}{6}\right)h^2 + O(h^3),\\ &\leq \widetilde{M}h. \end{aligned}\tag{5.3.18}$$

Then by Lemma 5.3.5 and (5.3.18) we have

$$\begin{aligned}\max_{0\leq i\leq n}|(\varpi-\widetilde{\nu})_i| &\leq \max_{1\leq j\leq n-1}\left|L^{h,\tau}(\varpi-\widetilde{\nu})_j\right|,\\ &\leq \widetilde{M}h. \end{aligned} \tag{5.3.19}$$

From equations (5.3.15) and (5.3.18) the local truncation error of SFDM is given by

$$\begin{aligned}\left|L^{h,\tau}(\theta-\widetilde{\nu})_j\right| &= \left|L^{h,\tau}(\theta-\varpi+\varpi-\widetilde{\nu}_j\right|,\\ &\leq \left|L^{h,\tau}(\theta-\varpi)_j\right|+\left|L^{h,\tau}(\varpi-\widetilde{\nu})_j\right)|,\\ &\leq \widetilde{M}\left(\tau+h\right). \end{aligned} \tag{5.3.20}$$

Then using Lemma 5.3.5 to estimate the bounds on $|(\theta-\widetilde{\nu})|$, we get

$$\max_{0\leq i\leq n}|(\theta-\widetilde{\nu})_i| \leq \max_{1\leq j\leq n-1}\left|L^{h,\tau}(\theta-\widetilde{\nu})_j\right| \leq \widetilde{M}\left(\tau+h\right). \tag{5.3.21}$$

Similarly, the local truncation error of the FOFDM (5.3.11) is given by

$$\left|L^{h,\tau}(\theta-u)_j\right| = \left|L^{h,\tau}(\theta-\varpi+\varpi-u)_j\right| = \left|L^{h,\tau}(\theta-\varpi)_j\right|+\left|L^{h,\tau}(\varpi-u)_j\right|. \tag{5.3.22}$$

From lemma 5.3.3

$$\left|L^{h,\tau}(\theta-\varpi)_j\right| = \widetilde{S}\tau. \tag{5.3.23}$$

The truncation error for the spatial descretization is given by

$$\begin{aligned}\left[L^{h,\tau}(\varpi-u)_j\right] &= -\epsilon\varpi_j''-B\varpi_j'+\left(\frac{1}{\tau}-Q\right)\varpi_j\\ &\quad -\left(-\epsilon\frac{\varpi_{j+1}-2\varpi_j+\varpi_{j-1}}{\psi_j^2}-B\frac{\varpi_{j+1}-\varpi_j}{h}\right)\\ &\quad +\left(\frac{1}{\tau}-\eta\right)\varpi_j,\\ &= -\epsilon\varpi_j''-B\varpi_j'+\frac{\epsilon}{\psi_j^2}\left[h^2\varpi_j''+\frac{h^4}{12}\varpi^{(iv)}(\zeta_1)\right]\\ &\quad +\frac{Bh}{2}\left(\varpi_j''+\frac{h}{3}\varpi_j'''+\frac{h^2}{12}\varpi^{(iv)}(\zeta_2)\right), \end{aligned}$$

where $\zeta_1 \in (y_{j-1}, y_{j+1})$ and $\zeta_2 \in (y_j, y_{j+1})$. Using the Taylor series expansion, we have

$$\frac{\epsilon}{\psi_j^2} = \frac{\epsilon}{h^2} - \frac{B}{2h} + \dots. \tag{5.3.24}$$

This implies that

$$\begin{aligned}\left[L^{h,\tau}(\varpi - u)_j\right] &= -\epsilon\varpi_j'' \\ &\quad + \left[\frac{\epsilon}{h^2} - \frac{B}{2h} + \dots\right]\left[h^2\varpi_j'' + \frac{h^4}{12}\varpi^{(iv)}(\zeta_1)\right] \\ &\quad + \frac{Bh}{2}\left(\varpi_j'' + \frac{h}{3}\varpi_j''' + \frac{h^2}{12}\varpi^{(iv)}(\zeta_2)\right).\end{aligned} \tag{5.3.25}$$

Further simplifications lead to

$$\left[L^{h,\tau}(\varpi - u)_j\right] = \left[\frac{\epsilon\varpi_j^{(iv)}}{12} + \frac{B\varpi_j'''}{6}\right]h^2 + O(h^5).$$

Using Lemma 5.3.1 we obtain

$$\left|L^{h,\tau}(\varpi - u)_j\right| \leq \left|\frac{\widetilde{C}\epsilon}{12}\left(1 + \epsilon^{-4}e^{-\lambda y/\epsilon}\right) + \frac{\widetilde{C}B}{6}\left(1 + \epsilon^{-3}e^{-\lambda y/\epsilon}\right)\right|h^2 + O(h^5).$$

Now applying Lemma 7 in [103]

$$\begin{aligned}\left|L^{h,\tau}(\varpi - u)_j\right| &\leq \widetilde{C}\left(\frac{\epsilon h^2}{12} + \frac{Bh^2}{6}\right) + O(h^5), \\ &\leq \widetilde{S}h^2,\end{aligned} \tag{5.3.26}$$

since $\epsilon h^2 < h^2$. Then by Lemma 5.3.1 and (5.3.26) we have

$$\begin{aligned}\max_{0\leq i\leq n}\left|(\varpi - u)_i\right|, &\leq \max_{1\leq j\leq n-1}\left|L^{h,\tau}(\varpi - u)_j\right|, \\ &\leq \widetilde{S}h^2.\end{aligned} \tag{5.3.27}$$

From equations (5.3.23) and (5.3.27) the local truncation error of FOFDM is given by

$$\begin{aligned}\left|L^{h,\tau}(\theta-u)_j\right| &= \left|L^{h,\tau}(\theta-\varpi+\varpi-u)_j\right|, \\ &\leq \left|L^{h,\tau}(\theta-\varpi)_j\right| + \left|L^{h,\tau}(\varpi-u_j)\right|, \\ &\leq \widetilde{S}\left(\tau+h^2\right). \end{aligned} \tag{5.3.28}$$

Then using Lemma 5.3.5 to estimate the bounds on $|(\theta-u)|$, we get

$$\max_{0\leq i\leq n}|(\theta-u)_i|, \quad \leq \quad \max_{1\leq j\leq n-1}\left|L^{h,\tau}(\theta-u)_j\right| \leq \widetilde{S}\left(\tau+h^2\right).$$

We therefore establish that

$$\max_{0\leq i\leq n}|(\theta-u)_i| \leq \widetilde{S}\left(\tau+h^2\right). \tag{5.3.29}$$

5.4 Results and discussions

In this section we begin by presenting some numerical results followed by a discussion on the results.

The pointwise errors are estimated as:

$$e^{\Delta t,N}(y,t) = |u^N(y,t) - u^{2N}(y,t)|,$$

where N is the spatial discretization parameter, Δt is the time descritization parameter and w is the numerical solution. The maximum absolute error at all mesh points are evaluated using the double mesh principle

$$E^{N,\Delta t} = \max_N e^{\Delta t,N}(y,t),$$

and the rates of convergence are computed using the formula([60])

$$r_N = \frac{\log(E^{N,\Delta t}/E^{2N,\Delta t/4})}{\log 2}.$$

Equation (5.3.1) is solved using the standard finite difference method and the fitted operator finite difference method. The accuracy of a numerical method is achieved by computing the maximum absolute errors as depicted in Tables 5.4.1.

Table 5.4.1: Maximum absolute errors and orders of convergence associated with SFDM and FOFDM for $V_o = 0.2$, $\iota = 0.2$, $t = 1$, $\tau = 0.02$, $Q = 0.1$, $A = 0.5$, $R = 0.5$.

P_r	N	10	20	40	80
	Δt	0.02	0.02/4	$0.02/4^2$	$0.02/4^3$
5	SFDM	8.17E-2	5.30E-2	3.15E-2	1.74E-2
	r_N	0.62	0.75	0.86	
	FOFDM	1.88E-3	4.49E-4	1.11E-4	2.76E-5
	r_N	0.74	2.06	2.00	
10	SFDM	1.08E-1	8.704E-2	5.58E-2	3.27E-2
	r_N	0.31	0.64	0.77	
	FOFDM	1.11E-3	3.08E-4	7.27E-5	1.83E-5
	r_N	1.85	2.08	1.99	
20	SFDM	1.02E-1	1.14E-1	8.88E-2	5.66E-2
	r_N	-	0.36	0.65	
	FOFDM	1.23E-4	8.44E-5	1.54E-5	3.70E-6
	r_N	0.54	2.45	2.06	
40	SFDM	7.52E-2	1.07E-1	1.14E-1	8.88E-2
	r_N	-	-	0.36	
	FOFDM	6.13E-7	4.54E-6	2.82E-7	4.30E-7
	r_N	-	4	-	

The maximum absolute error values inform us on the closeness of the solution of a numerical method to the exact solution. For a fixed value of ϵ the maximum absolute error decreases as the number of grid points, N increases. The table of results suggests that the SFDM and FOFDM are first order and second order convergent respectively. The result agrees with theoretical results which showed that for SFDM and the FOFDM the local truncation error is first order and second order respectively (see equation (5.3.20) and (5.3.28)). The table also show that the maximum absolute errors of the FOFDM are smaller than that of the SFDM whereas the order of convergence is larger for the FOFDM than for the SFDM. Since the value of ϵ can assume small values in this paper we use the FOFDM to analyze the temperature, velocity, and concentration profiles of the double diffusive MHD convective flow. It is observed from Figure 5.4.1(a) that for small Prandtl number P_r the solution of both the

SFDM and the FOFDM are close to the exact solution. As potrayed by Figure 5.4.1(a) the solution of the FOFDM almost coinicides with the exact solution and so the solution of the FOFDM is better than the solution of the SFDM. As depicted in Figure 5.4.1(b) when the value of P_r is increased the solution of the FOFDM remains close to the exact solution where as the solution of the SFDM differs significantly from the analytical solution. Figure 5.4.1(c) depicts the effect of the radiation parameter R, Prandtl number P_r and heat generation Q on the temperature profile. We observed that as the value of the radiation parameter R increases the temperature profile increases. It is also shown in Figure 5.4.1(c) that an increase in the Prandtl number P_r decreases the thermal boundary layer thickness. In other words an increase in P_r results in faster cooling of the plate. It is further illustrated in Figure 5.4.1(c) that an increase of the heat generation parameter Q increases the temperature profile.

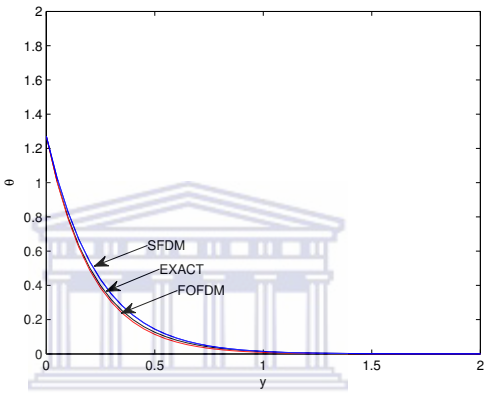

(a) Temperature profiles for different methods for $P_r = 7$, $R = 0.5$, $\iota = 0.1$, $t = 1$, $Q = 1$.

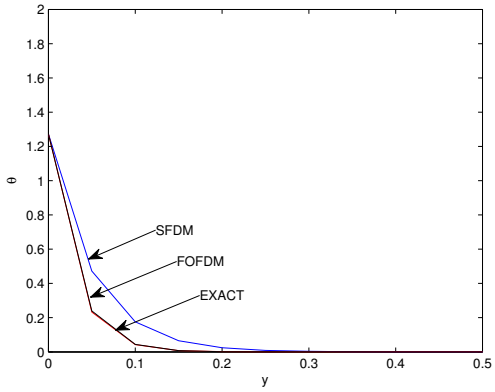

(b) Temperature profiles for the different methods for $P_r = 50$, $R = 0.5$, $Q = 1$.

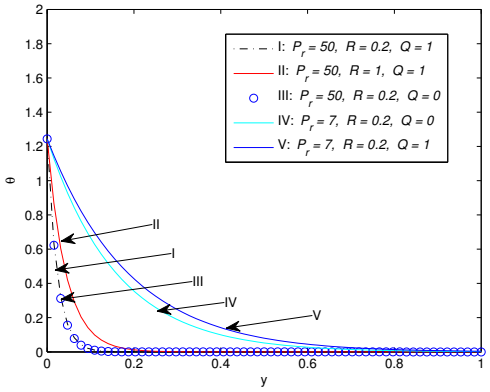

(c) The effect of R, P_r and Q on the temperature profile.

Figure 5.4.1: Temperature profiles for $\iota = 0.2$, $A = 0.5$, $t = 1$, $N = 64$.

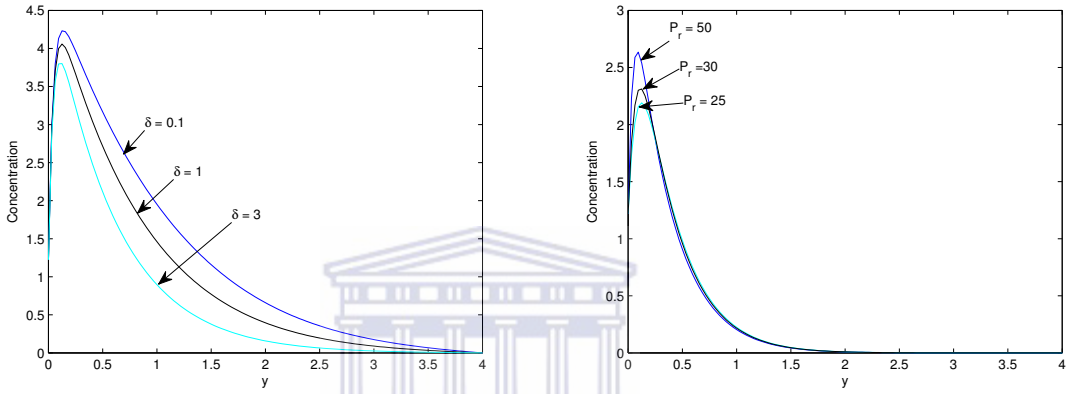

(a) The effect of δ on the concentration profile for $P_r = 50$, $S_c = 0.1$, $S_o = 5$.

(b) The effect of P_r on the concentration profile for $\delta = 1$, $S_c = 0.1$, $S_o = 5$.

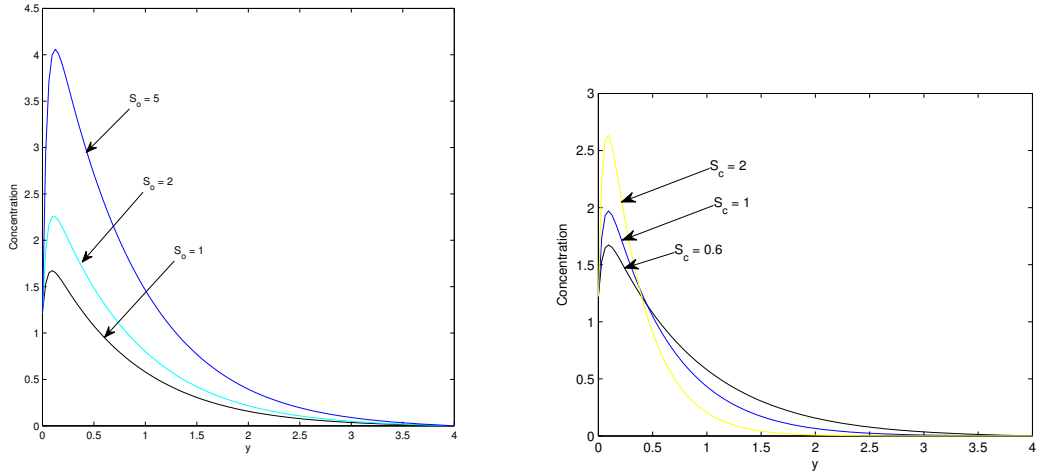

(c) The effect of S_o on the concentration profile for $P_r = 50$, $S_c = 0.6$, $\delta = 1$.

(d) The effect of S_c on the concentration profile for $P_r = 50$, $\delta = 1$, $S_o = 1$.

Figure 5.4.2: Concentration profiles for $\iota = 0.2$, $A = 0.5$, $Q = 1$, $N = 64$.

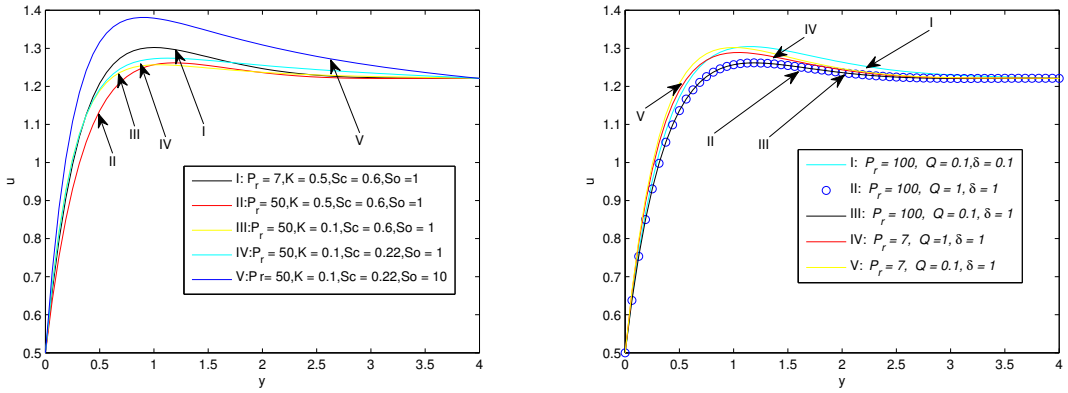

(a) The effect of P_r, K, S_c, and S_o on the velocity profile for $G_m = 1.0$, $\delta = 1$, $\iota = 0.2$

(b) The effect of Q and δ on the velocity profile for $G_r = 2$, $G_m = 1$, $\iota = 0.2$.

Figure 5.4.3: Velocity Profiles for $A = 0.5$, $\tau = 0.2$, $N = 64$.

Figures 5.4.2(a) - 5.4.2(d) presents the effects of the parameters δ, P_r, S_o and S_c on the concentration profile. Figure 5.4.2(a) shows that an increase in the chemical reaction parameter δ decreases the concentration distribution across the boundary layer.

The concentration profile increases as the Prandtl number P_r increases as depicted in Figure 5.4.2(b). Figure 5.4.2(c) shows that the concentration profile increases with increasing Soret number S_o. The concentration profile increases near the vertical porous plate and decreases far away from the porous plate as the Schmidt number increases as illustrated in Figure 5.4.2(d).

Figure 5.4.3(a) displays the velocity profile for various values of the Prandtl number P_r, Soret number So, permeability parameter K and Schmidt number S_c. It is observed that increasing the values of the Schmidt number S_c results in the decrease of the velocity distribution across the boundary layer. It is depicted in the same Figure that as the Soret number S_o increases the velocity profile increases. In other words the velocity increases due to greater thermal diffusion. It is also shown that as the Prandtl number P_r increases, the velocity profile decreases. Figure 5.4.3(a) also shows that as the permeability parameter K increases, the velocity profile decreases near the vertical plate and increases far away from the plate.

Figure 5.4.3(b) depicts the effect of heat generation Q and the chemical reaction parameter δ on the velocity profile. It is shown that for small Prandtl number P_r, the velocity profile increases with increasing heat generation parameter Q. However, for large Prandtl number

$P_r = 50$ say, there is no noticeable change in the velocity profile as the values of Q are varied. Figure 5.4.3(b) also shows that the increase in the chemical reaction parameter δ results in the increase of the velocity profile. The accuracy of our method is ascertained by calculating the numerical values of the skin friction coefficient C_f and $NuRe^{-1}$ where Nu is the Nusselt number and Re_x is the Reynolds number. These values are compared with those obtained by Mohamed [99] as depicted in Table 5.4.2 and Table 5.4.3.

Table 5.4.2: Numerical values of C_f for $P_r = 0.71, G_r = 2, M = 0.0, U_p = 0.5, \iota = 0.2, t = 1, N_1 = 0.1, A = 0.5, R = 0.5, Q = 0.1, \delta = 1$.

So	G_r	S_c	Mohamed [99] C_f	Our Method C_f
0.0	1.0	0.6	3.9338820	3.9338810
1.0	0.0	0.6	3.3651510	3.3651510
1.0	1.0	0.22	3.9740650	3.9676878

Table 5.4.3: Numerical values of $NuRe_x^{-1}$ for $P_r = 0.71, G_r = 2, M = 0.0, U_p = 0.5, \iota = 0.2, t = 1, N_1 = 0.1, A = 0.5, R = 0.5, Q = 0.1, \delta = 1$.

So	G_r	S_c	Mohamed [99] $NuRe_x^{-1}$	Our Method $NuRe_x^{-1}$
0.0	1.0	0.6	0.6781036	0.6781936
1.0	0.0	0.6	0.6781036	0.6781036
1.0	1.0	0.22	0.6781036	0.6781036

5.5 Summary

In this chapter, we analyzed the effect of a first order homogenous chemical reaction and thermal radiation on MHD free convection heat and mass transfer of viscous fluid past a semi-infinite vertical moving plate with heat generation and soret effects. The governing equations are solved numerically. The fitted numerical method is applied on the singularly perturbed part of the differential model. The perturbation parameter ϵ is a function of P_r and R where R is small and P_r can assume very large values. As ϵ become smaller and smaller the SFDM fails to give reliable results except for the FOFDM. We observed that the truncation

error for the FOFDM is second order convergent. Since we assumed small values of ϵ we used the FOFDM to analyze the temperature, concentration and velocity profiles as different parameters vary. We deduced the following.

- Temperature increases with increase in the value of the radiation parameter R and heat generation parameter Q and it decreases with the increase in the value of the Prandtl number P_r.

- Concentration increases with increase in the value of the Prandtl number, Soret number S_o, and Schmidt number S_c near the plate and it decreases with increasing chemical reaction parameter δ, Schmidt number S_c far away from the plate.

- Velocity increases with increase in the value of the Soret number S_o, chemical reacton parameter δ, and permeability parameter K far from the plate. On the other hand the velocity decreases with an increase in the value of Prandtl number P_r, permeability parameter K near the plate and Schmidt number S_c.

In the next chapter, we study the effects of thermophoresis, viscosity, chemical reaction and radiation on MHD flow over an inclined plate.

Chapter 6

A fitted numerical method to investigate the effect of thermophoresis, viscosity, chemical reaction and radiation on an MHD flow over an inclined plate

The fitted numerical method on unsteady transient MHD free convective and mass transfer flow with thermophoresis past an inclined permeable plate in the presence of chemical reaction, thermal radiation and temperature dependent viscosity is investigated. We design a suitable fitted operator finite difference method (FOFDM) to solve a model constructed by Alam *et al.* [8]. The governing non-linear partial differential equations in the current model are transformed by a suitable similarity transformation to a system of ordinary differential equations which are then solved numerically using the fitted operator finite difference method (FOFDM). The superiority of the proposed FOFDM over the standard finite difference method (SFDM) is proved theoretically and numerically. Furthermore, we illustrate the effect of various parameters on the temperature, concentration and velocity profiles using the FOFDM. It is observed that an increase in the viscosity parameter leads to a decrease in

the temperature and an increase in the velocity. Results also show that an increase in the thermophoretic parameter leads to a decrease in the concentration.

6.1 Introduction

The simulation of the solution of a transient MHD free convective heat and mass transfer flow with thermophoresis past an inclined permeable plate in the presence of chemical reaction and temperature dependent viscosity using the the FOFDM is carried out. Existence of a temperature gradient in a gas medium causes small particles in the gas to move in the direction of decreasing temperature. A consequence of the temperature gradient is that the average velocities of gas molecules colliding on one side of a molecule is different from the average velocities of gases colliding on the other side, a phenomenon termed 'thermophoresis'. When a cold plate is placed in the hot particle laden gas flow, particles are deposited on it due to the thermophoretic force. The magnitude of the thermophoretic force is a function of the gas properties, particle properties and the temperature gradient. Thermophoretic deposition finds application in the production of optical fibre, production of ceramic powders in high temperatures aerosol flow reactors and in polymer separation.

According to Alam *et al.* [8] thermophoresis is worth considering if the particle involved are around 10mm in radius and the temperature gradient is of order 5K/mm. Mills *et al.* [97] studied the effect of wall suction and thermophoresis on aerosol-particle deposition from a laminar boundary layers on a flat plate. Thakurta *et al.* [161] did numerical computations on the deposition rate of small particles on the wall of a turbulent channel flow by employing the direct numerical simulation (DNS). Ye *et al.* [163] on the other hand studied the thermophoretic effect of particle deposition on a free standing semi conductor wafer in a clean environment. Han and Yoshida [63] analyzed numerically the cluster thermal plasma deposition process under the effects of thermophoresis. In their study Han and Yoshida [63] found out that the thickness of the concentration boundary layer was suppressed by the thermophoretic force and therefore concluded that the effect of thermophoresis play a more dominant role than that of diffusion. Alam *et al.* [7] studied numerically the effect of thermophoresis on surface deposition flux on hydromagnetic free convective heat and mass transfer flow along a semi infinite permeable inclined flat plate taking into account heat generation. It was deduced

that thermophoresis enhances surface mass flux. Walker *et al.* [162] studied the deposition efficiency of a small particle caused by thermophoresis in a laminar flow in a tube.

The study on thermophoresis presented so far ignored the effect of thermal radiation yet there are numerous high temperature systems such as heat exchangers and internal combustion in which the effect of radiation may not be ignored in comparison with heat transfer by conduction and convection. Yoa *et al.* [164] studied numerically the thermophoresis in a laminar tube flow taking into account the particle radiation. Akbar and Ghiaasiaan [4] analyzed numerically the combined effects of radiation heat transfer and thermophoresis on the transport of mono-disperse and poly-disperse soot particle. Sohn *et al.* [150] studied the radiation effect on the thermophoresis for a gas-particle two phase laminar flow. Recently Alam *et al.* [5] studied numerically the thermal radiation interaction of thermophoresis on free-forced convection heat and mass transfer flow along a semi-infinite permeable inclined flat plate.

The existence of chemical reaction in convective heat and mass transfer process affect the diffusion rate. The effect of a chemical reaction depends on whether the reaction is heterogenous or homogenous. A heterogenous reaction occur at an interface whereas a homogenous reaction occur as a single phase volume reaction. A reaction is said to be of order m, if the reaction rate is proportional to the m-th power of the concentration. It follows then that a reaction is first order if the rate of the reaction is directly proportional to the concentration.

Most fluids have foreign bodies present in them which causes some kind of chemical reaction. The study or analysis of such reactions is helpful in enhancing or improving processes such as polymer production and food processing. The problem of first order chemical reaction in the neighborhood of a flat plate for both destructive and generative reaction was studied by Chambre and Young [25]. Das *et al.* [42] analyzed the effect of first order homogenous reaction on the flow past an impulsively started infinite vertical plate in the presence of uniform heat flux and mass transfer. Muthucumaraswamy and Ganesan [110] analyzed the effect of a chemical reaction on an unsteady flow past an impulsively started vertical plate with uniform mass flux in the presence of heat transfer. Recently Alam *et al.* [5] analyzed the effects of thermophoresis and first order chemical reaction on unsteady hydromagnetic free convection and mass transfer flow past an impulsively started infinite inclined porous plate in the presence of heat generation/absorption.

Most studies mentioned so far assume constant fluid physical properties. It is known however that some physical properties such as viscosity, change with temperature. To predict accurately the flow behavior and heat transfer rate the variation of viscosity deserve consideration. In line with this argument Kafoussias and William [78] analyzed the thermal diffusion and diffusion thermo effects on mixed free-forced convective mass transfer boundary layer flow with temperature dependent viscosity. The effect of variable viscosity on hydrodynamic flow and heat transfer past a continuously moving porous boundary with radiation was studied by Seddeck [139]. Recently, Molla and Hossain [100] analyzed the effects of chemical reaction, heat and mass diffusion in natural convection flow from an isothermal sphere with temperature dependent viscosity. The effects of higher order chemical reaction and thermophoresis on an unsteady MHD free convective heat and mass transfer flow past an impulsively started infinite inclined porous plate in the presence of thermal radiation with temperature dependent viscosity was studied by Alam *et al.* [8]. These authors solved the problem using a sixth-order Runge-Kutta integration scheme with Nachtsheim-Swigert shooting method.

In this chapter, we numerically solve the model proposed in [8] by using a fitted operator finite difference method (FOFDM). In this chapter it is assumed that the coefficient of the energy equation is very small rendering the equation singularly perturbed and so the usual standard finite difference method will produce very poor results as is going to be demonstrated theoretically and numerically in this paper. We therefore construct or design the FOFDM in such a way that the denominator function of the classical second order derivative is replaced with a positive function that captures significant properties of the energy equation and thus provide reliable numerical results. A considerable amount of literature exists regarding the singularly perturbed differential equations (see Burie *et al.* [21], Murray [105], Roos *et al.* [132], Ansari *et al.* [11], Bashier and Patidar [14], Lubuma and Patidar [86], Kumar and Kadalbajoo [85], Beckett and Mackenzie [16]).

The rest of the chapter is organized as follows. In section 6.2 we describe the model. Section 6.3 is concerned with the numerical method and its analysis. Section 6.4 deals with the numerical results and their discussion and we conclude the chapter in Section 6.5.

6.2 Description of model

We consider the unsteady convective heat and mass transfer flow of a viscous incompressible electrically conducting fluid past an accelerating vertical infinite inclined porous plate with an angle α to the vertical in the presence of a transverse magnetic field B_o and a chemical reaction with significant radiation effect. Let the $x-$axis be directed along the inclined plate and the $y-$axis be normal to the plate. Let u and v be the velocity components along $x-$ and $y-$ axes, respectively. We assume that the plate starts moving impulsively in its own plane with a velocity U_o at time $t \geq 0$. Then the magnetohydrodynamic unsteady convective boundary layer equations under usual Boussinesq and boundary-layer approximation [8] read

$$\frac{\partial v}{\partial y} = 0, \tag{6.2.1}$$

$$\frac{\partial u}{\partial t} + v\frac{\partial u}{\partial y} = \frac{1}{\rho_\infty}\frac{\partial}{\partial y}\left(\nu\frac{\partial u}{\partial y}\right) + g\beta(T - T_\infty)\cos\alpha - \frac{\sigma {B_0}^2}{\rho}u, \tag{6.2.2}$$

$$\frac{\partial T}{\partial t} + v\frac{\partial T}{\partial y} = \frac{\lambda_g}{\rho_\infty c_p}\frac{\partial^2 T}{\partial y^2} - \frac{1}{\rho c_p}\frac{\partial q_r}{\partial y}, \tag{6.2.3}$$

$$\frac{\partial C^*}{\partial t} + v\frac{\partial C^*}{\partial y} = D\frac{\partial^2 C^*}{\partial y^2} - \frac{\partial}{\partial y}(V_T C^*) - K_l {C^*}^{m^*}, \tag{6.2.4}$$

where ν is the kinematic viscosity, β is the volumetric coefficient of thermal expansion, β^* is the volumetric coefficient of expansion with concentration, ρ_∞ is the ambient density of the fluid, σ is the electrical conductivity of the fluid, g is the acceleration due to gravity, T is the temperature of the fluid in the boundary layer, T_∞ is the temperature of the fluid far away from the plate, C^* is the concentration of fluid in the boundary layer, ${C^*}_\infty$ is the concentration of the fluid far away from the plate and D is the molecular diffusivity, K_l is the chemical reaction parameter, c_p is the specific heat capacity, λ_g is the thermal conductivity of the fluid, q_r is the radiation heat flux, B_0 is the magnetic induction, V_T is the thermophoresis velocity and m^* is the order of the chemical reaction. The associated boundary conditions [8] are

$$\begin{aligned} t \leq 0,\ u = v = 0,\ T = T_\infty,\ C^* = C^*_\infty \text{for all } y, \\ t > 0\ u = U_o,\ v = \pm v(t)\ T = T_w,\ C = C_w = 0 \text{ at } y = 0, \\ u = 0,\ T = T_\infty,\ C^* = C^*_\infty = 0 \text{ as } y \to \infty, \end{aligned} \tag{6.2.5}$$

where $v(t)$ is the time dependent viscosity at the porous plate. The radiative heat flux q_r is described by the Rosseland approximation (see Brewster [19], Alam *et al.* [8]) such that

$$q_r = (4\sigma_1/3k_1)\partial T^4/\partial y, \tag{6.2.6}$$

where σ_1 and k_1 are the Stefan-Boltzman constant and the mean absorption coefficient, respectively. We introduce the following dimensionless variables

$$\eta = \frac{y}{l_o},\ \theta(n) = \frac{T - T_\infty}{T_w - T_\infty},\ C(\eta) = \frac{C^*}{C^*_\infty}, \tag{6.2.7}$$

where

l_o is the time dependent length scale and the dimensionless temperature θ can also be written as

$$\theta = \frac{T - T_r}{T_w - T_\infty} + \theta_r \tag{6.2.8}$$

where

$$\theta_r = \frac{T_r - T_\infty}{T_w - T_\infty} = constant, \tag{6.2.9}$$

and its value is determined by by the viscosity temperature characteristics of the fluid under consideration and the operating temperature difference $\Delta t = T_w - T_\infty$.

By introducing appropriate relations into the equations (6.2.1)- (6.2.4) (see Alam *et al.* [8]) we then obtain the following set of ordinary differential equations

$$f'' + \eta\left(\frac{l_o}{\nu}\frac{dl_o}{dt}\right)\left(\frac{\theta_r - \theta}{\theta_r}\right)f' + V_o\left(\frac{\theta_r - \theta}{\theta_r}\right)f' + \left(\frac{\theta'}{\theta_r - \theta}\right)f'$$
$$+G_r\left(\frac{\theta_r - \theta}{\theta_r}\right)\theta\cos\alpha - M\left(\frac{\theta_r - \theta}{\theta_r}\right)f = 0, \tag{6.2.10}$$
$$-\eta\left(\frac{l_o}{\nu}\frac{dl_o}{dt}\right)\theta' - V_o\theta' = \left(\frac{3R+4}{3RP_r}\right)\theta'', \tag{6.2.11}$$
$$-\eta\left(\frac{l_o}{\nu}\frac{dl_o}{dt}\right)\phi' - V_o\phi' = \frac{1}{S_c}\phi'' - \tau\left(\phi\theta'' + \phi'\right) - K\phi'', \tag{6.2.12}$$

with corresponding boundary conditions

$$f = 1,\ \theta = 1,\ C = 0 \text{ as } \eta = 0, \tag{6.2.13}$$
$$f = 0,\ \theta = 0,\ C = 0 \text{ as } \eta \to \infty,$$

where $P_r = \rho_\infty c_p \nu/\lambda_g$ is the Prandtl number, $S_c = \nu/D$ is the Schmidt number, $M = \sigma B_o^2 l_o^2/\nu\rho_\infty$ is the local magnetic parameter, $G_r = g\beta(T_w - T_\infty)l_o^2/\nu U_o$ is the local Grashof number, $R = \lambda_g k_1/4\sigma_1 T_\infty^3$ is the radiation parameter, and $K = K_l l_o^2/\nu$ is the local chemical chemical reaction parameter and primes denote differentiation with respect to η.

The equations (6.2.10)-(6.2.12) are locally similar except the term $(l_o/\nu)dl_o/dt$ where t appears explicitly yet local similarity conditions requires that the term $(l_o/\nu)dl_o/dt$ be a constant. In line with the work of Satter and Hassain [136] and Alam *et al.* [8] we assume $(l_o/\nu)dl_o/dt = \lambda_g$ (a constant). We choose $\lambda_g = 2$ which corresponds to the usual scaling factor for various unsteady boundary layer flows (see Schlichting [137]). We therefore obtain the following non-dimensional non-linear ordinary differential equations which are locally similar in time:

$$f'' + (2\eta + V_o)\left(\frac{\theta_r - \theta}{\theta_r}\right) f' + \left(\frac{\theta'}{\theta_r - \theta}\right) f'$$
$$+ G_r \left(\frac{\theta_r - \theta}{\theta_r}\right) \theta \cos\alpha - M\left(\frac{\theta_r - \theta}{\theta_r}\right) f = 0 \tag{6.2.14}$$
$$\theta'' + (2\eta + V_o)\left(\frac{3RP_r}{3R+4}\right)\theta' = 0, \tag{6.2.15}$$
$$C'' + S_c(2\eta + V_o)C' - \tau S_c(C\theta'' + C') - S_c K C'' = 0, \tag{6.2.16}$$

with the corresponding boundary conditions as depicted in equation (6.2.13).

6.3 Construction and analysis of the numerical method

In this section we are going introduce the FOFDM which is the appropriate method used to solve the singularly perturbed temperature equation. We state the temperature equation in

the form

$$L\theta := \epsilon\theta'' + (2\eta + V_o)\theta' = 0, \tag{6.3.1}$$

where $\epsilon = (3R+4)/(3RP_r)$ and the primes denote the derivative with respect to η.

The following lemma provides bounds on the solution of the problem (6.2.15).

Lemma 6.3.1. *Let θ be the solution of (6.2.15) with u(0) = 1 and u(4) = 0. Then for $0 \leq k \leq 4$,*

$$|\theta^{(k)}(\eta)| \leq \widetilde{C}\left(1 + \epsilon^{-k}e^{-\lambda\eta/\epsilon}\right)$$

for all $\eta \in \overline{\Omega}$ where $0 < \epsilon < 1$, $\widetilde{C}$ is independent of ϵ, and $0 < \lambda < (2\eta + V_o)$.

Proof. See [96].

We will approximate the solution of the temperature equation on a uniform mesh which we describe below.

Let n be a positive integer. Consider the following partition of the interval [0,4]:

$$\eta_0 = 0,\ \eta_i = \eta_0 + ih,\ i = 1(1)n,\ h = \eta_i - \eta_{i-1},\ \eta_n = 4.$$

On this partition, the standard finite difference method (SFDM) used to discretly approximate (6.2.15) reads

$$\epsilon\frac{\nu_{j+1} - 2\nu_j + \nu_{j-i}}{h^2} + (2\eta + V_o)\frac{\nu_{j+1} - \nu_j}{h} = 0, \tag{6.3.2}$$

where ν is an approximation for θ and h is the step-size in the discretization of the region of interest. As ϵ become smaller and smaller the standard finite difference method (SFDM) fails to provide fairly accurate approximation of the true solution. To obtain more reliable results we design a fitted numerical technique whereby the denominator of the approximation to the second derivative h^2 is replaced by a function ψ_j^2, which is a function of $\epsilon,\ \eta,\ V_o$, and h. The resulting FOFDM reads

$$L^h u_j \equiv \epsilon \frac{u_{j+1} - 2u_j + u_{j-i}}{\psi^2} + (2\eta + V_o)\frac{u_{j+1} - u_j}{h} = 0, \tag{6.3.3}$$

where u is an approximation for θ obtained by using this FOFDM and

$$\psi_j^2 = \frac{h\epsilon}{(2\eta + V_o)}\left[\exp\left(\frac{(2\eta + V_o)h}{\epsilon}\right) - 1\right]. \tag{6.3.4}$$

The function ψ_j^2 is obtained by using the theory of finite differences as indicated in [86]. The function ψ_j^2 captures significant behavior of the solution particularly when the solution in the layer region has steep gradient. The layer region is located in the neighborhood of the inclined plate near the left end of the interval. We begin by analyzing the FOFDM (6.3.3) for stability and convergence before the numerical simulations.

Lemma 6.3.2. (Discrete minimum principle) *Assume that the mesh function ϕ_i satisfies $\phi_0 \geq 0$ and $\phi_n \geq 0$. Then, $L^h\phi_i \leq 0$ for all $i = 1(1)n-1$, implies that $\phi_i \geq 0$ for all $i = 0(1)n$.*

Proof. The proof follows the same lines as the proof of the discrete minimum principle in [96] as shown below. Choose k such that $\phi_k = \min_i \phi_i$ and assume that $\phi_k \leq 0$. It follows that $k \notin \{0, n\}$, $\phi_{k+1} - \phi_k \geq 0$ and $\phi_k - \phi_{k-1} \leq 0$. Then

$$\begin{aligned} L^h\phi_k &= \frac{\epsilon}{\psi_k^2}\left(\phi_{k+1} - 2\phi_k + \pi_{k-1}\right) + \frac{2\eta_k + V_o}{h}\left(\phi_{k+1} - \phi_k\right), \\ &= \frac{\epsilon}{\psi_k^2}\left(\phi_{k+1} - \phi_k + \phi_{k-1} - \phi_k\right) + \frac{(2\eta_k + V_o)}{h}\left(\phi_{k+1} - \phi_k\right) \\ &\geq 0, \end{aligned} \tag{6.3.5}$$

a clear contradiction. Therefore

$$\phi_k \geq 0 \text{ so } \phi_i \geq 0 \ \forall i,\ i = 1(1)n, \text{ which completes the proof.}$$

The following lemma is a consequence of the above discrete minimum principle.

Lemma 6.3.3. (Uniform stability estimate) *If ξ_i is any mesh function such that $\xi_0 = \xi_n = 0$ then*

$$|\xi_i| \leq \frac{4}{\lambda} \max_{1 \leq j \leq n-1} \left|L^h \xi_j\right| \text{ for } 0 \leq i \leq n.$$

Proof. Let

$$\widetilde{C} = \frac{1}{\lambda} \max_{1\leq j\leq n-1} |L^n \xi_j|,$$

and $a \geq \lambda \geq 0$ where $a = 2\eta + V_o$. Introduce the mesh functions $\vartheta_j^+, \vartheta_j^-$ defined by $\vartheta_j^\pm = \widetilde{C}(4-\eta_j) \pm \xi_j$. From equation (6.3.3)

$$\begin{aligned} L^h \vartheta_j^\pm &= \frac{\left(\vartheta_{j+1}^\pm - 2\vartheta_j^\pm + \vartheta_{j-1}^\pm\right)}{\psi_j^2} + \frac{a_i}{h}\left(\vartheta_{j+1}^\pm - \vartheta_j^\pm\right), \qquad (6.3.6) \\ &= \frac{\left(\widetilde{C}(4-\eta_{j+1}) \pm \xi_{j+1} - 2(\widetilde{C}(4-\eta_j) \pm \xi_j) + \widetilde{C}(4-\eta_{j-1}) \pm \xi_{j-1}\right)}{\psi_j^2} \\ &\quad + a_j \frac{\widetilde{C}(4-\eta_{j+1}) \pm \xi_{j+1} - \widetilde{C}(4-\eta_j) \mp \xi_j}{h}, \\ &= \frac{\pm\xi_{j+1} \mp 2\xi_j \pm \xi_{j-1}}{\psi_j^2} + a_i \frac{\pm\xi_{j+1} \mp \xi_j}{h} - Ca_i, \\ &= \pm L^h \xi_j - Ca_i, \\ &= \pm L^h \xi_j - \frac{a_i}{\lambda} \max_{0\leq i\leq n-1} |L^h \xi_i| \\ &\leq 0, \end{aligned}$$

since $a_i/\lambda \geq 0$. By the minimum principle, we have

$$\zeta_j^\pm \geq 0 \text{ for } 0 \leq j \leq n$$

and therefore

$$\zeta_j^\pm = \widetilde{C}(4-\eta_j) \pm \xi_j \geq 0 \text{ for } 0 \leq j \leq n.$$

This implies that $|\xi_j| \leq (4-\eta_j)\widetilde{C} = (4-\eta_j)\frac{1}{\lambda}|L^h \xi_i| \leq \frac{4}{\lambda} \max_{0\leq i\leq n-1} |L^h \xi_i|$, which completes the proof.

Now the truncation error for the spatial descretization is given by

$$\begin{aligned}\left[L^{h,\tau}(\theta-u)_j\right] &= -\epsilon\theta_j'' - (2\eta+V_o)\theta_j' + \frac{1}{\tau}\theta_j \\ &\quad - \left(-\epsilon\frac{\theta_{j+1}-2\theta_j+\theta_{j-1}}{\psi_j^2} - (2\eta+V_o)\frac{\theta_{j+1}-\theta_j}{h} + \frac{1}{\tau}\theta_j\right), \\ &= -\epsilon\theta_j'' - (2\eta+V_o)\theta_j' + \frac{\epsilon}{\psi_j^2}\left[h^2\theta_j'', + \frac{h^4}{12}\theta^{(iv)}(\zeta_1)\right] \\ &\quad + \frac{(2\eta+V_o)h}{2}\left(\frac{2\theta_j'}{h} + \theta_j'' + \frac{h}{3}\theta_j''' + \frac{h^2}{12}\theta^{(iv)}(\zeta_2)\right), \end{aligned} \tag{6.3.7}$$

where $\zeta_1 \in (y_{j-1}, y_{j+1})$ and $\zeta_2 \in (y_j, y_{j+1})$. Using the Taylor series expansion, we have

$$\frac{\epsilon}{\psi_j^2} = \frac{\epsilon}{h^2} - \frac{(2\eta+V_o)}{2h} + \ldots. \tag{6.3.8}$$

This implies that

$$\begin{aligned} L^{h,\tau}(\theta-u)_j &= -\epsilon_j'' \\ &\quad + \left[\frac{\epsilon}{h^2} - \frac{(2\eta+V_o)}{2h} + \ldots\right]\left[h^2\theta_j'' + \frac{\theta^{(iv)}(\zeta_1)}{12}h^4\right] \\ &\quad + \frac{(2\eta+V_o)}{2}\left(h\theta_j'' + \frac{h^2}{3}\theta_j''' + \frac{\theta^{(iv)}(\zeta_2)}{12}h^3\right). \end{aligned}$$

Further simplifications lead to

$$L^{h,\tau}(\theta-u)_j = \left(\frac{\epsilon\varpi^{(iv)}(\zeta_1)}{12} + \frac{(2\eta+V_o)}{6}\varpi_j'''\right)h^2 - \left(\frac{(2\eta+V_o)\varpi^{(iv)}(\zeta_1)}{24}\right)h^3 + O(h^5).$$

Using Lemma 6.3.1, we obtain

$$\left|L^{h,\tau}(\theta-u)_j\right| \leq \left|\frac{\widetilde{C}\epsilon}{12}\left(1+\epsilon^{-4}e^{-\lambda y/\epsilon}\right) + \frac{\widetilde{C}(2\eta+V_o)}{6}\left(1+\epsilon^{-3}e^{-\lambda y/\epsilon}\right)\right|h^2 + O(h^5).$$

Now applying Lemma 7 in [103]

$$\begin{aligned}\left|L^{h,\tau}(\theta-u)_j\right| &\leq \widetilde{C}\left(\frac{\epsilon h^2}{12}+\frac{(2\eta+V_o)h^2}{6}\right)+O(h^5),\\ &\leq \widetilde{B}h^2,\end{aligned} \tag{6.3.9}$$

since $\epsilon h^2 < h^2$. Then by Lemma 6.3.3 and (6.3.9) we have

$$\begin{aligned}\max_{0\leq i\leq n}\left|(\theta-u)_i\right|, &\leq \max_{1\leq j\leq n-1}\left|L^{h,\tau}(\theta-u)_j\right|,\\ &\leq \widetilde{B}h^2.\end{aligned} \tag{6.3.10}$$

6.4 Results and discussions

Numerical results are presented in this section followed by a discussion on the results. Using the double mesh principle the pointwise errors are estimated as:

$$e^N(\eta) = |u^N(\eta) - u^{2N}(\eta)|, \tag{6.4.1}$$

where N is the spatial discretization parameter. The maximum absolute errors are given by

$$E^N = \max_N e^N(\eta), \tag{6.4.2}$$

Since ϵ is inversely proportional to P_r we calculate the maximum absolute error in the FOFDM solution by varying P_r and n while keeping other parameters constant. The numerical rates of convergence are computed using the formula ([51])

$$r_N = \frac{\log(E^N/E^{2N})}{\log 2}. \tag{6.4.3}$$

Numerical experiments that confirm the first order convergence of the SFDM solution and the second order convergence of the FOFDM solution is depicted in Table 6.4.1.

The energy equation (6.2.11) is solved using the SFDM and the FOFDM and the solutions are compared. Alam *et al.* [8] solved a similar problem numerically with $P_r = 0.71$ and $P_r = 7$ using a sixth-order Runge-Kutta integration scheme with Nachtcheim-Swiggert shooting

method. In this chapter we consider a case where P_r is large enough to ensure that the perturbation parameter ϵ which multiplies the highest derivative is small enough to render the energy equation singularly perturbed. In order for us to check on the accuracy and convergence rate of our numerical method we use the double mesh principle since there is no exact solution available. As depicted in Table 6.4.1, the SFDM is first order convergent and the FOFDM is second order convergent.

Table 6.4.1: Maximum absolute errors and orders of convergence associated with SFDM and FOFDM for $V_o = 0.5$ and $R = 0.5$.

P_r	n	5	10	20	40	80
5	SFDM	5.26E-2	3.56E-2	2.12E-2	1.17E-2	6.15E-3
	r_n	0.56	0.75	0.86	0.93	
	FOFDM	1.88E-2	4.54E-3	1.21E-3	3.03E-4	7.56E-5
	r_n	2.05	1.91	2.00	2.00	
10	SFDM	6.34E-2	4.38E-2	2.89E-2	1.70E-2	9.13E-3
	r_n	0.53	0.60	0.77	0.90	
	FOFDM	1.89E-2	1.03E-2	2.51E-3	6.24E-4	1.56E-4
	r_n	0.88	2.04	2.01	2.00	
20	SFDM	6.07E-2	6.15E-2	4.04E-2	2.48E-2	1.38E-2
	r_n	-	0.61	0.70	0.85	
	FOFDM	3.86E-2	1.70E-2	5.10E-3	1.27E-3	3.23E-4
	r_n	1.18	1.74	2.01	1.98	
40	SFDM	4.66E-2	6.89E-2	5.65E-2	3.65E-2	2.12E-2
	r_n	-	0.30	0.63	0.78	
	FOFDM	4.04E-5	1.12E-2	1.05E-2	2.59E-3	6.76E-4
	r_n	-	0.10	2.02	1.94	

The order of convergence of the FOFDM is higher than the order of the SFDM. The FOFDM has smaller maximum absolute errors as compared to the SFDM and therefore we conclude that the FOFDM exhibit better accuracy. We analyze the temperature, velocity, and concentration profiles of our problem using the FOFDM since we are dealing with a singular perturbation parameter multiplying the highest derivative in the energy equation. Figure 6.4.1 shows that as the radiation parameter R increases the temperature profile decreases.

We depict in Figure 6.4.2(a) that as the Schmidt number S_c increases the concentration boundary layer thickness decreases. In Figure 6.4.2(b) we notice that the concentration profile

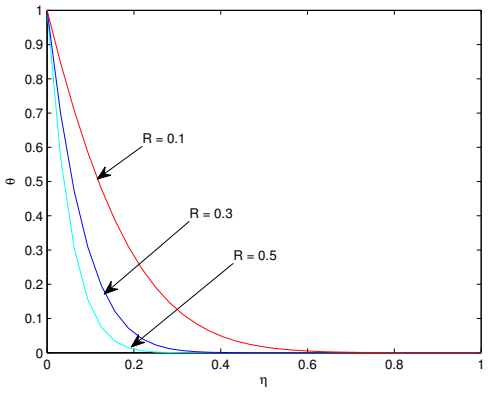

Figure 6.4.1: Temperature profile for different values of R with $V_o = 0.5$, $P_r = 50$, $n = 64$.

decreases with increasing thermophoretic parameter τ. The concentration profile increases as you move from the plate to about $\eta = 1$ and thereafter it decreases to a terminal value. The effect of the chemical reaction parameter K on the concentration is depicted in Figure 6.4.2(c) and it is clear that the concentration decreases for $K > 0$ and increases for $K < 0$.

The effect of the angle of inclination α to the vertical direction on the velocity profile is displayed in Figure 6.4.3(a). For small Prandtl number P_r the effect of varying α is significant and it is shown that the velocity profile decreases with increasing α. However when the Prandtl number is large, $P_r = 50$ say the graph for $\alpha = 0$ and $\alpha = 30^o$ coincides.

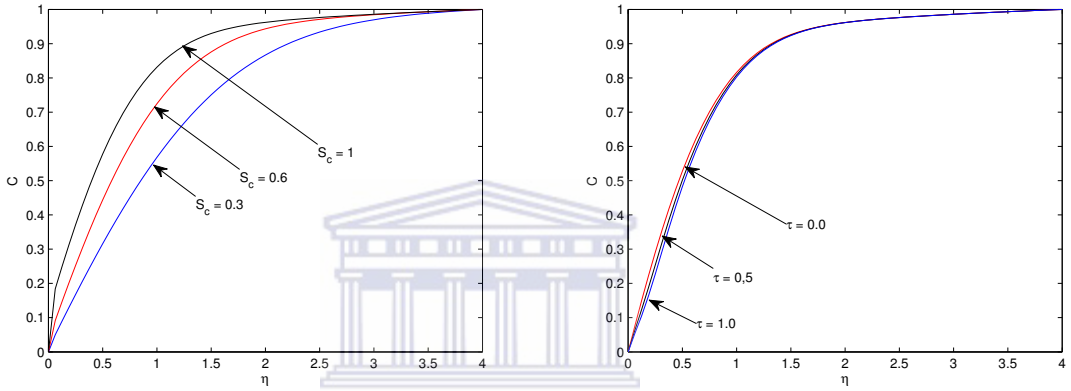

(a) Concentration profiles for different values of S_c with $\tau = 0.1$, $K = 0.1$.

(b) Concentration profiles for different values of τ with $S_c = 1$.

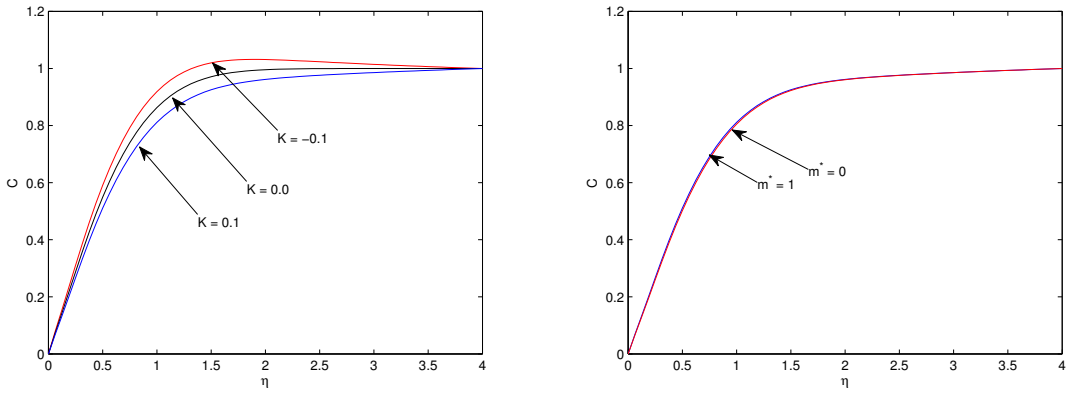

(c) Concentration profiles for different values of K with $\tau = 0.1$, $S_c = 1$.

(d) Concentration profiles for different values of m^* with $\tau = 0.1$, $S_c = 1$, $R = 0.5$.

Figure 6.4.2: Concentration profiles for $V_o = 0.5$, $R = 0.5$, $P_r = 50$, $n = 64$.

Figure 6.4.2(d) shows the effect of the order of chemical reaction m^* on the concentration distribution. We note that as the order of concentration m^* increases concentration profile also increases.

The effect of the magnetic parameter M on the velocity profile is depicted in Figure 6.4.3(b). We show that increasing the magnetic parameter M results in a decrease of the fluid velocity.

The results just discussed above agreed with those of Alam et al. [8] except for the shift in the profile due to varied size of the parameters. Figure 6.4.3(a) stands out in this respect as we have observed that for $P_r = 7$, the velocity profile increase with decreasing α whereas no change is noticed in the profile for $\alpha = 0^o$ and $\alpha = 30^o$ when $P_r = 50$ (see Figure 6.4.3(a)). Table 6.4.2 depicts the effect of P_r and R on the Nusselt number (Nu). From the table we observe that as the radiation parameter R increases the Nusselt number increases for air ($P_r = 0.70$) and for water ($P_r = 7.0$). Table 6.4.2 also compares the values of the Nusselt number obtained by Alam *et al.* [8] and those obtained by our method. The two methods agree to four decimal places which confirms the accuracy of our method.

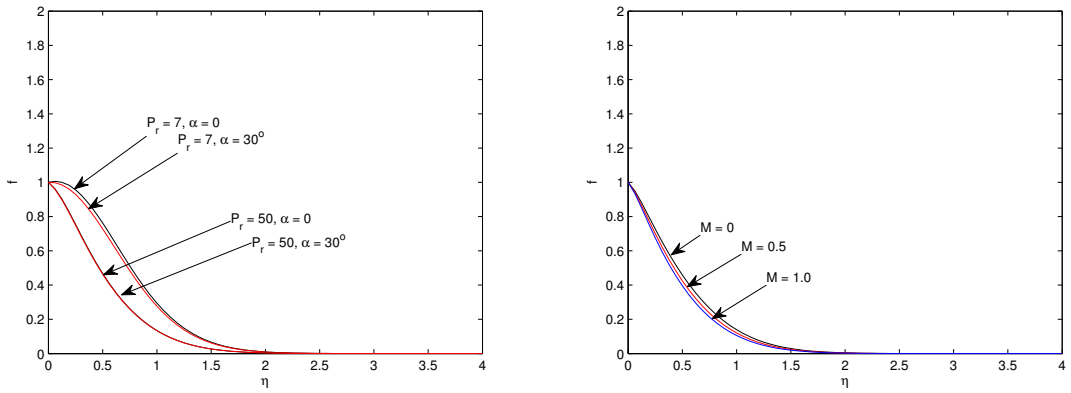

(a) Velocity profiles for different values of α and P_r with $\alpha = 30^o$, $M = 0.4$.

(b) Velocity profiles for different values of M with $\tau = 0.1$, $\alpha = \pi/6$.

Figure 6.4.3: Velocity profiles for $V_o = 0.5$, $S_c = 0.6$, $R = 0.3$, $Q_r = 2.0$, $G_r = 6$, $n = 64$.

Table 6.4.2: Effect of P_r and R on the Nusselt number Nu.

V_o	P_r	R	Alam [8]	Our method
0.5	0.70	0.1	0.2651156	0.2651126
0.5	0.70	0.3	0.4464034	0.4463955
0.5	0.70	0.6	0.5969869	0.5969729
0.5	7.00	0.1	0.9503326	0.9502978
0.5	7.00	0.3	1.7149534	1.7148449
0.5	7.00	0.6	2.4109572	2.4107490

6.5 Summary

The FOFDM gave reliable results, especially when P_r was large. The concentration, velocity and temperature profiles were studied using the FOFDM and the results which mostly agreed with previous findings are

- Radiation reduces the fluid velocity and fluid temperature.
- The fluid concentration decreases with increasing chemical reaction parameter.
- Concentration increases with increasing order of a chemical reaction.
- The concentration increases steadily for $0 \leq \eta \leq 1$ and decreases for $\eta > 1$. The effect of the thermophoretic parameter to the concentration is clearly noticed close to the plate. The concentration decreases with increasing thermophoretic parameter.
- The effect of the angle of inclination to the velocity profile is well pronounced for small P_r.
- The effect of the viscosity parameter θ_r is to decrease the temperature and to increase the velocity.
- The effect of the presence of a magnetic field is to reduce the velocity flow field.

In the next chapter, the effects of unsteady MHD free convection past a vertical permeable plate with heat source and suction or injection are studied.

Chapter 7

Analysis of radiation absorption and chemical effects on unsteady MHD free convection past a vertical plate with heat source and suction or injection using a fitted method

A fitted numerical study for the problem of a two-dimensional unsteady MHD free convection flow of a viscous, incompressible, electrically conducting, heat generation/absorbing fluid past a vertical infinite porous flat plate in the presence of a transverse magnetic field, radiation absorption, chemical reaction and suction or injection is reported. We extend the work of Shivaiah and Rao [143]. In this work, the governing partial differential equations describing the problem stated above are transformed by a suitable similarity transformation resulting in a system of ordinary differential equations. The singularly perturbed part of the governing equations of flow field is simulated using the fitted operator finite difference method (FOFDM). We observe that the FOFDM is second order convergent unlike the classical approaches which are first order convergent. In addition to high order of convergence the FOFDM proves to be more accurate than the classical finite difference methods that have been used to solve

problems such as the one of interest in this work. We observe that an increase in either the the heat source parameter or the radiation absorption parameter leads to an increase in the temperature and velocity.

7.1 Introduction

The study of combined heat and mass transfer problems with chemical reactions have received considerable amount of attention lately. The study has enormous practical applications in engineering and science. MHD flows find applications in the field of stellar, planetary magnetospheres, materiology, MHD accelerators, polymer production and manufacture of ceramics only to mention a few. Free convection currents are caused by either temperature difference or concentration differences.

Das *et al.* [42] studied the effect of homogenous first order chemical reaction on a flow past an impulsively started infinite vertical plate with uniform heat flux. Muthucumaraswamy and Ganesan [109] reported on the effect of the chemical reaction and injection on a flow in an unsteady upward motion of an isothermal plate. Muthucumaraswamy and Ganesan [108] studied the diffusion and first order chemical reaction on an impulsively started infinite vertical plate with varying temperature. Chamkha [27] analysed an MHD flow past a vertical permeable surface in the presence of heat generation/absorption and a chemical reaction. Prasad [122] reported on the effect of a reaction rate on the transfer of a chemically reactive species in a non-Newtonian fluid immersed in a porous medium. Recently Ghaly and Seddeek [59] investigated the effect of chemical reaction on laminar flow past a semi-infinite horizontal plate with temperature dependent viscosity. Ibrahim *et al.* [71] studied the effect of the chemical reaction and radiation absorption on unsteady MHD free convective flow past a semi-infinite vertical permeable moving plate with heat source and suction.

The effect of radiation on MHD flow has recieved considerable attention lately. Many processes in engineering and science occur at high temperatures and acquisation of such knowledge is important as we look at areas such as nuclear power plants, gas turbines, missiles, satellites and propulsion devices for aircrafts. AboEldahab [2] studied the radiation effect in heat transfer in an electrically conducting fluid at a stretching surface. Seddeek [138] analysed the effect of radiation and variable viscosity on unsteady forced convection flows

in the presence of a magnetic field. Cortell [38] considered the effect viscous dissipation and radiation on the thermal boundary layer over a non-linearly stretching sheet. Abel and Mahesha [1] investigated heat transfer in MHD viscoelastic fluid flow over a stretching sheet with variable thermal conductivity, non-uniform heat source and radiation. Pal and Talukdar [116] examined an unsteady MHD convective heat and mass transfer in a boundary layer slip flow past a vertical permeable plate with thermal radiation. The study of the effects of chemical reaction and radiation absorption on transient hydro-magnetic natural convection flow with wall transpiration and heat source was carried out by Ibrahim [71]. Devi [50] investigated the effects of a chemical reaction on the MHD flow in the presence of heat transfer. The differential model in our current study resembles that of Ibrahim [71] except that the boundary conditions are different. We modify the work of Shivaiah and Rao [143] by adding the effect of radiation absorption.

The objective of this study is to examine the singularly perturbed part of the governing equations of flow field using the FOFDM. The solution of the singular perturbation problems (SPPs) is known to have large gradients when the coefficient of the highest derivative is very small. Solving SPPs using standard finite difference methods producess very poor results as we will show theoretically and numerically. To avoid use of these unreriable methods we adopt the FOFDM designed so as to capture the behavior of the solution within the boundary layer region. Beckett and Mackenzie [16] studied the convergence of finite difference approximations on equally distributed grids to a singularly perturbed boundary value problem using an upwind scheme. Whereas Beckett and Mackenzie considered steady flows the current study examines unsteady flows. Other sources of literature consulted on singularly perturbed partial differential equations include, Doolan *et al.* [51], Miller *et al.* [96], Munyakazi and Patidar [102], and references therein. Research on singularly perturbed steady convection diffusion problems have been carried out using different methods as stated in Beckett and Mackenzie [16] but none has been carried out so far using the FOFDM.

The rest of the chapter is organized as follows. In Section 7.2, the description of the model is presented. Section 7.3 deals with the construction of the numerical method and its analysis. Section 7.4 on the other hand is concerned with the numerical results which supports the theory as well as the study of the effects of the flow parameters using FOFDM. Finally we conclude the chapter in Section 7.5.

7.2 Description of the model

We consider the unsteady two-dimensional free convective mass transfer flow of a viscous incompressible electrically conducting fluid past a vertical infinite porous flat plate in the presence of a transverse magnetic field in the presence of suction or injection. Let the x^*-axis be directed upward along the plate and the y^*-axis normal to the plate. Let u^* and v^* be the velocity components along x^* and y^* axes respectively. At $t^* = 0$, the plate and fluid are at the same temperature T^*_∞ and same concentration C^*_∞. Then the magnetohydrodynamic unsteady free convective boundary layer equations under usual Boussinesq's approximation (a modification of the model in [143]) reads

$$\frac{\partial v^*}{\partial y^*} = 0, \tag{7.2.1}$$

$$\frac{\partial u^*}{\partial t^*} + v^*\frac{\partial u^*}{\partial y^*} = \nu\frac{\partial^2 u^*}{\partial {y^*}^2} + g\beta(T^* - T^*_\infty) + g\beta^*(C^* - C^*_\infty) - (\frac{\sigma {B_O}^2}{\rho} + \frac{\nu}{\kappa_p})u^*, \tag{7.2.2}$$

$$\frac{\partial T^*}{\partial t^*} + v^*\frac{\partial T^*}{\partial y^*} = \alpha\frac{\partial^2 T^*}{\partial {y^*}^2} + \frac{Q_0}{\rho c_p}(T^* - T^*_\infty) + Q^*_l(C^* - C_\infty), \tag{7.2.3}$$

$$\frac{\partial C^*}{\partial t^*} + \nu^*\frac{\partial C^*}{\partial y^*} = D\frac{\partial^2 C^*}{\partial y^* 2} - K^*_l(C^* - C^*_\infty), \tag{7.2.4}$$

where, ν is the kinematic viscosity, α is the thermal diffusivity, β is the volumetric coefficient of thermal expansion, β^* is the volumetric coefficient of expansion with concentration, ρ is the density, σ is the electrical conductivity of the fluid, g is the acceleration due to gravity, T^* is the temperature of fluid inside thermal boundary, T^*_∞ is the temperature of the fluid in the free stream, C^* is the species concentration in the boundary layer, C^*_∞ is the species concentration in the free stream, c_p is the specific heat capacity, B_0 is the magnetic induction, Q_o is the heat generation constant, Q^*_l is the coefficient of proportionality for the absorption of radiation, K^* is the permeability of the porous medium, D is the coefficient of chemical molecular diffusivity, K^*_l is the rate of chemical reaction. The boundary conditions [143] are

$$\begin{aligned} t^* \le 0: \ & u^* = 0, \ v^* = 0, \ T^* = T^*_\infty, \ C = C^*_\infty \text{ for all } y^*, \\ t^* > 0: \ & u^* = 0, \ v^* = v(t), \ T^* = T^*_w, \ C^* = C_w \text{ at } y^* = 0, \\ & u^* = 0, \ T^* = T^*_\infty, \ C^* = C^* = C^*_\infty \text{ as } y^* \to \infty, \end{aligned} \tag{7.2.5}$$

where, $v(t)$ is the suction velocity at the plate. From the continuity equation it is deduced that the suction velocity $v(y) = -V_o$. The negative constant indicates that the suction is directed towards the plate. We nondimensionalize (7.2.2) to (7.2.4) by introducing the following non-dimensional quantities

$$\begin{aligned}
&u = u^*/\widetilde{V_0},\ V_o = v^*/V_o,\ y = \widetilde{V_o}y^*/V_o,\ \theta = (T^* - T^*_\infty)/(T^*_w - T^*_\infty),\ t = \widetilde{V_o}^2 t^*/V_o,\\
&C = (C^* - C^*_\infty)/(C^*_w - C^*_\infty),\ M = (\sigma B_o^2\ V_o)/(\rho\widetilde{V_o}^2),\ P_r = V_o\rho C_p/k,\ K = k_p\widetilde{V_o}^2/V_o^2,\\
&G_r = (g\beta V_o(T^*_w - T^*_\infty))/(\widetilde{V_o}^3),\ G_m = (g\beta^* V_o(C^*_w - C^*_\infty))/(\widetilde{V_o}^3),\ Q = Q_o V_o/\rho C_p\widetilde{V_o}^2,\\
&Q_l = (V_o Q^*_l(C_w - C_\infty))/((T_w - T_\infty)\widetilde{V_o}^2),\ \delta = K^*_l V_o^2/\widetilde{V_o}^2,\ S_c = V_o/D,
\end{aligned} \tag{7.2.6}$$

where, M is the magnetic parameter, κ is the thermal conductivity, V_0 is the reference velocity, K_l is the chemical reaction parameter, G_r is the Grashof number of heat transfer, G_m is the Grashof number of mass transfer, S_c is the Schmidt number, Q is the heat source parameter and Q_l is the absorption of radiation parameter. Using (7.2.5) and (7.2.6), equations (7.2.2)-(7.2.4) reduces to

$$\frac{\partial u}{\partial t} - V_o\frac{\partial u}{\partial y} = \frac{\partial^2 u}{\partial y^2} + G_r\theta + G_m C - \left(M + \frac{1}{K}\right)u, \tag{7.2.7}$$

$$\frac{\partial \theta}{\partial t} - V_o\frac{\partial \theta}{\partial y} = \frac{1}{P_r}\frac{\partial^2 \theta}{\partial y^2} + Q\theta + Q_l C, \tag{7.2.8}$$

$$\frac{\partial C}{\partial t} - V_o\frac{\partial C}{\partial y} = \frac{1}{Sc}\frac{\partial^2 C}{\partial y^2} - \delta C. \tag{7.2.9}$$

The corresponding initial and boundary conditions are

$$\begin{aligned}
t \le 0:&\ u = 0,\ \theta = 0,\ C = 0 \text{ for all } y,\\
t \ge 0:&\ u = 0,\ \theta = 1,\ C = 1 \text{ at } y = 0,\\
&u \to 0,\ \theta \to 0,\ C \to 0,\ \text{as } y \to \infty.
\end{aligned} \tag{7.2.10}$$

The set of equations (7.2.7) to (7.2.9) together with the corresponding boundary conditions (7.2.10) are non-linear and coupled and so analytical solutions are difficult to find. The finite difference method is used to find an approximate solution to the problem. To solve the

perturbed part of the differential model we employ the FOFDM which is described in the next section.

7.3 Construction and analysis of the numerical method

We introduce the FOFDM to solve the energy equation. The FOFDM is compared with the standard finite difference method (SFDM). The energy equation (7.2.8) is stated in the form:

$$L\theta := \frac{\partial \theta}{\partial t} - V_o \frac{\partial \theta}{\partial y} - \frac{1}{P_r}\frac{\partial^2 \theta}{\partial y^2} - Q\theta = Q_l C. \tag{7.3.1}$$

We denote by N a positive integer and approximate the solution to (7.3.1) on a uniform mesh and let the interval [0,4] be divided into N equal sub-intervals:
$y_0 = 0,\ y_i = y_0 + ih,\ i = 1(1)N,\ h = y_i - y_{i-1},\ y_N = 4.$
Let τ be the uniform step size on

$$\Omega^{\tau,m} = \left\{ (y, t_j) : y \in \Omega, t_j = j\tau = \frac{j}{m},\ \forall\ 0 < j \leq m \right\}. \tag{7.3.2}$$

Denote the approximation of θ by the unknown ϖ and the approximation of C by unknown ϱ. By performing the time semi-discretization by Euler method at time level n gives

$$\frac{\varpi^n - \varpi^{n-1}}{\tau} - V_o \varpi_y^n - \epsilon \varpi_{yy}^n - Q\varpi^n = Q_l \varrho^n, \tag{7.3.3}$$

subject to

$$\begin{aligned} \widetilde{v}^n(0) = 1,\ \varrho^n(0) = 1,\ 0 < n < m, \\ \widetilde{v}^n(4) = 0,\ \varrho^n(4) = 0,\ 0 \leq n < m, \end{aligned} \tag{7.3.4}$$

where $\epsilon = 1/P_r$. This implies

$$-\epsilon \varpi_{yy}^n - V_o \varpi_y^n + \left(\frac{1}{\tau} - Q \right) \varpi^n = \widetilde{f}, \tag{7.3.5}$$

subject to

$$\varpi^n(0) = 1,\ \varrho^n(0) = 1,\ \varpi^n(4) = 0,\ \varrho^n(4) = 0, \tag{7.3.6}$$

where $\widetilde{f} = (1/\tau)\varpi^{n-1} + Q_l\varrho^n$.

For the sake of simplicity we rewrite equation (7.3.5) without the time level notation "n" in the following form

$$-\epsilon\varpi''(y) - V_o\varpi' + \left(\frac{1}{\tau} - Q\right)\varpi(y) = \widetilde{f}, \tag{7.3.7}$$

subject to

$$\varpi(0) = 1,\ \varpi(4) = 0, \tag{7.3.8}$$

where $\widetilde{f} = (1/\tau)\varpi^* + Q_l\varrho$.

Note that ϖ^* is defined as the previous time level value of ϖ.

The following lemma provides bounds on the solution of the problem (7.3.1).

Lemma 7.3.1. *Let ϖ_ϵ be the solution of (7.3.1). Then for $0 \le k \le 4$,*

$$|\varpi^{(k)}(y)| \le \widetilde{C}\left(1 + \epsilon^{-k}e^{-\lambda y/\epsilon}\right)$$

for all $y \in \overline{\Omega} = [0, 4]$, where $0 < \epsilon \le 1$, $\widetilde{C}$ is independent of ϵ, and $0 < \lambda < V_o$.

Proof. See [96].

Next we discretize (7.3.5) in space using the standard finite difference method and denote the approximation of ϖ by $\widetilde{\nu}$ to give

$$L^{h,\tau}\widetilde{\nu}_j \equiv -\epsilon\frac{\widetilde{\nu}_{j+1} - 2\widetilde{\nu}_j + \widetilde{\nu}_{j-1}}{h_j^2} - V_o\frac{\widetilde{\nu}_{j+1} - \widetilde{\nu}_j}{h} + \left(\frac{1}{\tau} - Q\right)\widetilde{\nu}_j = \widetilde{f}_j. \tag{7.3.9}$$

In this chapter we let SFDM stand for the standard finite difference method, FOFDM stand for fitted operator finite difference method. For very small values of ϵ, the SFDM gives inaccurate approximation of the true solution as the maximum absolute errors suggest. We design a

fitted numerical technique so as to achieve reliable results by replacing the denominator of the approximation to the second derivative h^2 by a function ψ_j^2, which is a function of P_r, V_o and h. The proposed FOFDM reads

$$L^{h,\tau}u_j \equiv -\epsilon\frac{u_{j+1}-2u_j+u_{j-1}}{\psi_j^2} - V_o\frac{u_{j+1}-u_j}{h} + \left(\frac{1}{\tau}-Q\right)u_j = \widetilde{f}_j, \tag{7.3.10}$$

where u is an approximation for ϖ obtained using this FOFDM and

$$\psi_j^2 = \frac{\epsilon h\left(\exp\left(\frac{V_o h}{\epsilon}\right)-1\right)}{V_o}. \tag{7.3.11}$$

The function ψ_j^2 is obtained by the theory of finite differences as indicated in [86]. The function ψ_J^2 mimics the behavior of the solution in the boundary layer region. The layer region is located in the neighborhood of the vertical plate near the left end of the interval. Before the numerical simulation of the MHD flow using the FOFDM we begin by analyzing the FOFDM for stability and convergence.

Analysis of the numerical method

The local truncation error of the time semi-discritization by the forward implicit Euler scheme is denoted by $\widetilde{e_n} = \theta(y,t_n) - \varpi(y)$, where $\varpi(y)$ is the solution of (7.3.5). The amount of error $\widetilde{e_n}$ is the contribution of each time step to the global error of the time semi-discretizaton. The following lemmas depict the order of the local and global error related to the problem (7.3.5).

Lemma 7.3.2. (Local error estimate) *If* $|\varpi^{(k)}(y)| \leq \widetilde{C},\ y \in [0,4],\ 0 \leq k \leq 2$, *then the local error estimate is given by* $||\widetilde{e_n}|| \leq \widetilde{C}\tau^2$.

The following lemma relates to the global error, E_n.

Lemma 7.3.3. (Global error estimate) *The global error* $E_n = \Sigma_{n=0}^{m}\widetilde{e_n}$ *satisfies*

$$||E_n|| \leq \widetilde{C}\tau,\ \forall\ 1 \leq n \leq m.$$

The global error of the time semi-discretization is of the first order, that is, $||\theta - \varpi|| \leq \widetilde{C}\tau$. We discretize spatially to find the local truncation error $|(\varpi - u)|$ where ϖ is the exact solution

with respect to space and u is the approximation of θ for the FOFDM. We are going to consider a few lemmas which are pivotal in the analysis of the error of the solution obtained using the fitted operator finite difference method.

The differential operator $L^{h,\tau}$ defined in (7.3.10) satisfies the following discrete maximum principle for all $\phi \in C^2(\overline{\Omega})$,

Lemma 7.3.4. (Discrete maximum principle) *Assume that the mesh function $\phi(y)$ satisfies $\phi(0) \geq 0$ and $\phi(4) \geq 0$. Then, $L^{h,\tau}\phi(y) \geq 0$ for all $y \in \Omega = (0,4)$ implies that $\phi(y) \geq 0$ for all $y \in \overline{\Omega}$.*

Proof. The proof follows the same lines as the proof of the discrete maximum principle in [96] as shown below. Choose k such that $\phi_k = \min_i \phi_i$ and suppose that $\phi_k \leq 0$. Then $k \notin \{0, n\}$, $\phi_{k+1} - \phi_k \geq 0$ and $\phi_k - \phi_{k-1} \leq 0$. Thus

$$\begin{aligned} L^{h,\tau}\phi_k &= -\frac{\epsilon}{\psi_k^2}\left(\phi_{k+1} - 2\phi_k + \phi_{k-1}\right) - \frac{V_o}{h}\left(\phi_{k+1} - \phi_k\right) + \left(\frac{1}{\tau} - Q\right)\phi_k, \qquad (7.3.12) \\ &= -\frac{\epsilon}{\psi_k^2}\left(\phi_{k+1} - \phi_k + \phi_{k-1} - \phi_k\right) - \frac{V_o}{h}\left(\phi_{k+1} - \phi_k\right) + \left(\frac{1}{\tau} - Q\right)\phi_k \\ &\leq 0, \end{aligned}$$

which is a contradiction. It follows $\phi_k \geq 0$ and so $\phi_i \geq 0 \ \forall i,\ i = 1(1)n$, which completes the proof. The following lemma is a consequence of the discrete maximum principle.

Lemma 7.3.5. (Uniform stability estimate) *If ξ_i is any mesh function such that $\xi_0 = \xi_n = 0$ then*

$$|\xi_i| \leq \frac{4}{\lambda} \max_{1 \leq j \leq n-1} \left| L^h \xi_j \right| \ \text{for } 0 \leq i \leq n.$$

Proof. Let

$$\widetilde{C} = \frac{1}{\lambda} \max_{1 \leq j \leq n-1} \left| L^n \xi_j \right|,$$

and introduce the mesh functions $\vartheta_i^+, \vartheta_i^-$ where $\vartheta_i^\pm = \widetilde{C}(4-y_i) \pm \xi_i$. Then

$$\begin{aligned} L^{h,\tau}\vartheta_i^\pm &= -\frac{\epsilon}{\psi_i^2}\left(\vartheta_{i+1}^\pm - 2\vartheta_i^\pm + \vartheta_{i-1}^\pm\right) - \frac{a(y)}{h}\left(\vartheta_{i+1}^\pm - \vartheta_i^\pm\right) + b_i\vartheta_i^\pm, \\ &= -\epsilon\frac{\pm\xi_{i+1} \mp 2\xi_i \pm \xi_{i-1}}{\psi_i^2} - a_i\frac{\pm\xi_{i+1} \mp \xi_i}{h} + b_i(\pm\xi_i) + \widetilde{C}a_i + b_i\widetilde{C}(4-y_i), \\ &= \pm L^{h,\tau}\xi_i + \widetilde{C}a_i + b_i\widetilde{C}(4-y_i), \\ &= \pm L^{h,\tau}\xi_i + \frac{a_i}{\lambda}\max_{\Omega} L^{h,\tau}\xi_i + b_i\widetilde{C}(4-y_i) \\ &\geq 0, \end{aligned} \tag{7.3.13}$$

since $a_i/\lambda \geq 1$. By the maximum principle it implies

$$\vartheta_i^\pm \geq 0 \text{ for } 0 \leq i \leq n,$$

and therefore

$$\vartheta_i^\pm = \widetilde{C}(4-y_i) \pm \xi_i \geq 0 \text{ for } 0 \leq y_i \leq 4.$$

This reduces to

$$|\xi_i| \leq \widetilde{C}(4-y_i).$$

Since $4 - y_i \leq 4$,

$$|\xi_i| \leq \frac{4}{\lambda}|L^{h,\tau}\xi_i|, \tag{7.3.14}$$

which completes the proof.

Now we attempt to establish the local truncation error of the FOFDM. In the analysis of these errors, $\widetilde{M}$ denote a positive constant, independent of h and ϵ and may assume different values in different inequalities and equations. The local truncation error of the FOFDM (7.3.10) is given by

$$\left|L^{h,\tau}(\theta-u)_j\right| = \left|L^{h,\tau}(\theta-\varpi+\varpi-u)_j\right| = \left|L^{h,\tau}(\theta-\varpi)_j\right| + \left|L^{h,\tau}(\varpi-u)_j\right|. \tag{7.3.15}$$

From lemma 7.3.3

$$\left|L^{h,\tau}(\theta-u_j\right| = \widetilde{M}\tau. \tag{7.3.16}$$

Now the truncation error for the spatial descretization is given by

$$\begin{aligned} L^{h,\tau}(\varpi - u)_j &= -\epsilon\varpi_j'' - V_o\varpi_j' + \left(\frac{1}{\tau} - Q\right)\varpi_j \\ &\quad - \left(-\epsilon\frac{\varpi_{j+1} - 2\varpi_j + \varpi_{j-1}}{\psi_j^2} - V_o\frac{\varpi_{j+1} - \varpi_j}{h}\right) - \left(\frac{1}{\tau} - Q\right)\varpi_j, \\ &= -\epsilon\varpi_j'' + V_o\varpi_j' - \frac{\epsilon}{\psi_j^2}\left[h^2\varpi_j'' + \frac{\varpi^{(iv)}(\zeta_1)}{12}h^4\right] \\ &\quad + \frac{V_o h}{2}\left(\varpi_j'' + \frac{h}{3}\varpi_j'''\right) + \frac{h^2}{12}\varpi^{(iv)}(\zeta_2), \end{aligned} \tag{7.3.17}$$

where $\zeta_1 \in (y_{j-1}, y_{j+1})$ and $\zeta_2 \in (y_j, y_{j+1})$. Using the Taylor series expansion, we have

$$\frac{\epsilon}{\psi_j^2} = \frac{\epsilon}{h^2} - \frac{V_o}{2h} + \ldots. \tag{7.3.18}$$

This implies that

$$\begin{aligned} L^{h,\tau}(\varpi - u)_j &= -\epsilon\varpi_j'' \\ &\quad + \left[\frac{\epsilon}{h^2} - \frac{V_o}{2h} + \ldots\right]\left[h^2\varpi_j'' + \frac{\varpi^{(iv)}(\zeta_1)}{12}h^4\right] \\ &\quad + \frac{V_o}{2}\left(h\varpi_j'' + \frac{h^2}{3}\varpi_j''' + \frac{\varpi^{(iv)}(\zeta_2)}{12}h^3\right). \end{aligned} \tag{7.3.19}$$

Further simplifications lead to

$$L^{h,\tau}(\varpi - u)_j = \left(\frac{\epsilon\varpi^{(iv)}(\zeta_1)}{12} + \frac{V_o}{6}\varpi_j'''\right)h^2 - \left(\frac{V_o\varpi^{(iv)}(\zeta_1)}{24}\right)h^3 + O(h^5).$$

Using Lemma 7.3.1 we obtain

$$\left|L^{h,\tau}(\varpi - u)_j\right| \leq \left|\frac{\widetilde{C}\epsilon}{12}\left(1 + \epsilon^{-4}e^{-\lambda y/\epsilon}\right) + \frac{\widetilde{C}V_o}{6}\left(1 + \epsilon^{-3}e^{-\lambda y/\epsilon}\right)\right|h^2 + O(h^5).$$

Now applying Lemma 7 in [103] yields

$$\begin{aligned}\left|L^{h,\tau}(\varpi-u)_j\right| &\leq \widetilde{C}\left(\frac{\epsilon h^2}{12}+\frac{V_o h^2}{6}\right)+O(h^5)\\ &\leq \widetilde{M}h^2,\end{aligned} \tag{7.3.20}$$

since $\epsilon h^2 < h^2$. Then by Lemma 7.3.5 and (7.3.20) we have

$$\begin{aligned}\max_{0\leq i\leq n}\left|(\varpi-u)_i\right|, &\leq \max_{1\leq j\leq n-1}\left|L^{h,\tau}(\varpi-u)_j\right|,\\ &\leq \widetilde{M}h^2.\end{aligned} \tag{7.3.21}$$

From equation (7.3.16) and (7.3.20) the local truncation error is given by

$$\begin{aligned}\left|L^{h,\tau}(\theta-u)_j\right| &= \left|L^{h,\tau}(\theta-\varpi+\varpi-u)_j\right|,\\ &\leq \left|L^{h,\tau}(\theta-\varpi)_j\right|\left|+\right|L^{h,\tau}(\varpi-u)_j\right|,\\ &\leq \widetilde{M}\left(\tau+h^2\right).\end{aligned} \tag{7.3.22}$$

The next section presents some numerical results followed by a discussion on them.

7.4 Results and discussions

Since the exact solution is not available the maximum errors at all the mesh points are estimated using the double mesh principle as:

$$e^{\Delta t,N}(y,t)=|u^N(y,t)-u^{2N}(y,t)|, \tag{7.4.1}$$

where N is the spatial discretization parameter, Δt is the time discretization parameter, u is the solution of (7.3.1). The maximum absolute errors are given by

$$E^{N,\Delta t}=\max_N e^{\Delta t,N}(y,t), \tag{7.4.2}$$

and the rates of convergence are given by

$$r_N = \frac{\log(E^{N,\Delta t}/E^{2N,\Delta t/4})}{\log 2}, \tag{7.4.3}$$

Table 7.4.1: Maximum absolute errors and orders of convergence associated with SFDM and FOFDM for $V_o = 0.1$, $\tau = 0.1$, $Q_l = 1.0$, $Q = 0.1$.

P_r	N	10	20	40	80
	Δt	0.1	0.1/4	$0.1/4^2$	$0.1/4^3$
5	SFDM	5.32E-2	1.90E-2	8.20E-3	3.80E-3
	r_N	1.49	1.21	1.11	
	FOFDM	3.91E-2	1.04E-2	3.00E-3	9.56E-4
	r_N	1.91	1.79	1.65	
10	SFDM	6.19E-2	2.50E-2	1.16E-2	5.80E-3
	r_N	1.31	1.11	0.92	
	FOFDM	4.37E-2	1.20E-2	3.50E-3	1.10E-3
	r_N	1.86	1.78	1.54	
20	SFDM	6.90E-2	3.09E-2	1.60E-2	8.60E-3
	r_N	1.16	0.95	0.90	
	FOFDM	5.00E-2	1.33E-2	3.90E-3	1.20E-3
	r_N	1.91	1.75	1.70	
40	SFDM	7.24E-2	3.71E-2	2.10E-2	1.21E-2
	r_N	0.96	0.82	0.80	
	FOFDM	6.44E-2	1.55E-2	4.50E-3	1.40E-3
	r_N	2.05	1.78	1.68	

Equation (7.3.1) is solved using the standard finite difference method and the fitted operator finite difference method. Since the exact solution is not available the double mesh principle is applied. In Table 7.4.1 the spatial descretization takes the values $N = 10,\ 20,\ 40,\ 80$ and the time descretization parameter take the values $\Delta t = 0.1\ , 0.1/4,\ 0.1/4^2,\ 0.1/4^3$. We divide the step sizes into a different ratio so that we accommodate at the same time the first order convergence in time and the second order convergence in space. For a fixed value of ϵ the maximum absolute error decreases as the number of grid points, N increases. From the tabulated results we show that the maximum absolute errors of the FOFDM are comparatively smaller than the usual standard methods.

As portrayed in Table 7.4.1, the FOFDM and the SFDM are second order and first order convergent, respectively. The result agrees with theoretical results which showed that the local truncation errors of the FOFDM are of order $O\left(\tau + h^2\right)$.

Since we regard large values of P_r in this chapter we use the FOFDM to analyze the temperature, velocity and concentration profiles of the MHD free convective flow past an infinite vertical porous plate with heat sources in the presence of a chemical reaction and suction or injection. Figure 7.4.1(a) is obtained by plotting the temperature profile with $G_r = 2.0$, $G_m = 2.0$, $M = 1$, $K = 0.5$, $\delta = 0.5$, $P_r = 0.71$, $S_c = 0.6$ and $Q_l = 0$. The resulting temperature profiles in Figure 7.4.1(a) coincides with those obtained by Shivaiah [143], which guarantees the correctness of our method.

The temperature profiles in Figure7.4.1(a) displays the effect of the Prandtl number, the suction parameter and heat source parameters on the temperature. We notice from Figure 7.4.1(a) that the temperature flow field increases as the heat source parameter Q increases. On the other hand the temperature flow field decreases with increasing Prandtl number P_r and suction parameter V_o. Figure 7.4.1(b) shows the effect of parameters such as the Schmidt number S_c, chemical reaction parameter δ and suction parameter V_o on the concentration profile. We observe that the concentration distribution decreases with increasing Schmidt number, chemical reaction parameter and suction parameter. The effects of magnetic parameter M, suction parameter V_o, permeability parameter K and heat source parameter Q are depicted in Figure 7.4.1(c). As expected, we observe that the magnetic parameter and suction parameter retards the velocity flow field. We also observe that the velocity flow field increases with increasing permeability parameter and increasing heat source parameter.

We modify the work by Shivaiah and Rao [143] by including the effect of the radiation absorption parameter Q_l. Figure 7.4.2(a) depicts the temperature profile for the case $Q_l = 0$, which looks exactly the same as the one by Shivaiah and Rao [143]. Figures 7.4.2(b) depict the graph of temperature profile against y for different values of heat absorption parameter Q_l in the boundary layer region. We notice that the absorption radiation parameter increases temperature in the boundary layer. The radiated heat is absorbed by the fluid which increases the fluid temperature within the boundary layer. The effect of Q_l is less pronounced as you move further away from the porous boundary. Figure 7.4.2(c) depicts the graph of velocity profile against y for various values of the radiation absorption parameter Q_l. The effect of

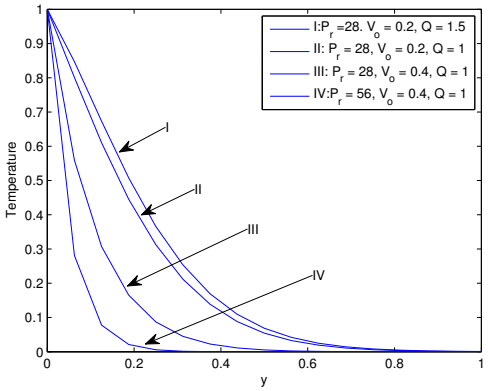

(a) The effect of P_r, V_o and Q on the temperature profile for $N = 64$.

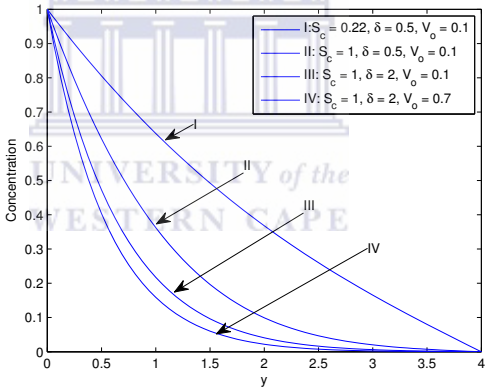

(b) The effect of S_c, V_o and δ on the Concentration profile for $N = 64$.

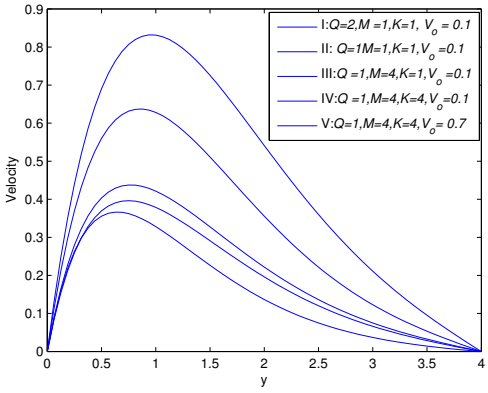

(c) The effect of M, V_o, Q and K on the Velocity profile for $N = 64$.

Figure 7.4.1: Temperature, concentration and velocity profiles with $Q_l = 0$.

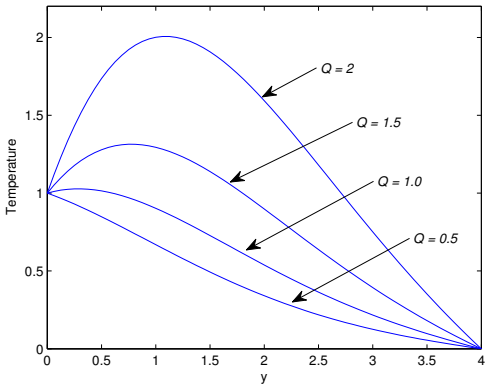

(a) Temperature profiles for different values of Q with $P_r = 0.71$,$S_c = 0.5$, M =1, $K = 0.5$, $\delta = 0.4$, $Q_l = 0$, $n = 64$.

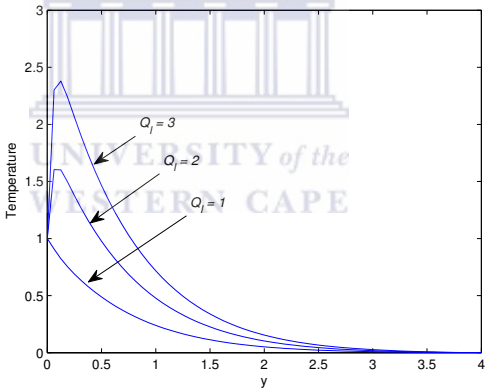

(b) Effect of Q_l on temperature with $P_r = 50$, $S_c = 0.6$, $K = 0.5$, $\delta = 0.5$, $Q = 1$, $G_m = G_r = 2$, $V_o = 0.2$, $n = 64$.

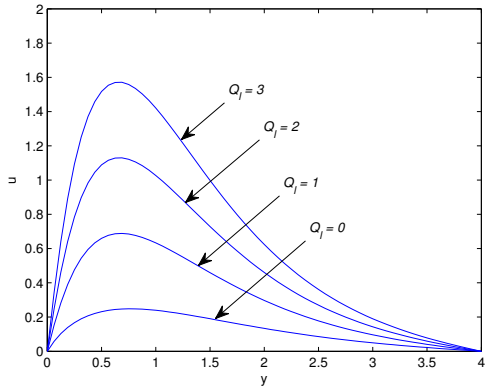

(c) Effect of Q_l on velocity with $P_r = 50$, $S_c = 1$, $K = 0.5$, $\delta = 0.5$, $Q = 0.1$, $G_m = G_r = 2$, $V_o = 0.5$, M = 1, $n = 64$.

Figure 7.4.2: Effect of Q_l on temperature and velocity.

increasing the values of the absorption parameter Q_l is to increase the boundary layer due to the increase in the buoyancy force wich speeds up the flow rate.

7.5 Summary

The study of unsteady free convective mass transfer flow of viscous incompressible electrically conducting fluid past a vertical infinite porous plate with heat sources in the presence of a chemical reaction, radiation absorption, transverse magnetic field and suction/injection using the FOFDM was carried out. The governing equations were non-dimensionalized by introducing similarity variables and then solved numerically using the fitted operator finite difference method. Since large values of P_r were assumed in this chapter the fitted operator finite difference method was used to analyze the temperature, concentration and velocity profiles as parameters such as the suction parameter, Prandtl number, Schmidt number, magnetic parameter, permeability parameter, chemical reaction parameter, absorption of radiation parameter and heat source parameter vary. We observed that using the FOFDM gives more accurate results with an improved order of convergence. The effect of the different parameters on the velocity, concentration and temperature profiles are summarized as follows.

- The temperature flow field increases with the increase in the heat source parameter and radiation absorption parameter whereas it decreases with the increase in Prandtl number and suction parameter.

- The concentration flow field decreases with the increase in the Schmidt number, chemical reaction parameter and suction.

- The velocity flow field decreases with increasing magnetic parameter and suction parameter whereas it increases with increasing permeability parameter and heat source parameter and radiation absorption parameter.

Chapter 8

Concluding remarks and scope for further research

In this thesis, we have designed, analyzed and implemented a class of fitted numerical methods to solve differential models describing unsteady magneto-hydrodynamic flow. The governing partial differential equations were transformed by a suitable similarity transformation to a system of ordinary differential equations. In each case, a fitted operator finite difference method (FOFDM) was developed to solve the ordinary differential equations. These methods were analyzed for stability and convergence. Both theoretical and numerical investigations done in this thesis show that proposed FOFDM are superior to the standard finite difference method.

As far as the **scope for further research** is concerned, we sought to

- design modified fitted operator finite difference methods to further improve the accuracy of the solutions for solving problems involving unsteady MHD flows;
- extend the study of unsteady MHD flows to higher dimensions;
- solve unsteady MHD flows that include dissipative heat and radiation, and
- extend the proposed approaches to solve other classes of unsteady MHD flows.

Bibliography

[1] M.S. Abel and N. Mahesha, Heat transfer in MHD viscoelastic fluid flow over a stretching sheet with variable thermal conductivity, non-uniform heat source and radiation, *Applied Methematical Modelling* **32(10)** (2008) 1965-1983.

[2] E.M. AboEldahab, Radiation effect on heat transfer in electrically conducting fluid at a stretching surface with uniform free stream, *Journal of Physics D: Applied Physics* **33(24)** (2000) 3180-3185.

[3] M. Acharya, L.P. Singh and G.C. Dash, Heat and mass transfer over an accelerating surface with heat source in presence of suction and blowing, *International Journal of Engineering Science* **37** (1999) 189-211.

[4] M.K. Akbar and S.M. Ghiaasiaan, Radiation heat transfer and soot thermophoresis in laminar tube flow, *International Journal of Heat and Fluid Flow* **11(1)** (1990) 98-104.

[5] M.S. Alam, M.M. Rahman and M.A. Sattar, Effects of variable suction and thermophoresis on steady MHD combined free-forced convective heat and mass transfer flow over a semi-infinite permeable inclined plate in the presence of thermal radiation, *International Journal of Thermal Sciences* **47(6)** (2008) 758-765.

[6] M.S. Alam, M.M. Rahman and M.A. Sattar, MHD free convective heat and mass transfer flow past an inclined surface with heat generation, *Thamasat International Journal of Science and Technology* **11(4)** (2006) 1-8.

[7] M.S. Alam, M.M. Rahman and M.A. Sattar, Similarity solutions for hydromagnetic free convective heat and mass transfer flow along a semi-infinite permeable inclined flat plate

with heat generation and thermophoresis, *Nonlinear Analysis: Modelling and Control* **12(4)** (2007) 433-445.

[8] M.S. Alam, M.M. Rahman and M.A. Sattar, Transient magnetohydrodynamic free convective heat and mass transfer flow with thermophoresis past a radiate inclined permeable plate in the presence of variable chemical reaction and temperature dependent viscosity, *Nonlinear Analysis: Modelling and Control* **14(1)** (2009) 3-20.

[9] M.M. Alam and M.A. Satter, Transient MHD heat and mass tranfer flow with thermal diffusion in a rotating system, *Journal of Energy, Heat and Mass Transfer* **21** (1999) 9-21.

[10] T.K. Aldoss, M.A. Al-Nimr, M.A. Jarra and B. Al-Shaer, Mixed convection flow from a vertical plate embedded in porous medium in the presence of magnetic field, *Heat Transfer* **28(A)** (1995) 635-645.

[11] A.R. Ansari, S.A. Bakr and G.I. Shishkin, A parameter-robust finite difference method for singularly perturbed delay parabolic partial differential equation, *Journal of Computing and Applied Mathematics* **205** (2007) 552-566.

[12] A.Y. Bakier and R.S.R. Gorla, Thermal radiation effect on mixed convection from horizontal surfaces in saturated porous media, *Transport in Porous Media* **23** (1996) 357-363.

[13] W.H.H. Banks, Similarity solution of the boundary layer equations for a stretching wall, *Journal of Mechanics Theory and Application* **2**(1983) 375-392.

[14] E.B.M. Bashier and K.C. Patidar, A Novel fitted operator finite difference method for a singularly perturbed delay parabolic partial differential equation, *Applied mathematics and Computation* **217(9)** (2011) 4728-4739.

[15] M. Bhavana, D.C. Kesavaiah and A. Sudhakaraiah, The soret effect on free convective unsteady MHD flow over a vertical plate with heat source, *International Journal of Innovative Research in Science, Engineering and Technology* **2(5)** (2013) 1617-1628.

[16] G. Beckett and J.A. Mackenzie, Convergence analysis of finite difference approximations on equidistributed grids to a singularly perturbed boundary value problem, *Applied Numerical Mathematics* **35** (2000) 87-109.

[17] O.A. Beg, H.S. Takhar and A.K. Singh, Multiparameter perturbation analysis of unsteady oscillatory magnetconvection in porous media with heat source effects, *International Journal of Fluid Mechanics Research* **32(6)** (2005) 635-661.

[18] O.A. Beg, J. Zueco, S.K. Ghosh and A. Heidari, Unsteady magnetohydrodynamic heat tranfer in a semi-infinite porous medium with thermal radiation flux: Analytical and numerical study, *Advances in Numerical Analysis.* DOI:10.1155/2011/304124.

[19] M.Q. Brewster, *Thermal Radiative Transfer and Properties* John Wiley and Sons, New York, 1992.

[20] H.C. Brinkman, A calculation of viscous force extended by flowing fluid in a dense swarm of particles, *Applied Science Research* **A(1)** (1947) 27-34.

[21] J.B. Burie, A. Calonnec and A. Ducrot, Singular pertubation analysis of travelling waves for a model in Phytopathology, *Mathematical Modelling of Natural Phenomena* **1(1)** (2006) 49-62.

[22] P. Carragher and L.J. Crane, Heat trensfer on a continous stretching sheet, *Journal of Applied Mathematics and Mechanics* **62** (1982) 564-565.

[23] G.F. Carrier and H.P. Greenspan, The time-dependent magnetohydrodynamic flow past a flat plate, *Journal of Fluid Mechanics* **7** (1960) 22-32.

[24] R.D. Cess, The interaction of thermal radiation with free convection heat transfer, *International Journal of Heat and Mass Transfer* **9** (1966) 1269-1277.

[25] P.L. Chambre and J.D. Young, On the diffusion of a chemically reactive species in a laminar boundary layer flow, *Physics of Fluids* **1(1)** (1958) 48-54.

[26] A.J. Chamkha, A. Al-Mudhaf and I. Pop, Effect of heat generation or absorption on thermophoretic free convection boundary layer from vertical flat plate embedded in a

porous medium,*International Communication in Heat and Mass Transfer* **33** (2006) 1096-1102.

[27] A.J. Chamkha, MHD flow of a uniformly stretched vertical permeable surface in the presence of heat generation /absorption and a chemical reaction, *International Communications Heat and Mass Transfer* **30** (2003) 413-422.

[28] A.J. Chamkha, Unsteady hydromagnetic natural convection in a fluid-saturated porous medium channel, *Advances in Filtration and Separation Technology* **10** (1996) 369-375.

[29] A.J. Chamkha, Unsteady laminar hydromagnetic flow and heat transfer in porous channels with temperature-dependent properties, *International Journal of Numerical Methods for Heat and Fluid Flow* **11(5)** (2001) 430-448.

[30] A.J. Chamkha, Unsteady MHD convective heat and mass transfer past a semi-infinite vertical permeable moving plate with heat absorption, *International Journal of Engeneering Science* **42** (2004) 217-230.

[31] P. Chandrakala, Chemical reaction effects on MHD flow past an impulsively started isothermal vertical plate with uniform mass flux, *International Journal of Dynamics of Fluids* **6(2)** (2010) 181-193.

[32] P. Chandrakala, Chemical reaction effects on MHD flow past an impusively started semi-infinite vertical plate, *International Journal of Dynamics of Fluids* **6(1)** (2010) 77-89.

[33] P. Chandran, N.C. Sacheti and A.K. Singh, Unsteady hydromagnetic free convection flow with heat flux and accelarated boundary motion, *Journal of Physics Society* **67** (1998) 124-129.

[34] R. Choundury and A. Das, Magnetohydrodynamic boundary layer flows of non-newtonian fluid past a flat plate, *Indian Journal of Applied Mathematics* **31(11)** (2000) 1429-1441.

[35] C.Clavero and J.L.Gracia, On the uniform of a finite difference scheme for time dependent singularly perturbed reaction-diffusion problems, *Applied Mathematics and Computation* **216** (2010) 1478-1488.

[36] A.C. Cogley, W.C. Vincenti and S.E. Gilles, Differential approximation for radiation transfer in a non-gray gas near equilibrium, *American Institute of Aeronautics and Astronautics Journal* **6** (1968) 551-555.

[37] C.I. Cookey, A. Ogulu and V.M. Omubo-Pepple, Influence of viscous dissipation and radiation on unsteady MHD free-convection flow past an infinite heated vertical plate in a porous medium with time-dependent suction, *International Journal of Heat and Mass Transfer* **46** (2003) 2305-2311.

[38] R. Cortell, Effects of viscous dissipation and radiation on the thermal boundary layer over a non-linearly stretching sheet, *Physics Letters A* **372(5)** (2008) 631-636.

[39] R. Cortell, Flow and heat transfer of an electrically conducting fluid of second grade over a stretching sheet subject to suction and to a transverse magnetic field, *International Journal of Heat Mass Transfer* **49** (2006) 1851-1856.

[40] L.J. Crane, Flow past a stretching plate, *Journal of Applied Mathematical Physics* **21** (1970) 645-647.

[41] U.N. Das, R.K. Deka, and V.M. Soundalgekar, Effect of mass transfer on flow past an impulsively started infinite vertical plate with chemical reaction, *The Bulletin of GUMA* **5** (1998) 13-20.

[42] U.N. Das, R.K. Deka and V.M. Soundalgekar, Effects of mass transfer on flow past an impulsively started infinite vertical plate with constant heat flux and chemical reaction, *Forschung im Ingenieurwesen* **60(10)** (1994) 284-287.

[43] U.N. Das, R.K. Deka and V.M. Soundalgekar, Radiation effect on flow past an impulsively started vertical plate-an exact solution, *Journal of Theoretical Application in Fluid Mechanics* **1(2)** (1996) 111-115.

[44] U.N. Das, R.K. Deka, and V.M. Soundalgekar, Transient free convection flow of an elastico-viscous fluid past an infinite vertical plate, *Engineering Transactions* **43** (1995) 487-491.

[45] U.N. Das, R.K. Deka and V.M. Soundalgekar, Transient free convection flow past an infinite vertical plate with periodic temperature variation, *ASME Journal of Heat Transfer* **121(4)** (1999) 1091-1094.

[46] S.S. Das and M. Mitra, Unsteady mixed convective MHD flow and mass transfer past an accelerated infinite vertical porous plate with suction, *Indian Journal of Science and Technology* **2(5)** (2009) 18-22.

[47] U.N. Das, S.N. Ray and V.M. Soundalgekar, Mass transfer effects on flow past an impulsively started infinite vertical plate with constant mass flux-an exact solution, *Heat and Mass Transfer* **31** (1996) 163-167.

[48] S.S. Das, S.K. Sahoo and G.C. Dash, Numerical solution of mass transfer effects on unsteady flow past an accelerated vertical porous plate with suction, *Bulletin of the Malaysian Mathematical Sciences Society* **29(1)** (2006) 33-42.

[49] R.K. Deka and B.C. Neog, Unsteady MHD flow past a vertical oscillating plate with thermal radiation and variable mass diffusion, *Chamchuri journal of math,* **1**(2)(2009):79-92.

[50] S.P.A Devi and R. Kandasamy, Effects of chemical reaction, heat and mass transfer on MHD flow past a semi infinite plate, *Zeitschrift für Angewandte Mathematik und Mechanik* **80(10)** (2000) 697-701.

[51] E.P. Doolan, J.J.H. Miller and W.H.A. Schilders, *Uniform Numerical Methods for Problems with Initial and Boundary Layers,* Boole Press, Dublin, 1980.

[52] B.K. Dutta, P. Roy and A.S. Gupta, Temperature field in flow over a stretching sheet with uniform heat flux, *International Communications of Heat and Mass Transfer* **12** (1985) 89-94.

[53] E.M.A. Elbashbeshy and M.A.A. Bazid, The effect of temperature-dependent viscosity on heat trensfer over a continous moving surface with variable internal heat generation, *Applied Mathematics and Computation* **153** (2004) 721-731.

[54] M.A. El-Hakiem, MHD oscillatory flow on free convection-radiation through a porous medium with constant suction velocity, *Journal of Magnetism and Magnetic Materials* **220(2-3)** (2000) 271-276.

[55] M.A.A. El-Naby, E.M.E. Elbarbary and N.Y. Abdelazem, Finite difference solution of radiation effects on MHD unsteady free-convection flow on vertical porous plate, *Applied Mathematics and Computation* **151(2)** (2004) 327-346.

[56] W.G. England and A.F. Emery, Thermal radiation effects on the laminar free convection boundary layer of an absorbing gas, *Journal of Heat Transfer* **91**(1969) 37-44.

[57] P. Ganesan and P. Loganathan, Radiation and mass transfer effects on flow of an incompressible viscous fluid past a moving vertical cylinder, *International Journal of Heat and Mass Transfer* **45(21)** (2002) 4281-4288.

[58] B. Gebhart and L. Pera, The nature of vertical natural convection flows resulting from the combined buoyancy effects of thermal and mass diffusion, *International Journal of Heat and Mass Transfer* **14(12)** (1971) 2025-2050.

[59] A.Y. Ghaly and M.A. Seddeek, Chebyshev finite difference method for the effects of chemical reaction, heat and mass transfer on laminar flow along a semi-infinite horizontal plate with temperature dependent viscosity, *Chaos, Solitons and Fractals* **19** (2004) 61-70.

[60] J.L. Gracia and F.J. Lisbona, A uniformly convergent scheme for a system of reaction-diffusion equations, *Journal of Computational and Applied Mathematics* **206** (2007) 1-16.

[61] P.S. Gupta and A.S. Gupta, Heat and mass transfer on a stretching sheet with sunction and blowing, *Journal of Chemical Engineering* **55** (2009) 744-746.

[62] P.S. Gupta and A.S Gupta, Radiation effect on hydromagnetic convection in a vertical channel, *International Journal of Heat Mass Transfer* **17**(1974) 1437-1442.

[63] P. Han and T. Yoshida, Numerical investigation of thermophoretic effects on cluster transport during thermal plasma deposition process, *Journal of Applied Physics* **91(4)** (2002) 1814-1818.

[64] H. Hasimoto, Boundary layer growth on a flat plate with suction or injection, *Journal of the Physics Society of Japan* **12 (1)** (1957) 68-72.

[65] I.A. Hassanien and M.H. Obied Allah, Oscillatory hydromagnetic flow through a porous medium with variable permeability in the presence of free convection and mass transfer flow, *International Communications in Heat and Mass Transfer* **29(4)** (2002) 567-575.

[66] T. Hayat, M.Qasim and S. Mesloub, MHD flow and heat transfer over permeable stretching sheet with slip condition, *International Journal for Numerical methods in Fluids,* **66**(2011) 963-975.

[67] J.D. Hellums and S.W. Churchill, Computation of natural convection by finite-difference methods, *ASME International Development in Heat Transfer, Part V* (1961) 985-994.

[68] K.A. Helmy, MHD unsteady free convection flow past a vertical porous plate, *Zeitschrift fur Angewandte Mathematik und Mechanik* **98** (1998) 255-270.

[69] M.A. Hossain, M.M. Molla and L.S. Yaa, Natural convection flow along a vertical wavy surface temperature in the presence of heat generation/absorption, *International Journal of Thermal Science* **43** (2004) 157-163.

[70] M.A. Hossain and H.S. Takhar, Radiation effect on mixed convection along a vertical plate with uniform surface temperature, *Heat and Mass Transfer* **31** (1996) 243-248.

[71] F.S. Ibrahim, A.M. Elaiw and A.A. Bakr, Effect of the chemical reaction and radiation absorption on the unsteady MHD free convection flow past a semi infinite vertical permeable moving plate with heat source and suction, *Communications in Nonlinear Science and Numerical Simulations* **13(6)** (2008) 1056-1066.

[72] C.R. Illingworth, Unsteady laminar flow of gas near an infinite flat plate, *Mathematical Proceedings of the Cambridge Philosophical Society* **46** (1950) 603-613.

[73] A. Ishak, R. Nazar and I. Pop, Heat tranfer over an unsteady stretching permeable surface with prescribed wall temperature, *Nonlinear Analysis: Real World Applications* **10(5)** (2009) 2909-2913.

[74] A. Ishak, R. Nazar and I. Pop, MHD boundary-layer flow due to a moving extensible surface, *Journal of Engineering Mathematics* **62** (2008) 23-33.

[75] C. Israel-Cookey, A. Ogulu and V.B. Omubo-Pepple, Influence of viscous dissipation and radiation on unsteady MHD free-convection flow past an infinite heated vertical plate in a porous medium with time-dependent suction, *International Journal of Heat and Mass Transfer* **46(13)** (2003) 2305-2311.

[76] B.K. Jha, Effect of applied magnetic field on transient free convective flow in a vertical channel, *Indian Journal of Pure and Applied Mathematics* **29(4)** (1998) 441-445.

[77] M.K. Kadalbajoo, K.C. Patidar and K.K. Sharma, ϵ-Uniformly convergent fitted methods for the numerical solution of the problems arising from singularly perturbed general DDEs, *Applied Mathematics and Computation* **182** (2006) 119-139.

[78] N.G. Kafoussias and E.W. Williams, Thermal-diffusion and diffusion-thermo effects on mixed free-forced convective and mass transfer boundary layer flow with temperature dependent viscosity, *International Journal of Engineering Science* **33(9)** (1995) 1369-1384.

[79] R. Kandasamy, Effect of heat and mass transfer along a wedge with heat source and concentration in the presence of suction or injection, *Journal of Energy, Heat and Mass Transfer* **27** (2005) 305-316.

[80] Y.J. Kim and A.G. Fedorov, Transient mixed radiative convection flow past a moving semi-infinite vertical porous plate *International Journal of Heat and Mass Transfer* **46** (2003) 1751-1758.

[81] Y.J. Kim, Unsteady MHD convective heat transfer past a semi-infinite vertical porous moving plate with variable suction, *International Journal of Engineering Science* **38(8)** (2000) 833-845.

[82] H.K Kuiken, On boundary layers in fluid mechanics that decay algebraically along stretches of wall that are not vanishingly small, *IMA Journal of Applied Mathematics* **27** (1981) 387-405.

[83] M. Kumari and G. Nath, Development of two-dimensional boundary layer with an applied magnetic field due to an impulsive motion, *Indian Journal of Pure and Applied Mathematics* **30(7)** (1999) 695-708.

[84] M. Kumari and G. Nath, Unsteady MHD mixed convection flow over an impulsively stretched permeable vertical surface in a quesscent fluid, *International Journal of Non-Linear Mechanics* **45** (2010) 310-319.

[85] D. Kumar and M.K. Kadalbajoo, A parameter-uniform numerical method for time-dependent singularly perturbed differential-difference equations, *Applied Mathematical Modelling* **35** (2011) 2805-2819.

[86] J.M.S. Lubuma and K.C. Patidar, Contributions to the theory of non-standard finite difference methods and applications to singular perturbation problems. In R.E. Mickens (ed.): *Applications of Nonstandard Finite Difference Schemes*, World Scientific, Singapore, 2005, pp. 513–560.

[87] M.I. Loffredo, Extension of von Karman ansatz to magnetohydrodynamic, *Meccanica* **21(2)** (1986) 81-86.

[88] E. Magyari and B. Keller, Heat and mass transfer in the boundary layers on an exponentially stretching continous surface, *Journal of Physics: Applied Physics* **32** (1999) 577-585.

[89] E. Magyari and B. Keller, Exact solutions for self similar boundary-iayer flows induced by permeable strettching surfaces, *Europian Journal of Mechanics: B-Fluids* **19** (2001) 109-122.

[90] E. Magyari, M.E. Ali and B. Keller, Heat and mass transfer characteristics of the self similar boundary-layer flows induced by continous surfaces stretched with rapid decreasing velocities, *Heat and Mass Transfer* **38** (2001) 65-74.

[91] A. Mahmood and A. Ali, The effect of slip condition on unsteady MHD oscillatory flow of a viscous fluid in a planer channel, *Romanian Journal of Physics* **52(1-2)** (2007) 85-91.

[92] M.A. Mansour, N.F. El-Anssary and A.M. Aly, Effect of chemical reaction and viscous dissipation on MHD natural convection flows saturated in porous media with suction or injection, *International Journal of Applied Mathematics and Mechanics* **4(2)** (2008) 60-76.

[93] D. Mansutti, G. Pontrelli and K.R. Rajagopal, Steady flows of non-Newtonian fluids past a porous plate with suction or injection, *International Journal for Numerical Methods in Fluids* **17(11)** (1993) 927-941.

[94] M.K. Mazumdar and R.K. Deka, MHD flow past an impulsively started infinite vertical plate in presence of thermal radiation, *Romanian Journal of Physics* **52** (2007) 529-535.

[95] I.U. Mbeledogu, A.R.C. Amakiri and A. Ogulu, Unsteady MHD free convection flow of a compressible fluid past a moving vertical plate in the presence of radiative heat transfer, *International Journal of Heat Mass Transfer* **50(9-10)** (2007) 1668-1674.

[96] J.J.H. Miller, E. O'Riordan and G.I. Shishkin, *Fitted Numerical Methods for Singular Perturbation Problems* World Scientific, Singapore, 1996.

[97] A.F. Mills, Xu. Hang and F. Ayazi, The effect of wall suction and thermophoresis on aerosol-particle deposition from a laminar boundary layer on a flat plate, *International Journal of Heat and Mass Transfer* **27(7)** (1984) 1110-1113.

[98] J.P. Mishra, G.C. Shit and H.J. Rath, Flow and heat transfer of a MHD viscoelastic fluid in a channei with stretching walls, *Computer and fluids* **37**(1) (2008) 1-11.

[99] R.A. Mohamed, Double-diffusive convection-radiation interaction on unsteady MHD flow over a vertical moving porous plate with heat generation and soret effects, *Applied Mathematical Sciences* **3(13)** (2009) 629-651.

[100] M.M. Molla and M.A. Hossain, Effects of chemical reaction heat and mass diffusion in natural convection flow from an isothermal sphere with temperature dependent viscosity, *International Journal of Computer-Aided Engineering and Software* **23(7)** (2006) 840-857.

[101] J.B. Munyakazi and K.C. Patidar, A fitted numerical method for singularly perturbed parabolic reaction-diffusion problems, *Computational and Applied Mathematics* **32** (2013) 509-519.

[102] J.B. Munyakazi and K.C. Patidar, On Richadson extrapolation for fitted operator finite difference methods, *Applied Mathematics and Computation* **201** (2008) 465-480.

[103] J.B. Munyakazi and K.C. Patidar, Limitations of Richardson's extrapolations for a high order fitted mesh method for self-adjoint singularly perturbed problems, *Applied Mathematics and Computation* **32** (2009) 219-236.

[104] J.B. Munyakazi and K.C. Patidar, Novel fitted finite difference methods for singularly perturbed elliptic convection-diffusion problems in two dimensions, *Journal of Difference Equations and Applications* **18** (2012) 799-813.

[105] J.D. Murray, *Mathematical Biology: I. An Introduction* 3^{rd} ed. Springer-Verlag, Berlin, 2001.

[106] R. Muthucumaraswamy, Effects of suction on heat and mass transfer along moving vertical surface in the presence of chemical reaction, *Forschung im Ingenieurwesen* **67** (2002) 129-132.

[107] R. Muthucumaraswamy, The interaction of thermal radiation on vertical oscillating plate and variable temperature and mass difusion, *Theoretical Applied Mechanics* **33** (2006) 107-121.

[108] R. Muthucumaraswamy and P. Ganesan, Diffusion and first-order chemical reaction on impulsively started infinite vertical plate with variable temperature, *International Journal of Thermal Sciences* **41(5)** (2002) 475-479.

[109] R. Muthucumaraswamy and P. Ganesan, Effect of the chemical reaction and injection on flow characteristics in an unsteady upward motion of an isothermal plate, *Journal of Applied Mechanics and Technical Physics* **42(4)** (2001) 665-671.

[110] R. Muthucumaraswamy and P. Ganesan, First order chemical reaction on flow past an impulsively started infinite vertical plate with uniform heat and mass flux, *Acta Mechanica* **147(1-4)** (2001) 45-57.

[111] R. Muthucumaraswamy and P. Ganesan, On impulsive motion on a vertical plate with heat flux and diffusion on chemically reactive species, *Forschung im Ingenieurwesen* **66(1)** (2000) 17-23.

[112] R. Muthucumaraswamy and P. Ganesan, Unsteady flow past an impulsively started vertical plate with heat and mass transfer, *International Journal of Heat and Mass Transfer* **34(2)** (1998) 187-193.

[113] R. Muthucumaraswamy and B. Janakiraman, MHD and radiation effects on moving isorthemal vertical plate with variable mass difussion, *Theoretical Applied Mechanics* **33** (2006) 17-29.

[114] R. Nazar, N. Amin, D. Philip and I. Pop, Unsteady boundary layer flow in the region of the stagnation point on a stretching sheet, *International Journal of Engineering Science* **42** (2004) 1241-1253.

[115] B.C. Neog and R.K. Das, Flow past an electrically conducting fluid over a vertical oscillating plate with chemical reaction, *Journal of Mathematics* **2(1)** (2012) 12-16.

[116] D. Pal and B. Talukdar, Perturbation analysis of unsteady magnetohydrodynamic convective heat and mass transfer in a boundary layer slip flow past a vertical permeable plate with thermal radiation and chemical reaction, *Communications in Nonlinear Science and Numerical Simulation* **15(7)** (2010) 1813-1830.

[117] G. Palani and U. Srikanth, MHD flow past a semi-infinite vertical plate with mass transfer, *Nonlinear Analysis: Modelling and Control,* **14(3)** 345-356.

[118] A. Pantokratoras, Non-Darcian forced convection heat transfer over a flat plate in a porous medium with variable viscosity and variable Prandtl number, *Journal of Porous Media* **10(2)** (2007) 201-208.

[119] E.N. Parker, Cosmical magnetic fields, *Clareden Press, Oxford,* 1979.

[120] G. Pathal, C. Maheswari and S.S. Tak, Unsteady mass, momentum, and heat transfer in MHD free convection flow past along a vertical plate suddenly set in motion, *Bulletin of Pure and Applied Mathematics. Section E Mathematics* **24(1)** (2005) 173-183.

[121] K.C. Patidar, High order parameter uniform numerical method for singular perturbation problems, *Applied Mathematics and Computation* **188(1)** (2007) 720-733.

[122] K.V. Prasad, S. Abel and P.S. Datti, Diffusion of chemically reactive species of a non-Newtonian fluid immersed in a porous medium over a stretching sheet, *International Journal of Non-linear Mechanics* **38(5)** (2003) 651-657.

[123] V.R. Prasad, N. Bhakar Reddy and R. Muthucumaraswamy, Transient radiative hydromagnetic free convection flow past an impulsively started vertical plate with uniform heat and mass flux, *Theoretical Application in Mechanics* **33(1)** (2006) 31-63.

[124] V.R. Prasad, N. Bhakar Reddy and R. Muthucumaraswamy, Radiation and mass tranfer effects on two-dimensuional flow past an impulsively started infinite vertical plate, *International Journal of Thermal Sciences* **46** (2007) 1251-1258.

[125] U.S. Rajput and S. Kumar, Radiation effects on MHD flow past an impulsively started vertical plate with variable heat and mass transfer, *International Journal of Applied mathematics and Mechanics* **8(1)** (2012) 66-85.

[126] A. Raptis, Radiation and free convection flow through a porous medium, *International Communications in Heat and Mass Transfer* **25(2)** (1998) 289-295.

[127] A. Raptis and C. Perdikis, Viscous flow over a non-linearly stretching sheet in the presence of a chemical reaction and magnetic field, *International Journal of Non-linear Mechanics* **41** (2006) 527-529.

[128] A. Raptis, A.K. Singh and K.D. Rai, Finite difference analysis of unsteady free convective flow through a porous medium adjacent to a semi-infinite vertical plate, *Mechanics Research Communication* **14(1)** (1987) 9-16.

[129] G.V.R Reddy, C.V.R. Murthy and N.B. Reddy, Mixed convective MHD flow and mass transfer past an accelerated infinite vertical porous plate, *Mathematics Applied in Science and Technology* **1(1)** (2009) 27-37.

[130] P. Roja, T. Sankar Reddy and N.B. Reddy, Double-diffusive convection-radiation interaction on unsteady MHD flow of a micropolar fluid over a vertical moving porous plate

embedded in a porous medium with heat generation and soret effects, *The International Journal of Engineering and Science* **1(2)** (2012) 201-214.

[131] H.-G. Roos, M. Stynes and L. Tobiska, *Numerical Methods for Singularly Perturbed Differential Equations: Convection-Diffusion and Flow Problems,* Springer-Verlag, Berlin, 1996.

[132] H.-G. Roos, M. Stynes and L. Tobiska, *Robust Numerical Methods for Singularly Perturbed Differential Equations: Convection-Diffusion-Reaction and Flow Problems,* Springer-Verlag, Berlin, 2008.

[133] N.C. Sacheti, P. Chandran and A.K. Singh, An exact solution for unsteady magnetohydrodynamics free convection flow with constant heat flux, *International Communications in Heat and Mass Transfer* **21(1)** (1994) 131-142.

[134] B.C. Sakiadis, Boundary layer behavior on continous solid surface: The boundary layer equations for two-dimensional and axisymmetric flow, *American Institute of Chemical Engineers Journal* **7(1)** (1961) 26-28.

[135] M.A. Satter, Free convection and mass tranfer flow through a porous medium past an infinite vertical porous plate with time dependent temperature and concentration, *Indian Journal of Pure and Applied Mathematics* **25(7)** (1994) 759-766.

[136] M.A. Sattar and M.M. Hossain, Unsteady hydromagnetic free convection flow with Hall current and mass transfer along an accelerated porous plate with time dependent temperature and concentration, *Canadian Journal of Physics* **70** (1992) 369-374.

[137] H. Schlichting and K. Gersten, *Boundary Layer Theory,* 6^{th} ed., McGraw-Hill, New York, 1968.

[138] M.A. Seddeek, Effects of radiation and variable viscosity on a MHD free convection flow past a semi-infinite flat plate with an aligned magneti field in the case of unsteady flow, *International Journal of Heat and Mass transfer* **45(4)** (2002) 931-935.

[139] M.A. Seddeek, The Effect of variable viscosity on hydromagnetic flow and heat transfer past a continously porous boundary with radiation, *International Communucations of Heat and Mass* **27** (2000) 1037-1048.

[140] M.A. Seddeek, A.A. Darwish and M.S. Abdelmeguid, Effects of chemical reaction and variable viscosity on hydromagnetic mixed convection heat and mass transfer for Hiemenz flow through porous media with radiation, *Communucations in Nonlinear Science and Numerical Simulation* **12(2)** (2007) 195-213.

[141] P.R. Sharma and D. Pareek, Steady free convection MHD flow past a vertical porous moving surface, *Indian Journal of Theoretical Physics* **50** (2002) 5-13.

[142] S. Shateyi, S.S. Motsa and P. Sibanda, The effects of thermal radiation, Hall currents, Soret, and Dufour on MHD flow by mixed convection over a vertical surface in porous media, *Mathematical Problems in Engineering*, 2010, Article ID 627475; DOI: 10.1155/2010/627475.

[143] S. Shivaiah and J.A. Rao, Chemical reaction effect on an unsteady MHD free convection flow past a vertical porous plate in the presence of suction or injection, *Theoretical and Applied Mechanics* **39(2)** (2012) 185-208.

[144] R. Siegel, Transient free convection from a vertical flat plate, *Transactions of the American Society of Mechanical Engineers* **80** (1958) 347-359.

[145] A.K. Singh, Effect of mass transfer on free convection in MHD flow of a viscous fluid, *Indian Journal of Pure and Applied Physics* **41** (2003) 262-274.

[146] A.K. Singh, Effects of thermal diffusion on MHD free convection flow through a vertical channel, *Journal of Energy, Heat and Mass Transfer* **27** (2005) 109-123.

[147] A.K. Singh, Numerical solution of unsteady free convection flow of an incompressible micropolar fluid past an infinite vertical plate with temperature gradient dependent heat source, *Journal of Energy, Heat and Mass Transfer* **24** (2002) 185-194.

[148] D. Singh, Unsteady hydromagnetic free convection flow past a vertical infinite flat plate, *Journal of the Physical Society of Japan* **19** (1964) 751- 755.

[149] A.K. Singh and V.M. Souindalgekar, Transient free convection in cold water past an infinite vertical porous plate, *International Journal of Energy Research* **14(4)** (1990) 413-420.

[150] Y.M. Sohn, S.W. Baek and D.Y. Kim, Thermophoresis of particles in gas-particle two-phase flow with radiation effect, *Numerical Heat Transfer, Part A: Applications* **41(2)** (2002) 165-181.

[151] V.M. Soundalgekar, Free convection effects on the flow past a vertical oscillating plate, *Astrophysics and Space Science* **66** (1979) 165-172.

[152] V.M. Soundalgekar, Free convection effects on steady MHD flow past a vertical porous plate, *Journal of Fluid Mechanics* **66(3)** (1974) 541-551.

[153] V.M. Soundalgekar and S.P. Akolkar, Effects of free convection currents and mass transfer on flow past a vertical oscillating plate, *Astrophysics and Space Science* **89** (1983) 241-254.

[154] V.M. Soundalgekar, U.N. Das and R. Deka, Transient free convection flow past an infinite vertical plate with periodic temperature variation, *ASME Journal of Heat Transfer* **121** (1999) 1091-1094.

[155] V.M. Soundalgekar and P. Ganesan, Finite-difference analysis of transient free convection with mass transfer on an isothermal vertical flat plate, *International Journal of Engineering Science* **19** (1981) 757-770.

[156] V.M. Soundalgekar, S.K. Gupta and R.N. Aranake, Free convection effects on MHD Stokes problem for a vertical plate, *Nuclear Engineering and Design* **51(3)** (1979) 403-407.

[157] V.M. Soundalgekar and H.S. Takhar, Radiative convective flow past a semi infinite vertical plate, *Modelling Measure and control,* **51** (1992) 31-40.

[158] V.M. Soundalgekar, A.G. Uplekar and B.S. Jaiswal, Transient free convection flow of dissipative fluid past an infinite vertical porous plate, *Archives of Mechanics* **56(1)** (2004) 7-17.

[159] H.S. Takhar and O.A. Beg, Effects of trnsverse magnetic field, Prandtl number and Reynolds number in non-Darcy mixed convective flow of an incompressible viscous fluid

past a porous vertical flat plate in a saturated porous medium, *International Journal of Energy Research* **21** (1997) 87-100.

[160] H.S. Takhar, A.K. Singh and G. Nath, Unsteady MHD flow and heat tranfer on a rotating disk in an ambient fluid, *International Journal of Thermal Science* **41**(2002) 147-155.

[161] D.G. Tharkuta, M. Chen, J.B. Mclaughlin and K. Kontomaris, Thermophoretic deposition of small particles in a direct direct numerical simulation of turbulent channel flow; *International Journal of Heat and Mass Transfer* **41(24)** (1998) 4167-4182.

[162] K.L. Walker, G.M. Homsy and F.T. Geyling, Thermophoretic deposition of small particles in laminar tube, *Journal of Colloid and Interface* **69** (1979) 138-147.

[163] Y. Ye, D.Y.H. Pui, B.Y.H. Liu, S. Opiolka, S. Blumhorst and H. Fissan, Thermophoretic effect of particle deposition on a free standing semiconductor wafer in a clean room, *Journal of Aerosol Science* **22** (1991) 63-72.

[164] S.J. Yoa, S.S. Kim and J.S. Lee, Thermophoresis of highly absorbing emitting particles in laminar tube flow, *International Journal of Heat and Fluid Flow* **11(1)** (1990) 98-104.